Together ahead. RUAG

Diplomarbeit

Low Resistive Torque Supply Harness and Piping Routing for High Power Plasma Thruster Pointing Mechanisms

ausgeführt zum Zwecke der Erlangung des akademischen Grades eines Diplom-Ingenieurs unter der Leitung von

Ao.Univ.Prof. Dipl.-Ing. Dr.techn. Manfred Grafinger

und

Dipl.-Ing. Paul Janu (RUAG SPACE AUSTRIA)

Institut für Konstruktionswissenschaften und Technische Logistik
Forschungsbereich Konstruktionslehre und Fördertechnik

eingereicht an der Technischen Universität Wien
Fakultät für Maschinenwesen und Betriebswissenschaften

von
Ingo Polonia
0728148 (066 482)
Hillerstraße 4/13-14
1020 Wien

Wien, im Jänner 2016

Ingo Polonia

Kurzfassung

Geometrische und mechanische Entwicklung eines elektrischen Kabelbaums mit geringem resistivem Störmoment für Verstellmechanismen von Hochleistungsplasmatriebwerken

Im Zuge dieser Diplomarbeit wurden verschiedene Möglichkeiten für die Verlegung der elektrischen Versorgungskabel für Plasmatriebwerke von Raumfahrzeugen untersucht, wobei spezielles Augenmerk auf die Festigkeitsberechnung und Minimierung des resistiven Störmoments durch die Steifigkeit der Kabel gelegt wurde. Der Kabelbaum wird hierbei um mehrere Rotationsachsen gespult und muss in der Lage sein, die Drehungen des Verstellmechanismus, welcher das Triebwerk relativ zur Raumsonde bewegt, mechanisch zu kompensieren. Nach einer theoretischen Diskussion der geometrischen und mechanischen Designparameter des Kabelbaums wurden verschiedene Versionen im Labor aufgebaut und Messungen des resistiven Moments sowie des Reibungsmoments vorgenommen. In den abschließenden Berechnungen wurde die Eignung des im Mechanismus verwendeten Rotationsaktuators bezüglich des vorherrschenden Störmoments verifiziert sowie eine Ermüdungsberechnung der Stromkabel, bestehend aus Kupferlitzen mit Polyimid-Isolierung, durchgeführt. Es konnte gezeigt werden, dass die schraubenförmige Wicklung des Kabelbaums sowie die Anordnung in mehreren Kabelschichten nicht nur eine enorme Verringerung des Platzbedarfs, sondern auch eine Erhöhung der Lebensdauer bewirkte. Da die Spannungsamplitude durch die Bewegung des Mechanismus klein gegen die Mittelspannung ist, sind die Kabelkomponenten dauerfest und können daher eine unbegrenzte Zahl an Lastzyklen ertragen. Des Weiteren erwies sich der im Labor aufgebaute Prüfstand als ein verlässliches und konservatives Modell im Bezug auf die Messungen des resistiven Störmoments sowie des Reibungsmoments des Kabelbaums.

Abstract

Low Resistive Torque Supply Harness and Piping Routing for High Power Plasma Thruster Pointing Mechanisms

This diploma thesis investigates different possibilities for the routing of the electric supply harness for plasma thrusters used in spacecrafts, with special attention to strength calculation and minimization of the resistive torque induced by the stiffness of the electric cables. Hereby, the electric cables are winded around several rotation axes and need to compensate the deployment carried out by the so-called pointing mechanism, which moves the thruster relatively to the spacecraft. After the geometric and mechanical parameters of the harness design were evaluated theoretically, different design versions were built in the laboratory and measurements of resistive and friction torque were performed. In the final calculations, the suitability of the chosen geared actuator regarding the prevailing resistive torque was verified and the fatigue lifetime of the cables (consisting of copper strands with a polyimide insulation) was assessed. It could be shown that the helical routing of the harness and the arrangement in multiple cable layers not only decreased the space requirement, but also had a positive effect on the fatigue life. Due to the stress amplitude during operation of the mechanism being small compared to the overall stress level, the material reaches the fail-safe region and is therefore able to resist an infinite number of cycles to failure. Furthermore, the test setup built in the laboratory turned out to be a reliable and conservative model regarding the measurements of resistive torque as well as friction torque of the cable harness.

Contents

Chapter 1

Introduction

In the past three decades, electric propulsion was frequently used to operate all kinds of spacecrafts including satellites and space probes. Electric thrusters were deployed instead of conventional chemical thrusters many times both in scientific missions as well as in commercial activities. Since the late 90's, electric propulsion systems experienced a rapid growth in employment especially for station keeping and orbit insertion applications in geosynchronous communication satellites. At the same time, this technology was more and more used also for deep-space scientific missions.[1] For example, the BepiColombo mission to Mercury by the EUROPEAN SPACE AGENCY (ESA) will be equipped with electric propulsion.[2]

The general benefit of this kind of propulsion is the greatly reduced need for propellant in comparison to traditional, i.e. chemical propulsion. Conventional thrusters generate thrust through the ejection of a hot gas, which has been heated by the chemical energy contained in the propellant. This implies a limitation of the attainable power and thrust values of this kind of propulsion, because only the energy which is already stored in the propellant can be used. On a contrary, an electric propulsion system feeds additional energy to the propellant material and thus separates the energy which can be used in the engine from the propellant mass. This means that the energy contained in one kilogram of propellant is no longer limited by the chemical ernergy which is stored in the fluid. The additional electric power can be provided by the solar arrays of the spacecraft as electrical energy in sufficient quantity.[3]

The reduction of required propellant mass results in the possibility of reaching objects at much greater distance, such as asteroids, with similar amounts of propellant. On the other hand, considering that a large proportion of the spacecraft's overall mass consists of propellant, the start mass can be sharply decreased. This leads directly to cost reduction, because either satellites can be launched using smaller and therefore cheaper rockets, or

[1] cf. Goebel and Katz, 2008, p. 3.
[2] cf. Turner, 2009, p. 167.
[3] cf. ibid., pp. 165–166.

the spacecraft can be equipped with higher amounts of payload.[4] The cost of transporting one kilogram of mass to Low Earth Orbit (LEO) is approximately 10,000 €.[5]

The advantageous propellant demand of electric propulsion systems is contrasted with their microscale thrust levels. This disadvantage is the reason why chemical propulsion was preferred for a long time, although the electric propulsion was already developed in the 1960's.[6] Common electrostatic propulsion units are only able to reach thrusts between 10 and 200 mN.[7] Compared to the thrust of conventional chemical propulsion, which can reach up to 10 MN,[8] we can see that a spacecraft equipped with electric thrusters has much lower levels of acceleration and therefore the duration of travel is many times higher.

If, for instance, a satellite with a start mass of 3000 kg shall be transferred from a geostationary transfer orbit (GTO) to a geostationary Earth orbit (GEO), a chemical thruster needs 1825 kg of propellant, while an electric thruster requires only 133 kg. However, the journey would take the conventional engine only about a week, while a satellite equipped with electric propulsion would be several months on the way.[9]

One kind of electric propulsion is the so-called electrostatic propulsion. This technique depends on plasma generation by ionizing a great proportion of the propellant. An electrostatic field is applied through biased grids, in which the ions taken from the plasma are highly accelerated in order to reach great exhaust velocities.[10] The mostly used propellants for this kind of propulsion are "heavy inert gases such as xenon",[11] because xenon has certain benefits compared to other materials such as for instance cesium and mercury.[12] This is the principle of a so-called *ion thruster*.

Another type of electrostatic propulsion is the *Hall effect thruster* (HET), which has been mainly developed by Russia until the mid-1990's. The ion current of a common ion thruster is limited because a positive charge (*space charge*) is established between its accelerating grids. In the Hall thruster, on the other hand, electrons which are held in a radial magnetic field neutralize this space charge. As a consequence, higher thrust values can be reached compared to the ion thruster.[13]

Current examples for ion thrusters are the *T-6 20-cm Kaufman thruster* which is developed by QINETIQ in England, and the *RIT-22* by the German company ASTRIUM (nowadays part of AIRBUS). Both of these systems are capable of producing thrust levels up to 200 mN.[14] Examples for Hall thrusters are the *PPS-1350-G* manufactured in France by

[4] cf. Altorfer, 2014, p. 5.
[5] cf. W. L. Gore & Associates. *GORE Space Cables and Assemblies*, p. 2. URL: see Bibliography.
[6] cf. Altorfer, 2014, p. 5.
[7] cf. Tajmar, 2003, p. 76.
[8] cf. ibid., p. 23.
[9] cf. Altorfer, 2014, p. 6.
[10] cf. Goebel and Katz, 2008, p. 4.
[11] Ibid., p. 1.
[12] cf. ibid., pp. 1–2.
[13] cf. Sforza, 2012, p. 557.
[14] cf. Goebel and Katz, 2008, pp. 437, 439.

SNECMA and the *Stationary Plasma Thruster* (SPT) by FAKEL in Russia.[15] The *SPT-140* will be part of the investigation of this diploma thesis.

One of the leading companies in Europe to produce mechanical equipment for the application of plasma propulsion systems on spacecrafts is RUAG SPACE GMBH or RUAG SPACE AUSTRIA (RSA). The company is the Austrian branch of the group RUAG SPACE, which is operating as a supplier in the fields of space flight on an international basis. RSA has successfully contributed to many European, Asian and US-American satellite missions, while some of the company's business segments also took a leading role in the non-space market. The product portfolio comprises the following different areas:

- On-board Electronics
- On-board Mechanisms
- Thermal Hardware
- Mechanical Ground Support Equipment[16]

One of the mechanisms developed for the ESA by RUAG SPACE is the *Electric Propulsion Pointing Mechanism* (EPPM), which is the main underlying component for the investigations of this diploma thesis. The EPPM is a device used to control the position and orientation of the electric propulsion unit by moving it around two or even three rotation axes. This is necessary in order to optimally adjust the direction of the thruster so its efficiency can be increased. That way, larger spacecrafts can be operated by electric propulsion and higher travel speeds can be reached.[17] Each rotation axis of the EPPM is equipped with a rotary geared actuator type *SA-15*, a high detent torque actuator which is capable of providing torques up to 12 Nm. The motor can revolve the thruster (or any other component attached to the EPPM) relatively to the spacecraft within a certain angular range (typically 90° up to 120°) around its rotation axis. This rotation angle is also called *deployment angle*.

Additionally, the propulsion units are mounted at the end of fold-out arms, so-called *booms*, so that the thrust vector points directly into the spacecraft's center of gravity. By this measure, it is possible to equip even larger and heavier spacecrafts with electric propulsion and enlarge the possibilities of this propulsion concept.[18] The deployment of these booms, i.e. their angular position relatively to the body of the spacecraft, is also controlled by the EPPM.

One problem a designer of EPPMs has to face is the energy and fuel transport from the satellite to the thruster. The cables and pipes which enable this transport are routed along the rotation axis and must be able to endure the induced deployment movement. As a

[15] cf. Goebel and Katz, 2008, pp. 440–441.
[16] cf. RUAG Space Austria. *RUAG SPACE GmbH*. URL: see Bibliography.
[17] cf. Altorfer, 2014, p. 6.
[18] cf. ibid., p. 6.

consequence, the cables and pipes need to have a certain flexibility in order to move along with the EPPM, as well as sufficient strength to withstand the permanently changing stress and strain conditions. Additionally, the flexural stiffness of the pipework and cable harness is a critical factor regarding the dimensioning of EPPM drive units, as it is responsible for the greater part of the rotational torque acting on the motor (resistive torque).[19]

This diploma thesis investigates different design alternatives for the electric cable harness and aims to find a best suited design by comparing these variants to each other by means of certain requirements (which will be defined in chapter 1.2). Prototypes of these design variants will be produced and assembled at a test bench in the laboratory, where they can be examined for their mechanical and geometric characteristics. Finally, mathematical predictions such as strength and torque calculations and a fatigue analysis shall be performed. This diploma thesis shall be helpful for future engineers facing similar design tasks, as they are able to draw on empirical and analytical results describing the behavior of the electric harness system.

1.1 Problem Statement

Plasma propulsion units are powered and fueled via multiple wires and pipelines which are routed via the corresponding thruster pointing mechanism. The xenon gas, which serves as propellant for the plasma thruster, as well as the electric energy have to be transported from the spacecraft to the thruster itself. Hereby, the xenon gas is led through small pipes made from stainless steel (i.e. the *piping*), while the electric power is transferred via multiple supply cables (the *harness*). The piping as well as the harness have to be routed from the spacecraft to the propulsion unit in such a way that the deployment movement of the EPPM on its several axes is not disturbed.

Figure 1.1 shows a schematic sketch of a pointing mechanism with two separate rotation axes. The thruster supply piping and harness is led from the spacecraft to the thruster around the first rotation axis, along the boom and around the second rotation axis. The *Hold Down & Release Mechanism* (HDRM) secures the pointing mechanism in the launch position during the launch of the spacecraft. Once it is in space, the HDRM releases the thruster pointing mechanism which is then able to rotate and revolve the thruster around its rotation axes. The deployed position of the mechanism is characterized by the respective deployment angle.

The pipework as well as the harness consists of a movable part and a fixed part. The movable part is the one routed around the respective rotation axis and has to compensate every rotational movement of the EPPM. The fixed part on the other hand lies in between the moving parts and is fixed to the boom for instance. It does not experience any dynamic

[19] cf. Janu, 2010, p. 9.

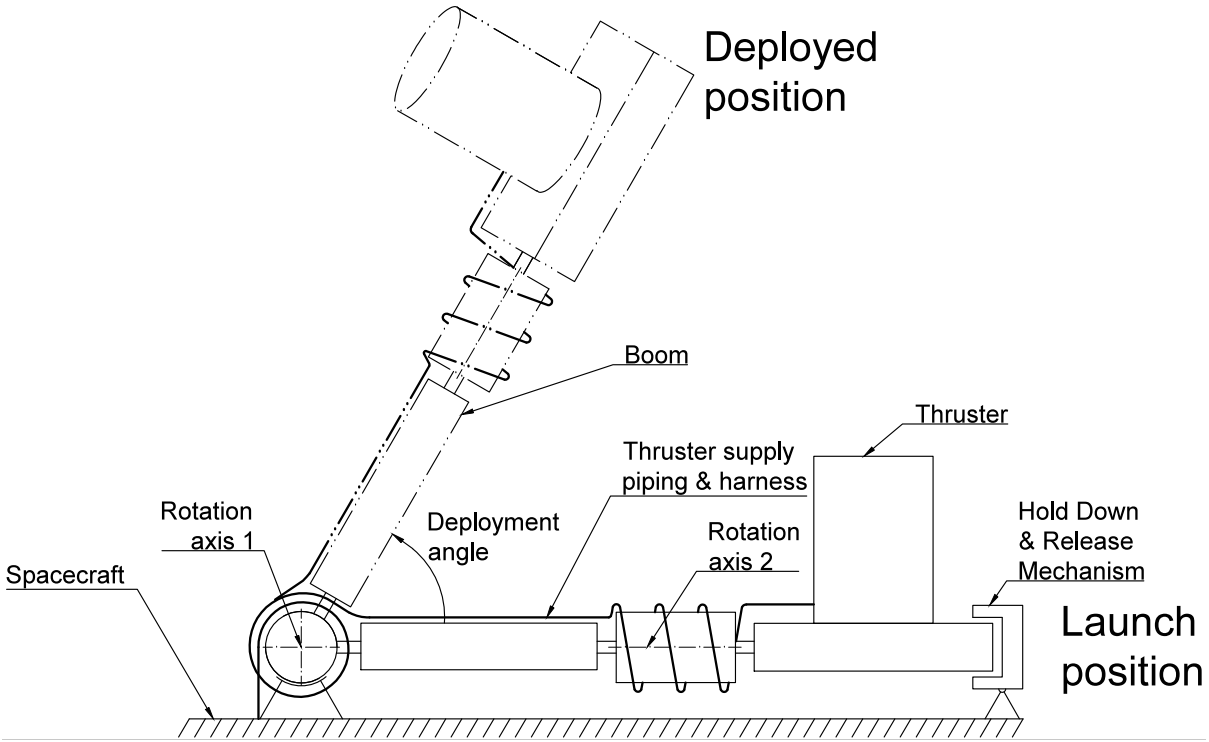

Figure 1.1: Schematic sketch of the Electric Propulsion Pointing Mechanism

flexure or deformation during the lifetime of the pointing mechanism.[20]

The focus of this diploma thesis lies on the investigation of construction alternatives of the movable electric cable harness. The piping as well as the fixed cable harness shall not be addressed as there are already existing solutions for these components. Also, only one rotation axis shall be considered, because the results of these considerations can be used for other axes analogously.

Due to the high number of electric cables and their quite large diameter, the cable harness has an immense flexural stiffness which has to be overcome by the motor in each rotational movement. As will be shown in chapter 2.2, the optimal form is to wind the harness helically around the rotation axis of the EPPM, whereby the torsional movement causes a bending of the cables. The cutting moment in the cables due to the flexure then acts upon the geared actuator and induces a so-called *spring torque*. The spring torque consists of a constant part, which is created by the initial bending of the cable harness into its helical form, and a variable part, which is created by the increase in bending due to deployment and pointing of the EPPM. The variable part depends on the deployment angle of the pointing mechanism and is superposed onto the constant part. In order to rotate the arm of the pointing mechanism, the actuator has to overcome the total spring torque, which must therefore lie below certain boundaries.

Another source of unwanted torque acting upon the motor is the friction between several parts of the movable cable harness, which is winded around the rotation axis (*friction*

[20] cf. Janu, 2010, p. 30.

torque). It poses an additional disturbance for the motor and should be kept as low as possible.

The individual harness cables themselves have to endure the constant stress and strain changes which they undergo due to the mechanism movement. At each rotation, the EPPM increases or decreases the curvature radius of the already prebent electricity cables and therefore induces superposing flexural stresses. It is necessary to ensure that the wires are strong enough to sustain these stress conditions for the entire lifetime of the thruster, because obviously maintenance is no longer possible once the spacecraft has left the Earth. Since the flexural stresses can be divided into a constant part (from prebending the cables) and a variable part with a certain amplitude (from the additional bending by the mechanism), a fatigue analysis of the harness is inevitable.

The possible space requirements of the construction variants of the cable harness are limited due to the dimensions of the rotary actuator centered in the axis of the pointing mechanism and the maximum dimensions, which the device is allowed to have (in axial and radial direction). Lastly, an important design consideration is the radiation, which the EPPM along with the cable harness is exposed to during its journey through space. Every installed component or material, i.e. electricity cables as well as connection elements, needs to have sufficient resistance against the radiation levels which occur in space.

1.2 Objective

In consultation with RUAG SPACE AUSTRIA, the following items have been defined as objective targets for the diploma thesis:

RSA-100: The used cables and all support components shall provide resistance against X-ray radiation up to a dosage of 100 Mrad.

RSA-110: The harness shall be designed applicable to mechanisms with deployment angles up to 120°.

RSA-120: The cables and all used components shall have a fatigue life of over 1000 large cycles (deployment by 120°) and 100 000 small cycles (pointing by $\pm$15°).

RSA-130: The axial installation length of the harness is limited to 150 mm. Additionally, the inner diameter of the harness helix shall be above 82 mm and the outer diameter shall be below 140 mm (see figure 1.2 for definition of geometric constraints).

RSA-140: The maximum resistive torque acting from the harness upon the rotary actuator shall be below 3 Nm. The proportion of the resistive torque which is caused by internal friction shall be small compared to the total torque.

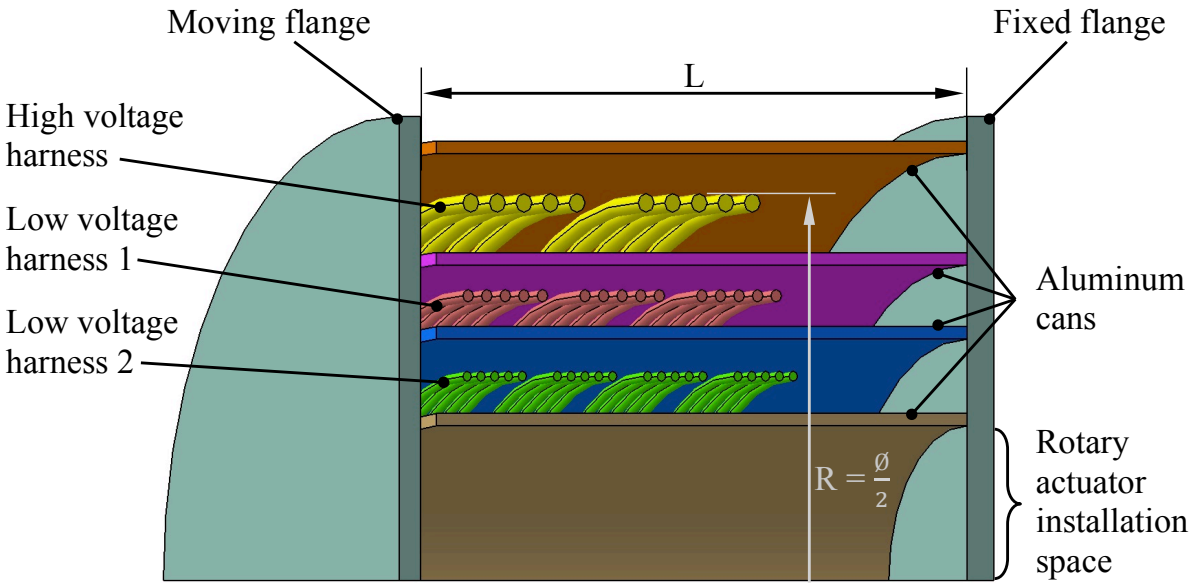

Figure 1.2: Cross-sectional sketch of one EPPM rotation axis

RSA-150: The high voltage harness and the low voltage harness have to be separated by an electromagnetic shielding in order to keep interferences low.

RSA-160: The high voltage harness shall consist of twenty electric cables with a nominal cross section of 1.5 mm^2 each, while the low voltage harness shall consist of twenty-seven cables size AWG 26. The data sheets of the two cable types can be found in appendix B.

These are the goals which have do be reached through the design of the cable harness and supporting components. In the diploma thesis, several different design alternatives will be created and tested in the laboratory. These design alternatives shall be examined in theory on their specific characteristics, features and their ability to fulfill the defined goals. After that, a breadboard testing will be performed where the different variants will be assembled and mounted to a test bench. In the test setup, the theoretical results can be verified by testing a variant in the real application and measuring certain characteristics, such as spring torque or space requirements.

While all of the defined goals have to be achieved, the goals RSA-130 (space requirements) and RSA-140 (maximum torque) are of particular importance concerning the breadboard testing. The effect of different design alternatives on the realizability of these goals will be examined mostly by measurements on the test bench.

The goal RSA-100 (radiation resistance) shall be achieved by a feasible choice of materials, and in order to check if goal RSA-120 (fatigue life) is reached, a mathematical stress analysis will be performed.

Lastly, the shielding between the high voltage and low voltage harness, which is demanded by goal RSA-150, will not only be attained by using shielded cables, but also by

the aluminum can lying in between these harnesses.

Some of the requirements are to be further explained:

ad RSA-100: The *absobed dose of radiation* is measured in the SI-unit `gray` (Gy), which is equal to an absorbed amount of energy of one Joule per kilogram.[21] The unit `rad`, which is mostly used in the United States, equals 10^{-2} Gy.[22] Therefore, 100 Mrad correspond to 1 MGy.

ad RSA-110: Typical deployment angles of pointing mechanisms range from 90° to 120°. For this diploma thesis, a design angle of 120° was used in order to cover the worst case.

ad RSA-130: Because the outer can, which serves as support for the piping, has a diameter of 140 mm, this is the highest possible value for the harness diameter. Additionally, the harness is built around a rotary geared actuator type *SA-15*, a high detent torque actuator developed by RUAG SPACE AUSTRIA. Therefore, the helically shaped harness shall provide enough space for the actuator, which has an outer diameter of 82 mm.

ad RSA-140: The torque acting on the motor can be split up in a spring torque (which is due to the required bending moment to bring the harness into a helical shape) and a friction torque (which is a consequence of friction between the harness and other components). The value of 3 Nm includes both of these components, whereby the spring torque shall be the dominating factor. Defining the margin to be 3 Nm is necessary in order to fulfill the equation for minimum actuator torque as given in chapter 4.7.5.3.1d of the Standard `ECSS-E-ST-33-01C` by the EUROPEAN CO-OPERATION FOR SPACE STANDARDIZATION. The validation of the chosen actuator, which is able to deliver an unpowered holding torque of 12 Nm, will be made in chapter 4.1.2.

ad RSA-160: The electric supply lines split up into a high voltage harness (which covers the thruster power supply) and a low voltage harness (which covers the motor power supply, thruster and motor control, and thruster and motor sensors). In figure 1.2, the basic structural design of one rotation axis is sketched. A detailed description of the used materials and electric cables will be given f.i. in chapter 4.1.1. The two harness types shall be separated from each other by an aluminum pipe with a wall thickness of 0.3 mm, a so-called *can*. This aluminum can provides electromagnetic shielding between the inner and the outer harness.

[21] cf. National Institute of Standards and Technology. *The International System of Units (SI)*, p. 25. URL: see Bibliography.

[22] cf. ibid., pp. 37–38

Chapter 2

Trade-Off Between Different Design Alternatives

One of the main tasks of this diploma thesis was to find a feasible solution for the design of the cable harness according to the given technical requirements. The practical part of this task was carried out at the Mechanical AIV (*"Assembly, Integration, Verification"*) of RUAG SPACE, where I created several different design alternatives and applied them to a test bench. That way, the geometric and mechanical properties of the individual alternatives were examined and certain characteristics such as the occurring resistive torque could be measured.

In the course of the design process, various intermediate versions of the harness were developed. A chronological overview of these versions as well as the particular measurement results will be given in chapter 3.3. In the current chapter, on the other hand, I will go into the description of certain features and parameters of the harness design.

Instead of illustrating the characteristics of the cable harness as a whole, I want to demonstrate different realization options for specific harness components. These options will be investigated in detail and analyzed for their individual advantages and disadvantages. Based on this analysis, I will rate the design variants regarding their effects on the geometric and mechanical characteristics of the cable harness. The goal is to find a rank order of variants and thus identify the best suited alternative.

2.1 Point Rating System

In order to compare the different design alternatives with each other and find a preferred design, the weighted point rating system according to Gerhard Pahl and Wolfgang Beitz will be used. This system should help to rate the individual advantages and disadvantages of the different variants in an objective way, with the effect of determining a rank order of these design alternatives and find the best suited design option.

„Bei der gewichteten Punktbewertung werden die identifizierten Kriterien entsprechend ihrer Bedeutung für den Erfolg des neuen Produktes gewichtet (Lindemann 2007). Das Vorgehen bei einer gewichteten Punktbewertung lässt sich in sechs Schritte gliedern:

1. **Bewertungskriterien festlegen**

   Die Bewertungskriterien werden aus Anforderungen abgeleitet, die in der Anforderungsliste aufgeführt sind, wobei diese auf die aktuelle Entscheidungsaufgabe zugeschnitten sein müssen.

2. **Gewichtung der Bewertungskriterien bestimmen**

   Die Gewichtung der Kriterien zueinander wird üblicherweise mit Zahlen zwischen 0 und 1 festgelegt, wobei die Summe aller Kriteriengewichte 1 ergeben muss.

3. **Eigenschaften der Varianten beschreiben**

   In diesem Schritt werden die qualitativen und quantitativen Eigenschaften der zu bewertenden Varianten in Bezug auf die Kriterien beschrieben.

4. **Eigenschaften mit Punkten bewerten**

   Die zuvor festgelegten Eigenschaften der Lösungsalternativen werden nach einer festgelegten Punkteskala (z. B. 1-4) bewertet.

5. **Punkte mit Gewichtung multiplizieren**

   Durch die Multiplikation der vergebenen Punkte der Varianten mit den Kriteriengewichten werden die gewichteten Punktzahlen berechnet.

6. **Aufsummieren der Resultate aus der Multiplikation von Kriteriengewichten mit den Punktzahlen für jede Variante**

   Durch die Summation der Punkte für jede Lösungsalternative entsteht eine Rangfolge der einzelnen Varianten. Die Lösung mit der höchsten Punktzahl ist die am besten bewertete Alternative für die vorliegende Aufgabe.“[23]

2.2 Cable Harness Routing Along the Rotation Axis

The cable harness establishes an electric connection between the fixed and the moving end of the geared actuator, whereby these two ends can be rotated relatively to each other about a certain, fixed angle. The goals are to keep

- the installation space requirements,

[23] Pahl and Beitz, 2013, pp. 387–388.

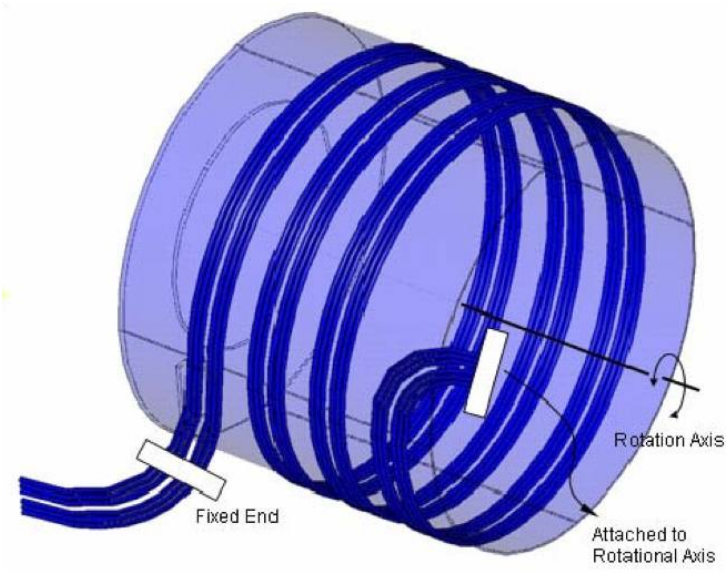

Figure 2.1: Torsion spring layout for the harness routing[24]

- the resistive torque acting upon the mechanism motor and
- the (flexural) stresses induced inside the electricity cables

as low as possible.

Several different design options for the routing of the harness itself have been investigated by RSA, whereby the *torsion spring layout* (see figure 2.1) stands out due to "advantages like the compact design, easy shielding implementation and definite deformation behaviour".[25] In this approach, winding the harness cables around the mechanism axis several times translates the applied torsional moment of the EPPM to a bending moment in the cables. The results are a lower stress level in the cables and better deformation characteristics. A trade-off between the different harness routing options left the torsion spring layout as best suited design alternative concerning i.a. low performance degradation and resistive torque as well as long lifetime of used parts and materials.[26]

2.3 Number of Windings

In order to reduce the mechanical stress conditions in the cables, the harness is winded around the rotational axis of the adjusting mechanism. This way, the cables are not experiencing the same torsional movement which prevails between the two mounting interfaces (flanges) of the mechanism. Instead, the torsional movement is transformed into a flexure of the cables. By bending the cable harness, it is brought into a helical shape which is mounted coaxial to the adjusting mechanism. Through applying an increased bending

[24] Figure taken from: Janu, 2010, p. 91
[25] Ibid., p. 118.
[26] cf. ibid., pp. 124–125.

moment onto the cables, the curvature radius of the helical harness is reduced and the ends of the helix are rotated against each other. This increases the flexural stresses in the cables, however these stresses are not as critical due to the great ratio of the curvature radius to the cable diameter.

The number of windings hereby represents an important parameter due to its great effect on the realization of the goals described above. While the general space requirements in axial and/or radial direction increase with the number of windings (depending on the winding form, see chapter 2.4), the amplitude of flexural stresses and torque acting on the mechanism decreases with increasing overall cable length, which in turn is proportional to the number of windings.

In order to explain this statement, the cables shall be considered as cantilever beams loaded by a bending moment. The length L of the beam as well as the flexural stiffness EJ_y shall be given. A constant bending moment acting on the beam leads to a curvature with constant radius R:

$$\frac{1}{R} = \frac{M}{EJ_y}. \tag{2.1}$$

The flexural stresses in the beam are described by

$$\sigma_b = \frac{M}{W} \tag{2.2}$$

with the section modulus W defined by the cross-sectional properties of the beam.

For inclined routing (see chapter 2.4.1), the radius of the harness helix can be assumed equal at every point on the harness. As the length of the cables is constant, the curvature radius dependent on the number of windings can be estimated with the following relation:

$$L = R_{start} \cdot 2\pi \cdot n_{start} = R_{end} \cdot 2\pi \cdot n_{end} \tag{2.3}$$

$$R_{start} = R_{end} \frac{n_{end}}{n_{start}}. \tag{2.4}$$

In this formula, the index *start* indicates values at the starting position of the pointing mechanism ($\varphi = 0°$), while the index *end* stands for values at the final deployment position ($\varphi = \varphi_{max}$). The minimum curvature radius R_{end} is determined mainly by the geometry of the EPPM, in particular by the diameter of the supporting can. R_{start} is the maximum curvature radius at an angle of $\varphi = 0°$. As our parameter n we will define n_{end}, which is the number of windings around the mechanism at the maximum deployment angle. The number of windings at 0° is n_{start} and can be calculated by

$$n_{start} = n_{end} - \frac{\varphi_{max}}{360°}. \tag{2.5}$$

Finally, the radial difference between the two extremal positions is

$$\Delta R = R_{start} - R_{end} = R_{end} \left(\frac{n}{n - \frac{\varphi_{max}}{360°}} - 1 \right) = R_{end} \left(\frac{\frac{\varphi_{max}}{360°}}{n - \frac{\varphi_{max}}{360°}} \right) \tag{2.6}$$

In this particular case, the maximum deployment angle is $\varphi_{max} = 120°$, which leads to the relation

$$\Delta R = R_{0°} - R_{120°} = R_{120°} \left(\frac{n}{n - \frac{120°}{360°}} - 1 \right) = R_{120°} \left(\frac{\frac{1}{3}}{n - \frac{1}{3}} \right). \tag{2.7}$$

A consequence of this result is that the difference in harness radius between the two extremal positions of the geared actuator is all the lower, the higher the number of windings around the rotation axis. This leads directly to a lower space requirement in radial direction, because the widening of the harness during the reversed rotation is smaller. On the other hand, a larger number of windings results in a higher space requirement in axial direction, if the individual windings are routed next to each other without overlapping.

According to equations (2.1) and (2.2), the maximum value of bending moment and cable stress is determined by the minimum curvature radius, which in turn depends on geometric circumstances only. However, a smaller radial difference causes smaller variations of moment and stress. A lower stress amplitude is benefical for the fatigue life of the harness, while a lower moment amplitude results in a more uniform load characteristic for the rotational actuator of the EPPM.

Taking all these thoughts into account, it is hard to fix an optimal number of windings for this specific task. In chapter 3.3, the impact of different winding numbers on the harness characteristics such as space requirements and resistive torque will be evaluated. These results will be used to specify the number of windings which is best suited to fulfill the targeted objectives.

2.4 Winding Form

After the cable harness is brought into a helical shape, it is mounted around the axis of the adjusting mechanism. There are several possible mounting forms: either the individual windings are positioned next to one another so they do not overlap at all, or the windings are overlapping so they lie partially above each other. An extreme form of the latter would be to position all windings above one another so the individual windings are not at all shifted against each other in axial direction.

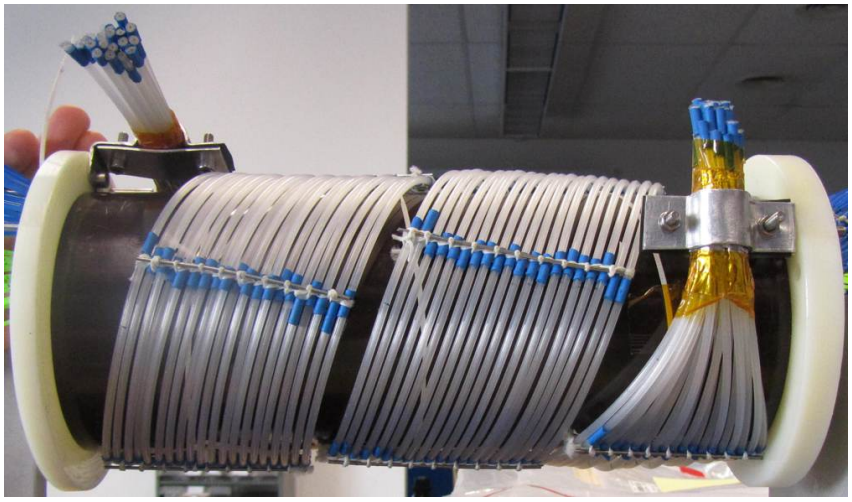

Figure 2.2: Inclined routing form of the cable harness[27]

2.4.1 Inclined Routing

Mounting the harness in a helical form where the windings are positioned next to each other without overlapping gives a spring-like shape with an approximately constant curvature radius of the cables along the axial length of the mechanism (see figure 2.2). This winding form will be used in breadboard testing and is the primary choice for the final design due to its many benefits.

When we look at the harness from a radial direction, the individual cables are tilted against the mechanism axis instead of being at a right angle to it. This inclined position is helpful for routing the cables away from the harness at both ends of the adjusting mechanism. Contrary to the version with overlapping windings, this form gives enough free space to conjoin the individual harness wires and lead them away from the mechanism in any desired direction (f.i. in radial or tangential direction).

While the space requirement in axial direction is relatively high, the diameter of the whole harness is reduced due to the fact that the individual windings do not lie above each other. Another benefit of this version is that the windings can be lashed to the underlying support can using lacing cord. This may be done in order to ensure a constant curvature radius and to decrease friction between the harness and the can. Without lacing cords, some windings would tend to advance towards the aluminum can and make unwanted contact with it, while the opposite side of the harness moves away from the can. In order to keep the harness cables from touching the can, lacing cords are used to tie the windings to the mechanism axis. As a result, the distance between the cables and the support can is limited similar to the concept of a spoked wheel. By this measure, it is possible to ensure a safety gap between the harness and the can.

[27] Figure taken from: Andre, 2014, p. 26

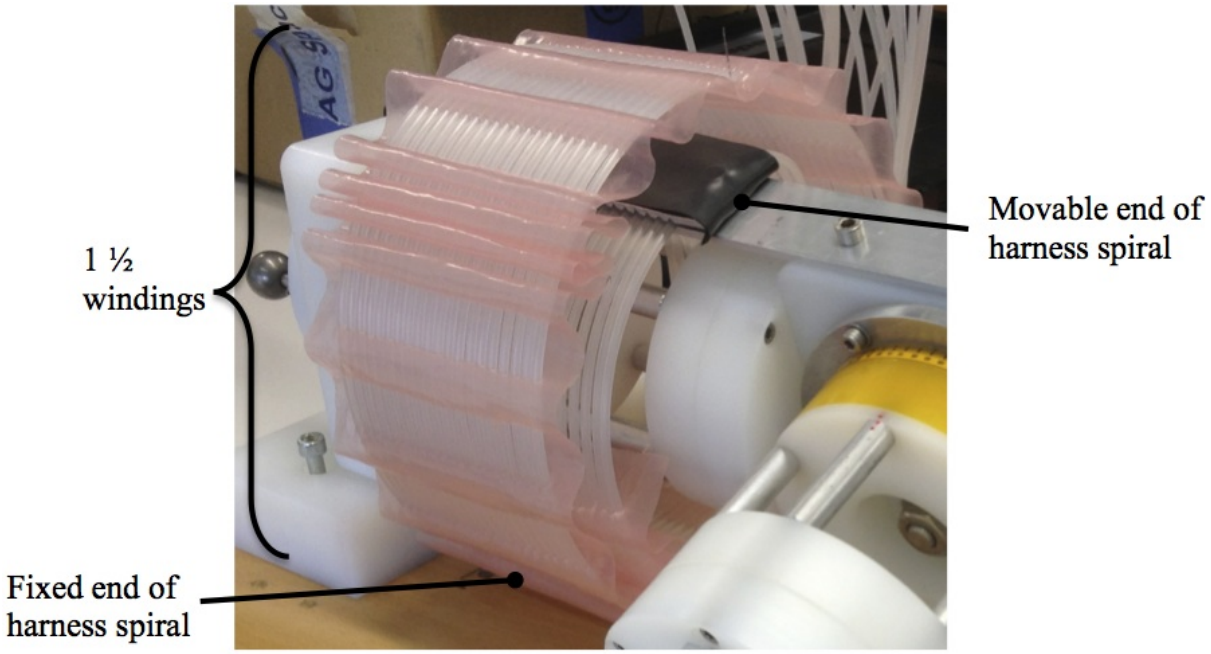

Figure 2.3: Perpendicular routing form of the cable harness

2.4.2 Overlapped or Perpendicular Routing

Positioning the windings partially above each other saves axial space at the cost of expanding in radial direction. The harness can be built shorter because the individual windings overlap each other and are clinched into one another. In order to prevent the windings from colliding and blocking themselves, it is necessary to ensure a safety gap between the individual winding layers. Omitting this would result in unwanted contact between the individual cable windings which are moving relatively to each other. This would lead to sliding friction and therefore increase the friction torque which is acting upon the moving part of the adjusting mechanism. So although the space requirement of the harness in axial direction can be greatly reduced, this brings along an enlargement of the overall diameter due to these safety gaps and due to the windings lying above each other.

The extreme form of the overlapped routing is the perpendicular routing, which is depicted in figure 2.3. Hereby all the windings are positioned completely above one another, so the helix of the cable harness is compressed into a spiral. The windings are routed from the inside to the outside in a spiral form, where the curvature radius of the cables is increasing steadily. The individual harness cables are positioned orthogonally to the mechanism axis, hence the term *perpendicular routing*. This form takes up minimal space in axial direction, but has large space requirements in radial direction.

In this form, the individual harness windings start to deviate to the left or the right of the ideal spiral form. If one tries to bring the cable harness into its spiral shape, it is difficult to keep it in this form without the windings wandering off (see figure 2.4). Generally the following can be stated: the higher the inclination of the cables against the axis (i.e. the

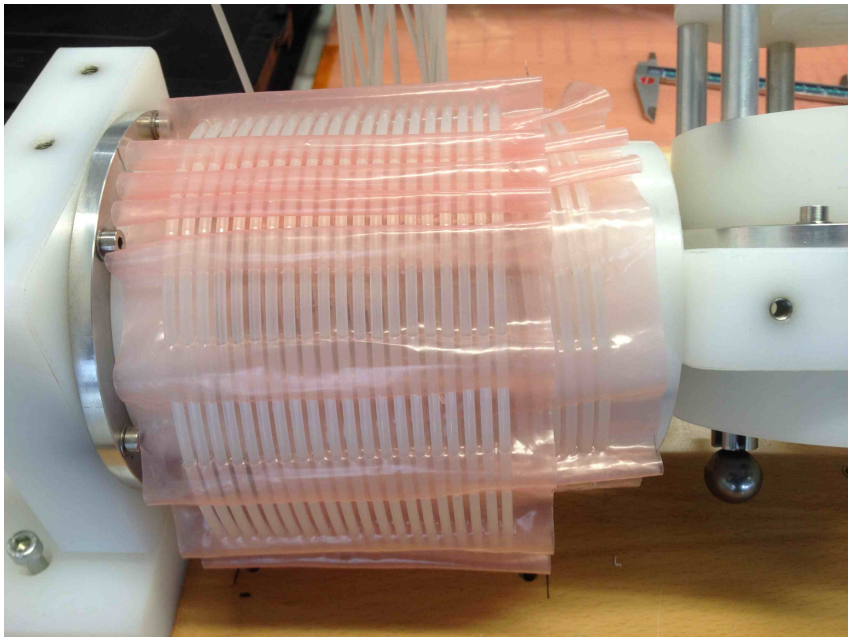

Figure 2.4: Deviation of the harness windings in the perpendicular routing form

slope of the helix), the better the geometric stability. The windings of the inclined routing are less likely to wander off and tend to stay in their position instead.

Also, the mechanical stress conditions at the inner end of the spiral are critical. Due to low values of the curvature radius at the inner end relatively to the outer end, the flexural cutting torque and therefore the flexural stresses in the cables reach a maximum value. Moreover, there is not enough space to route the cables away from the mechanism at the end of the spiral. Routing the cables in radial or tangential direction is not possible because all the other windings lie above this location. Therefore the cables can be led away only along the mechanism axis and have to perform a 90-degree turn in order to allow this kind of routing. This results either in high mechanical stresses due to the sharp turn or in a large installation space, if favorable values for the cable bending radius are chosen.

The contact between the cable layers which are overlapping each other results in sliding friction due to the relative movement between a single winding and the next one. The friction could be minimized by ensuring a safety distance between all the windings, which is a difficult task. The safety gap could again be created by using lacing cords, but the relative movement between the windings has to be taken into account. The harness windings cannot be connected directly to the underlying can, but would have to be laced together.

In the requirements defined in chapter 1.2, the space requirement in radial direction is a more critical design factor than that in axial direction. Due to the large space demand in radial direction, combined with the difficult assembly procedure, the geometric instability and increased friction torque, this method will be rejected. In the test setup we will therefore concentrate on the inclined routing form, especially as the greatest benefit which the overlapped routing would provide, namely the decrease of axial installation space, will be

accomplished by arranging the cables in multiple layers. This approach will be discussed in the following chapter.

2.5 Number of Cable Layers in Radial Direction

The preliminary studies about harness routing at RSA are summarized in the report *Thor Harness Routing Experimental*. According to this document, the moving harness cables should be connected side by side to form a ribbon cable in order to decrease the bending torque in the wires.[28] This method is also suggested by the cable manufacturer W. L. GORE & ASSOCIATES, or GORE for short. By packaging the wires into planar cables or so-called flat cables, tangling of the individual cables can be prevented.[29] The large number of cables of the harness is formed into a helical shape in order to wind it around the rotation axis of the EPPM and thus create an electric connection between the spacecraft and the plasma thruster. Due to the large deformations which are needed to form the helix, the cables undergo high stress and strain values. Without connecting the cables together, they would deviate and keep getting tangled. By forming this flat cable construction, the cables are able to "take individual round constructions"[30] and adapt to the high deformations and the large flexure resulting from their helical shape.

The idea is now to organize the harness in a flat cable of not only one, but multiple layers arranged above each other in radial direction of the harness. The cables have to be connected together using one of the methods described in chapter 2.6. Hereby, we do not only attach each cable to the ones lying right next to it (i.e. construct a single layer), but also the individual layers have to be connected together.

Doing this significantly reduces the space requirements of the harness in axial direction. For example, using two or three cable layers above each other while keeping the number of windings constant decreases the installation space to a half resp. a third. The radial space requirement, on the other hand, increases with each additional layer of cables, which represents a limitation of this method.

Apart from larger installation space, the radial enlargement has another disadvantage: basically the flexural stiffness of the harness and therefore the spring torque acting on the motor depends on the moment of inertia of the cross-sectional area. Increasing the radial extent of the harness by adding cable layers raises the moment of inertia, which results in a higher stiffness and spring torque. However, the effects are not that critical: because the individual layers are not rigidly connected, the cables can move relatively to each other and the cross sections will not stay flat. Not only are the cables able to move in their longitudinal

[28] cf. Andre, 2014, p. 15.

[29] cf. W. L. Gore & Associates. *FAQ - Improving Cable Performance in Harsh Environments*. URL: see Bibliography.

[30] Ibid.

direction, but also the layers themselves can evade normally to the plane the layer lies in. The latter movement causes a slight thickening of the harness in radial direction. Because of these movements, the stiffness of the harness will not increase as much as it would if the cable harness was a homogenous body. In chapter 3, the measurements taken during breadboard testing will show that the spring torque of a harness consisting of two or three layers still stays in the desired boundaries.

By building the harness with multiple cable layers, we can decrease the space requirement to a fraction of the original value, or we can increase the number of windings of the harness around the mechanism. According to chapter 2.3, the latter results in a reduced difference in harness diameter at minimal and maximal deployment angle. This has positive effects on the stress conditions in the cables and fatigue life of the harness.

During laboratory testing, different numbers of cable layers will be tested and the optimal number will be determined according to these results.

2.6 Conjunction of Individual Cables

In this chapter, I will discuss several different methods to connect the individual cables together in order to form the harness. After explaining the principles of these methods, I will describe their individual advantages and disadvantages before comparing them to each other and finding an optimal solution using the method *weighted point rating system* described in chapter 2.1.

2.6.1 Connection Using Lacing Cord and Metal Pins

At first, shrink tubes have to be applied to each cable in order to prevent damage and to ease the fixation of the lacing cords. The lacing cords cannot be tied well to the electric cables which are used for the EPPM due to their slippery insulation surface.[31] The shrink tubes stick to the surface of the cables very well, and as a consequence the lacing cord can be tied to the cable.[32]

The individual cables can be linked together starting at the first cable by tying a single overhand-knot at the shrink tube of the cable. One after the other, the wires can be added to the harness whereby each one is connected with another overhand-knot. Once all cables are connected together, the cable layer can be fixed with a double overhand knot (or reef knot).[33]

[31] cf. Andre, 2014, p. 10.
[32] cf. ibid., p. 14.
[33] cf. ibid., p. 18.

Figure 2.5: Connection of a flat cable layer by lacing cord[34]

Figure 2.6: Connection of a flat cable layer by lacing cord, reinforced by metal pins[35]

The result of this method can be seen in figure 2.5, whereby synthetic dummy cables made from Nylon were used. It is a rather simple connection form where the harness cables are linked together only at this particular location along the harness coil. Therefore, in order to stabilize the harness as a whole, the lacing cords have to be applied multiple times along the length of the harness. These connections should be located about every 10 cm of cable length.

Bending the harness into a helical shape will result in a movement of the middle cables orthogonally to the layer plane. The cables deviate from their flat position and the harness forms a bulge. In order to increase the geometric stability of the ribbon, two small metal pins with a diameter of 1.5 mm can be attached above and below the connection and fixed with lacing cord.[36] The result is depicted in figure 2.6.

The benefits of this version are high stability and strength of the connection, as well as low material cost. Due to the stiff connection between the cables, we get a stable harness which behaves the way it is supposed to. The reinforced connection by metal pins and

[34] Figure taken from: Andre, 2014, p. 19
[35] Figure taken from: ibid., p. 20
[36] cf. ibid., p. 19.

(a) Top view

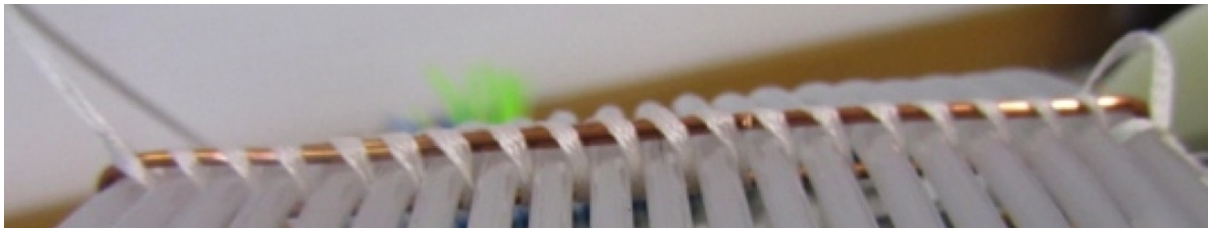

(b) Side view

Figure 2.7: Connection of a flat cable layer by a single bent copper pin[37]

lacing cord is resistant and therefore able to withstand high loads and deformations without loosening. The costs of the used components (f.i. the metal pins) are minimal and there is no need for a custom production. Adapting this connection method to a harness with more than one cable layer is possible by connecting the metal pins of different layers together with lacing cord.

On a contrary, we have vast amounts of time and effort needed during assembly. The process is time consuming, because it involves the application of shrink tubes, knotting together every single cable at every tube location along the length of the harness and finally the application and fastening of the metal pins.

Lastly, the shrink tubes with the attached metal pins pose an irregularity of the harness surface. When layers come into contact with each other or with the underlying can, the roughness results in additional friction which increases the friction torque of the harness.

2.6.2 Connection Using Ovally-Bent Copper Pins

If the two metal pins used in the method described above are replaced by a single bent copper pin, the application of shrink tubes to the electric wires can be omitted. Similar to the first method, the copper pin represents a linear connection between the cables and should therefore be applied about every 10 cm. As we can see in figure 2.7, it is bent ovally-shaped with overlapping ends so that it fully embraces the cable layer, therefore an additional connection between the individual cables themselves is not needed. The form of the copper pin is sufficient to keep all the cables of this layer together.

This version is in its characteristics similar to the variant using only straight metal pins.

[37] Figures taken from: Andre, 2014, p. 27

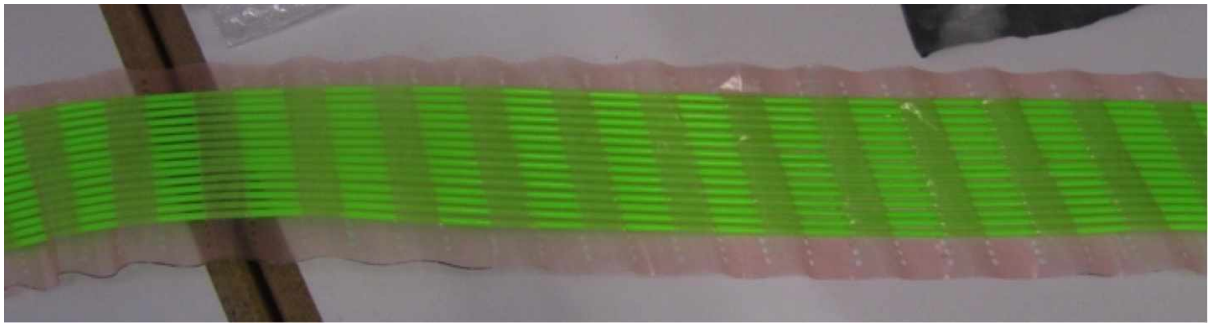

Figure 2.8: Connection of a flat cable layer by a thin synthetic film[38]

We get a stable harness with strong connections between the individual cables, and the components are cheap and easy to get. This method can also be used to create a harness with multiple layers, just like the method using straight pins. A large benefit towards the first method is the greatly reduced assembly time. There is no need to connect the cables together by lacing cord first, the copper pin can be attached to the wires right from the start.

A disadvantage is that the copper pin is not as fixed to the cables as the straight metal pins are. When force is applide to the copper pin, it can be moved along the harness in longitudinal direction of the cables. This is not a big problem, and the usage of shrink tubes at the location of the pin could eliminate this trouble. Still, we have to deal with increased friction and therefore higher friction torque when the pins scratch over the surface of the aluminum cans, for instance.

2.6.3 Connection Using a Perforated Plastic Film

Another possibility of cable connection is a thin elastic film made of plastic, which is about as broad and long as the unrolled cable harness. Along the length of the film there are circular perforations every few centimeters, in which the cables can be inserted in a wave-like shape. This means that the cables are routed through the first set of perforations from top to bottom, and through the next set from the bottom up, repeating this procedure all along the film. The result is a harness which is covered by the film along its whole length, as it can be seen in figure 2.8.

The film needs to be strong enough to keep all of the cables of the harness together without widening of the perforations or tearing of the film itself. If the film shows sufficient strength, this connection method provides a durable harness which can be bent into its helical form easily without losing its geometric stability.

A great advantage of this alternative is a vastly decreased friction between the cable harness and the underlying can. The film is made from a smooth material which allows the harness to slip over the surface of the aluminum can without creating much friction. Also, due to the fact that no additional material (like shrink tubes and metal pins in the

[38] Figure taken from: Andre, 2014, p. 28

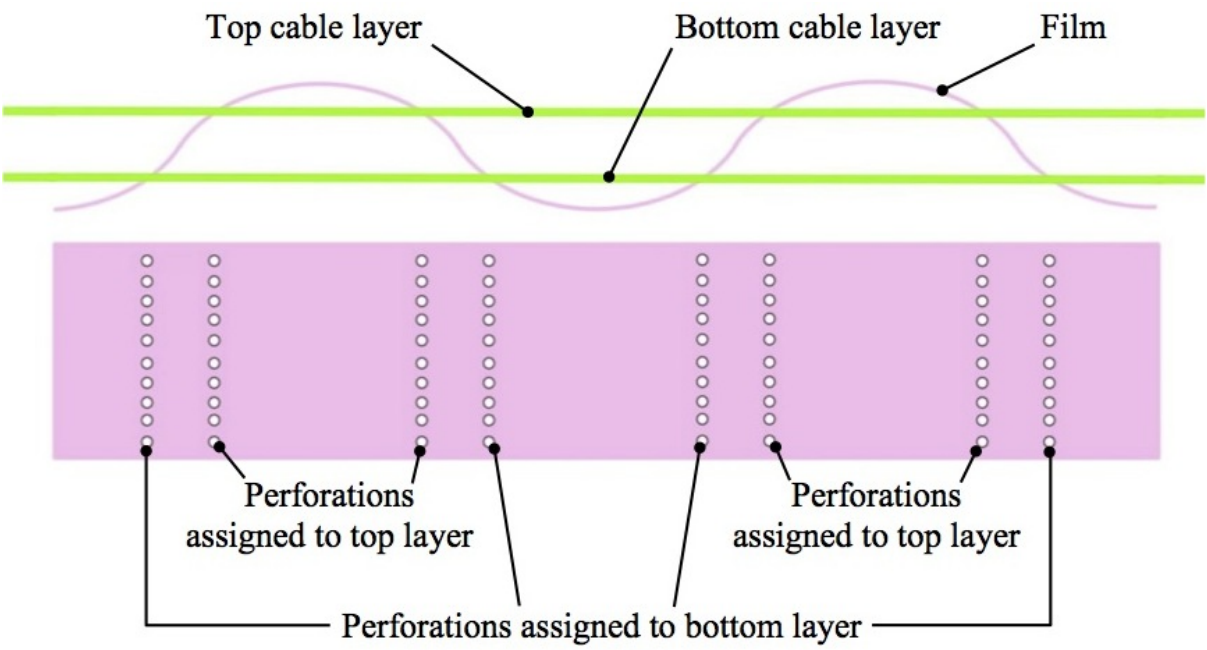

Figure 2.9: Sketch of the adaption of this method to a harness with two cable layers

other methods described above) apart from the film itself is used, the outer surface of the whole harness is flat and even. This reduces the possibility of some parts of the harness getting stuck somewhere, and therefore the overall friction of the moving harness is lower. Lastly, when a harness with more than one cable layer is built, the individual layers are kept together by the film and due to the negligible relative movement between the layers there is also no friction between them.

The method can also be adapted to a harness with multiple cable layers, while still using only one film. Hereby, the cables of each harness layer have to be put through only those perforations which are assigned to that particular layer. For example, for a harness with two cable layers, there are pairs of perforation sets assigned alternately to the top layer and to the bottom layer, respectively. This principle is depicted in figure 2.9.

The time expenditure for the assembly of the harness is much lower than that of the methods described above. The harness cables just have to be put through the perforations of the film in order to create the harness. On the other hand, a drawback of this method is that the film has to be produced solely for this particular use. The production methods require some effort and are investigated below. Also, the right material for the film has to be found, as it needs to be radiation resistant and must not have a Young's modulus higher than that of Kapton, in order that the surface of the electric cables is not scratched or damaged. The different options for the film material are also investigated below.

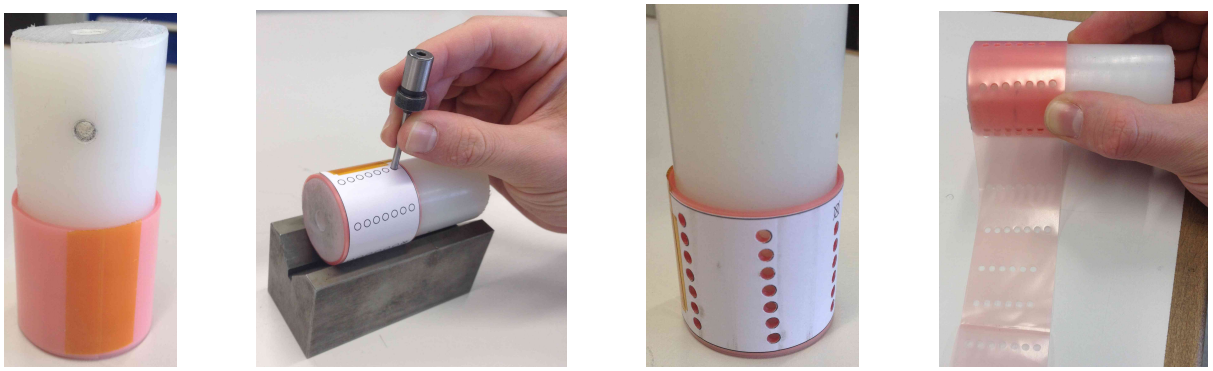

(a) (b) (c) (d)

Figure 2.10: Manufacturing the perforated film by manual stamping

2.6.3.1 Production Alternatives

As it turned out in the laboratory, the easiest method for the production of the perforated film is **manual punching**. A stamping tool of the right size (about the same diameter as the electric cables) is manually hammered into the film at all the locations where perforations are desired. This method requires little effort, but is rather time consuming.

It can be sped up drastically by using a plastic cylinder as stamping matrix. First, the film is coiled around this cylinder and fixed by adhesive tape (figure 2.10a). A punching sample can be printed out and fixed around the coiled film in order to ease the manual positioning of the stamp. Using a V-Block to support the cylinder, the perforations can now be punched with a hammer (figure 2.10b). If the stamp is emptied after every or every other hole, it is capable of perforating all the layers of the coiled film at once (figure 2.10c).

After stamping is done, the film can be uncoiled from the cylinder. As a result of the process we get sets of perforations in periodic distances along the length of the film (figure 2.10d).

Faster and more automated production methods would be **plotting** or **laser cutting**. RUAG SPACE owns a company plotter in Donaustadt, Vienna, but it has to be checked if the plotter is capable of perforating the film with sufficient accuracy. Laser cutting depends on the material of the film, because some materials would start to melt under the heat and therefore cannot be cut with a laser.

2.6.3.2 Choice of Material

There are several different film materials to be considered for this application. In order to be usable for space operations, they have to show certain characteristics. As defined in requirement RSA-100 in chapter 1.2, all used materials have to resist an X-ray radiation of at least 100 Mrad, which is equal to 10^6 Gy. The `gray` (Gy) is the SI-unit for the absorbed

dose of radiation and is equal to an absorbed energy of one Joule per kilogram mass.[39] Insufficient radiation resistance would cause the material to brittle and crack, which leads to disintegration of the cable harness. Furthermore, the Young's modulus of the used film material should not exceed the modulus of Kapton (which is typically about 2.5 GPa[40]), otherwise the insulation of the electric cables could be scratched or damaged. Lastly, the film used in the final application and the one used for the test setup should have about the same flexural stiffness.

The following materials are to be investigated for their usability in this application:

- **Polyamide (PA)** is a thermoplastic containing nitrogen whose units are linked by amide groups.[41] It is better known as *Nylon*, which is a trademark by the American company E. I. DU PONT DE NEMOURS AND COMPANY (short DUPONT).
- **Polyethylene (PE)** is the most important thermoplastic measured by its production volume.[42] The film used in the laboratory was made of low-density polyethylene (LDPE).
- **Polyetheretherketone (PEEK)** is a high-performance plastic in the polyaryletherketone family. It is available in amorphous and semi-crystalline form.[43]
- **Polyimide (PI)** is a polymer with imide groups in the main chain.[44] It is better known as *Kapton*, which is a trademark for a polyimide film by DUPONT. The insulation of the electric cables which are to be used is made of Kapton.
- **Polyoxymethylene (POM)**, also known as polyacetal, is a constructional thermoplastic with a linear structure and a high level of crystallinity.[45]
- **Polyphenylene sulfide (PPS)** is an organic polymer consisting of aromatic rings linked with sulfides.[46]
- **Polytetrafluoroethylene (PTFE)** is a plastic containing fluorine, made of tetrafluoroethylene.[47] It is better known under the trademark *Teflon* by DUPONT.

[39] cf. National Institute of Standards and Technology. *The International System of Units (SI)*, p. 25. URL: see Bibliography.
[40] cf. E. I. du Pont de Nemours and Company. *DuPont™ Kapton® HN polyimide film – Technical Data Sheet*, p. 2. URL: see Bibliography.
[41] cf. Domininghaus, 2008, p. 39.
[42] cf. ibid., p. 164.
[43] cf. ibid., p. 983.
[44] cf. Woebcken, 1998, p. 401.
[45] cf. Domininghaus, 2008, pp. 541–542.
[46] cf. ibid., p. 961.
[47] cf. Woebcken, 1998, p. 416.

- **Polyvinylidene fluoride (PVDF)** is a thermoplastic containing fluorine, made of vinylidene fluoride.[48] It is better known under the trademark *Kynar* by the French company ARKEMA.

An evaluation of the radiation resistance of these materials can be found on the homepage of ENSINGER GMBH, which is a German manufacturer of a large number of different industrial plastics. According to an article on their website, Gamma or X-ray radiation "often leads to a decrease in the elongation characteristics and the development of brittleness"[49] when plastics are exposed to this kind of radiation.

The webpage states the materials **PEEK**, which is produced by ENSINGER under the trademark *TECAPEEK*, and **PI**, which is produced as *TECASINT*, as especially resistant against nuclear radiation.[50] According to the diagram on the webpage, the radiation dose which reduces the elongation of these materials by a value up to 25 % amounts to 20 MGy for PEEK and 40 MGy for PI.[51] This means that these materials exceed the required radiation resistance by one order of magnitude. However, polyimide itself should not be used because the cable insulation is also made from the polyimide Kapton.

Other materials which provide the desired radiation resistance are **PPS** (*TECATRON*, resistant to about 1.5 MGy), **PVDF** (*TECAFLON PVDF*, also 1.5 MGy) and **PE** (*TECAFINE PE*, about 1.4 MGy).[52] According to the data sheet at the webpage, *TECATRON* shows an elastic modulus of 4.1 GPa and is therefore of no use.[53] The modulus of *TECAFLON PVDF* is only about 2.2 GPa, resulting in the material's suitability for this application.[54] Though the mechanical properties of *TECAFINE PE* could not be retrieved from the homepage, the Young's modulus of high-density polyethylene (HD-PE) is only about 0.8 GPa, which poses no risk of cable destruction.[55]

On a contrary, the materials **PTFE** (*TECAFLON PTFE*) and **POM** (*TECAFORM*) are sensitive to gamma radiation and therefore unfeasible for this application.[56] Also the material **PA** (*TECAMID*) can be omitted due to its radiation resistance of only about 0.1 MGy.[57]

As it can be seen in table 2.1, the three feasible materials for this task are polyethylene (PE), polyetheretherketone (PEEK) and polyvinylidene fluoride (PVDF). Hereby, the Young's modulus of PEEK is taken from the Austrian company LIPP-TERLER GMBH (short LITE GMBH), which produces a film under the trademark *LITE K (PEEK)* with a modulus of 2.3 GPa.[58]

[48] cf. Woebcken, 1998, p. 428.
[49] Ensinger GmbH. *Radiation resistance*. URL: see Bibliography.
[50] cf. ibid.
[51] cf. ibid.
[52] cf. ibid.
[53] cf. Ensinger GmbH. *TECATRON natural - Stock Shapes*. URL: see Bibliography.
[54] cf. Ensinger GmbH. *TECAFLON PVDF natural - Stock Shapes*. URL: see Bibliography.
[55] cf. http://www.engineeringtoolbox.com/young-modulus-d_417.html (visited on May 7, 2015).
[56] cf. Ensinger GmbH. *Radiation resistance*. URL: see Bibliography.
[57] cf. ibid.
[58] cf. http://www.lipp-terler.com/index.php?page=03german-lite_k (visited on June 30, 2015).

Short name	Trademark DuPont/Arkema	Trademark Ensinger	Radiation resistance	Young's modulus	Feasibility
PA	Nylon	TECAMID	$<$ 0.1 MGy		no
PE	-	TECAFINE PE	1.4 MGy	0.8 GPa	yes
PEEK	-	TECAPEEK	20 MGy	2.3 GPa	yes
PI	Kapton	TECASINT	40 MGy	2.5 GPa	no
POM	-	TECAFORM	$<$ 0.1 MGy		no
PPS	-	TECATRON	1.5 MGy	4.1 GPa	no
PTFE	Teflon	TECAFLON PTFE	$<$ 0.1 MGy		no
PVDF	Kynar	TECAFLON PVDF	1.5 MGy	2.2 GPa	yes

Table 2.1: Summary of the properties of the synthetic materials for the film

Ultimately, PEEK has been chosen as material for the harness due to its great radiation resistance and relatively low elastic modulus, which is slightly below that of Kapton. Furthermore, sufficiently thin foils are available from LITE GmbH at low cost.

The film used during breadboard testing had a thickness of 150 µm and was made of low-density polyethylene (LD-PE), which shows an elastic modulus of about 0.3 GPa.[59] As the material made by LITE GmbH shows a modulus of 2.3 GPa, the required thickness of this material in order to reach a similar flexural stiffness can be calculated by

$$EJ_y = E\,\frac{bh^3}{12} \tag{2.8}$$

$$\frac{EJ_{y,1}}{EJ_{y,2}} = \frac{E_1 h_1^3}{E_2 h_2^3} \tag{2.9}$$

$$h_{required} = \sqrt[3]{\frac{E_{old}}{E_{new}}}\,h_{old} = \sqrt[3]{\frac{0.3}{2.3}} \cdot 150\,\mu\text{m} \approx 76\,\mu\text{m}. \tag{2.10}$$

A request at LITE GmbH revealed that the company had a film made of the material *LITE K (PEEK amorph)* stocked with a thickness of 100 µm and a roll width of 236 mm. Finally, ten running meters of the material have been ordered for future RSA projects, amounting to a total cost of 200 €.

2.6.4 Comparison of the Conjunction Methods

In the last three chapters, different methods for the conjunction of individual cables to a cable harness have been discussed in detail. As a result of this discussion, the advantages and disadvantages of these methods have been found. In order to sort these construction alternatives by their suitability for this particular task, I will refer to the weighted point rating system presented in chapter 2.1.

[59] cf. for example http://www.makeitfrom.com/material-properties/Low-Density-Polyethylene-LDPE/ (visited on July 1, 2015).

According to this algorithm, the first step is to define certain assessment criteria for the individual construction alternatives. After that, these assessment criteria have to be weighted with a number between 0 and 1, whereby these weights must add up to 1. For the design alternatives regarding the conjunction of the cables, the following criteria have been defined:

Expenditure of time for production and assembly: The time and effort needed in order to produce and prepare the materials which are used by the respective alternative, and additionally the time and effort needed in order to assemble the cable harness. This factor is not as critical, because the EPPM will not be produced in large series. (weight: **10 %**)

Strength of the conjunction: The stability and durability of the used materials and connections. This is an important criterion due to the impossibility of maintenance during spaceflight. (weight: **22 %**)

Possibility of creating a multi-layer harness: A measure of how easily the respective procedure can be adapted to a harness with more than one cable layer. This is desirable because of the greatly reduced installation space for a multi-layer harness. (weight: **24 %**)

Effect on resistive torque (through friction): The increase (or decrease) in the torque of a cable harness built according to the respective design. As less torque leads to lighter and cheaper actuators, this is also a deciding factor. (weight: **24 %**)

Geometric stability of the resulting harness: A measure of the tendency of the cable harness to stay in its desired shape and form even if high loads and deformations are applied. Geometric instability might lead to an increase in friction or even destruction of the harness. (weight: **20 %**)

The third step is to describe the characteristics of the individual alternatives regarding the defined assessment criteria. These are shown in table 2.2. In the fourth step, these characteristics have to be rated, for instance by assigning every property a number from 1 (very bad) to 4 (very good).

In the fifth and sixth step, the assigned points of every characteristic are multiplied with the weight of the respective assessment criterion, before these weighted points are summed up individually for every design alternative. The design with the highest rating is the best suited alternative for this particular task. The results of this algorithm are depicted in table 2.3.

As we can see, the connection method with the perforated synthetic film is the best ranked method both in absolute terms (16 points against 14 points) as well as for the weighted assessment criteria (3.24 points against 2.70 points or less). Hereby, the lead

Criterion	**Method 1** Shrink tubes & metal pins	**Method 2** Bent copper pins	**Method 3** Synthetic film
Production & assembly	Applying shrink tubes, lacing cords & pins	Tying the pins to the cables	Punching of the film, inserting the cables
Conjunction strength	Great cohesion of materials	Pins are movable along the cables	Great cohesion of the harness
Multi-layer harness	By tying single layers together	By tying single layers together	By using a single film for multiple layers
Effect on torque	Great increase of friction	Great increase of friction	Practically none due to smooth surface
Geometric stability	Great due to pins	Great due to pins	Sufficient

Table 2.2: Characteristics of the presented methods for cable conjunction

Criterion	**Method 1** Shrink tubes & metal pins		**Method 2** Bent copper pins		**Method 3** Synthetic film	
	rating	wtd. pts.	rating	wtd. pts.	rating	wtd. pts.
Production & assembly (*weight: 0.10*)	3	0.30	4	0.40	3	0.30
Conjunction strength (*weight: 0.22*)	4	0.88	2	0.44	3	0.66
Multi-layer harness (*weight: 0.24*)	2	0.48	2	0.48	3	0.72
Effect on torque (*weight: 0.24*)	1	0.24	2	0.48	4	0.96
Geometric stability (*weight: 0.20*)	4	0.80	4	0.80	3	0.60
Sum	**14**	**2.70**	**14**	**2.60**	**16**	**3.24**

Table 2.3: Ranking of the cable conjunction methods

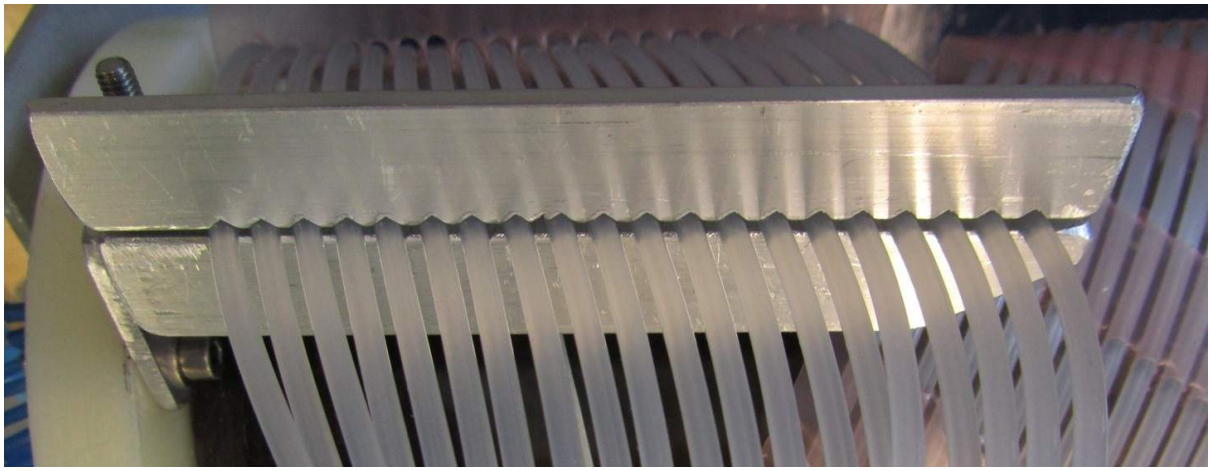

Figure 2.11: Harness fixation using milled metal brackets (initial test setup)[60]

of this method is even higher for the weighted points (lead by 20.0 % instead of 14.3 %), which means that it fulfills the set requirements better than both the other alternatives. As a result, this method will be chosen for the use during the breadboard testing as well as in the real mechanism.

2.7 Fixation of the Cable Harness to the Flanges

In this chapter, the different methods and possibilities of connecting the cable harness to the flanges of the EPPM shall be discussed. The rotation axis of the EPPM has a fixed flange on one end, which stays in place attached to the spacecraft, and a moving flange on the other end, which is rotated together with the electric thruster. Each end of the cable harness spiral must be fixed to one of the flanges. The fixation shall provide a stable connection between the harness and the flange without damaging the cables. The fixation methods described in chapters 2.7.1 to 2.7.3 were used and tested during breadboard testing. One of these methods will be chosen to fix the movable part of the cable harness to the two flanges of the geared actuator. The method described in chapter 2.7.4 on the other hand will be applied to the fixed part of the harness (f.i. to manage the cable routing along the booms), because this well-tried method is simple and sufficient for the low load levels at these locations.

2.7.1 Fixation Using Milled Metal Brackets

The harness fixation as it was used in the initial version of the test setup is depicted in figure 2.11. It consists of two metal brackets with twenty milled wedge-shaped grooves each. After all of the harness cables are put into these grooves, the brackets are pressed

[60] Figure taken from: Andre, 2014, p. 28

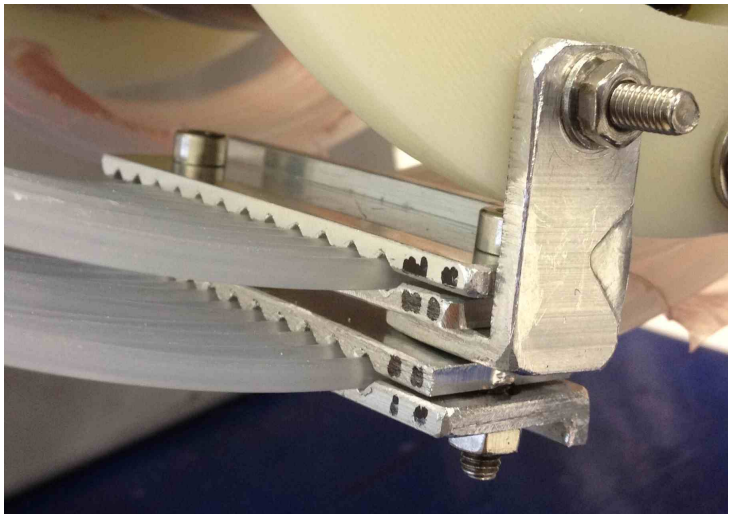

Figure 2.12: Fixation using milled metal brackets for a multiple-layer harness

together and fixed by screws to the left and the right of the harness. The clamping force ensures a fixation of the individual cables in longitudinal and lateral direction. Afterwards, the brackets are attached to one of the flanges of the EPPM by another screw.

This concept can be adapted for a multiple-layer harness by using another pair of brackets for each layer of the harness, see figure 2.12. Again, all of the brackets are fixed together by screws at both ends.

This method has several downsides: first, large effort has to be made during production and assembly of the brackets. Especially for the usage in a multi-layer harness there are accurate manufacturing tolerances, because the grooves and the drill holes have to fit together very well. The assembly of the brackets and cables in the laboratory turned out to be time-consuming not least because of the large stiffness of the cables. Putting the cables into their respective grooves and ensuring that they stay there while applying the counterpart bracket and tightening the bolts is a difficult task. Again, this is even harder when a harness with multiple cable layers is used.

The problems during production and assembly are not decisive factors because of the small number of mechanisms produced overall. What is much more important though is that the metal brackets are bent due to the fixation to the left and the right of the harness. This circumstance leads to large contact forces at the outer cables, while the cables in the middle are rather loose and therefore able to move longitudinally. Another problem is that the brackets are fixed to the flange with only one screw and are therefore movable. As a consequence, the angle of the harness support is inconstant.

Finally, the electric cables could also be damaged due to the high contact pressure which is needed for the cables to stay in place.

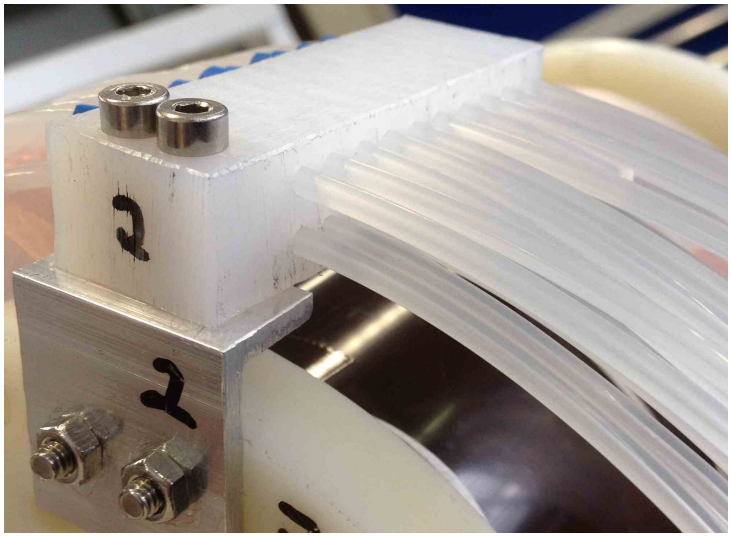

Figure 2.13: Harness fixation using a plastic block with drill holes

2.7.2 Fixation Using a Plastic Block With Drill Holes

The problems described above were addressed by using a plastic rectangular prism with twenty drill holes (see figure 2.13). The cables of the harness are inserted into these drill holes and kept there solely by dry friction between the cable surface and the inner surface of the hole. The block is mounted to the flange of the EPPM by a corner plate with four screws to increase stability.

The assembly of this kind of support is significantly easier because the cables just have to be plugged through the holes. Because of the circular shape of the drills the contact force is not as critical to the cables as in the method described above. Moreover, each and every cable is fixed in the same way and by the same contact force. It is still possible to move a single cable by a certain small amount if it is loaded with a force in longitudinal direction of the cable. However, it has been shown in the laboratory that the harness as a whole is fixed to the block as these longitudinal forces add up for each and every harness cable. This means that during the deployment of the mechanism, the harness is not able to move relatively to the support block and the method therefore provides a safe fixation of the harness helix.

This method has been tested with the dummy cables made from Nylon and works very well for this kind of wires. However, if the friction is not sufficient to keep the real electric cables in place, there is the option to apply shrink tubes to the cables at both entrances to the drill holes. When the shrink tubes are heated and fixed to the cables, their diameter is large enough to keep them from slipping through the hole.

Due to its great advantages, this method will be chosen to fix the movable part of the cable harness to the EPPM flanges. This means that both ends of the harness helix will be attached to their respective flange according to this method.

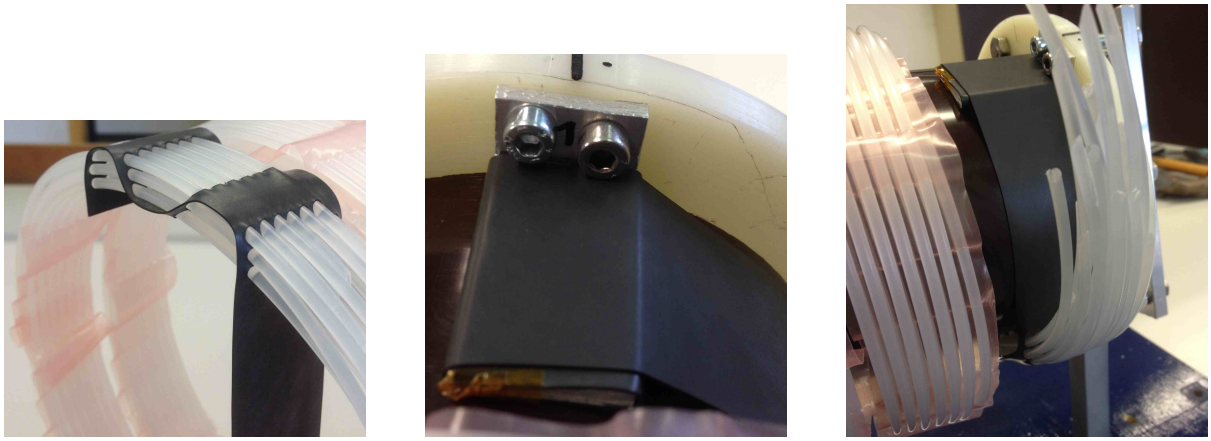

(a) (b) (c)

Figure 2.14: Harness fixation using a synthetic perforated belt

2.7.3 Fixation Using a Synthetic Belt

One disadvantage of the fixation method using the plastic block is the large space requirement of the block. In order to try to resolve that issue, a method in analogy to the connection of the cable harness by film (chapter 2.6.3) was developed. For this method, a synthetic belt made of Viton (which is a trademark by DUPONT) with a thickness of 0.5 mm was used. The belt was perforated several times, before the harness cables were pulled through these perforations (figure 2.14a). After that, the protruding end of the belt can be used to fix the harness to the flange with a small corner plate (figure 2.14b). If the belt is winded around the corner plate one and a half times, it can be held in place simply by adhesive tape due to the belt friction. The result of this method is depicted in figure 2.14c.

The basic idea of this method is that although the cables can be plugged through the perforations of the belt easily, a force which is applied to the protruding end in cable direction is not able to slip the belt off the cables. Similar to self-retention, the friction between the belt and cable surfaces prevents the wires from gliding out of the perforations. This theory has been confirmed in the laboratory. However, the belt was not able to withstand the loads during the rotation of the test mechanism and broke at the location of the smallest cross section (i.e. at the perforations nearest to the corner plate). The procedure was also tested using a thicker belt (about 1.3 mm), but it turned out to drastically complicate the assembly. It was almost impossible to put the cables through the perforations, so this method was rejected in favor of the variant using plastic support blocks.

2.7.4 Fixation Using a Clamp Part Support

According to the RSA Document *Flexlines – TN 2 Preliminary Designs, Analyses and Performance Predictions*, there is another option for the harness support. This method will not be used for the fixation of the harness spiral to the mechanism flanges (which will be

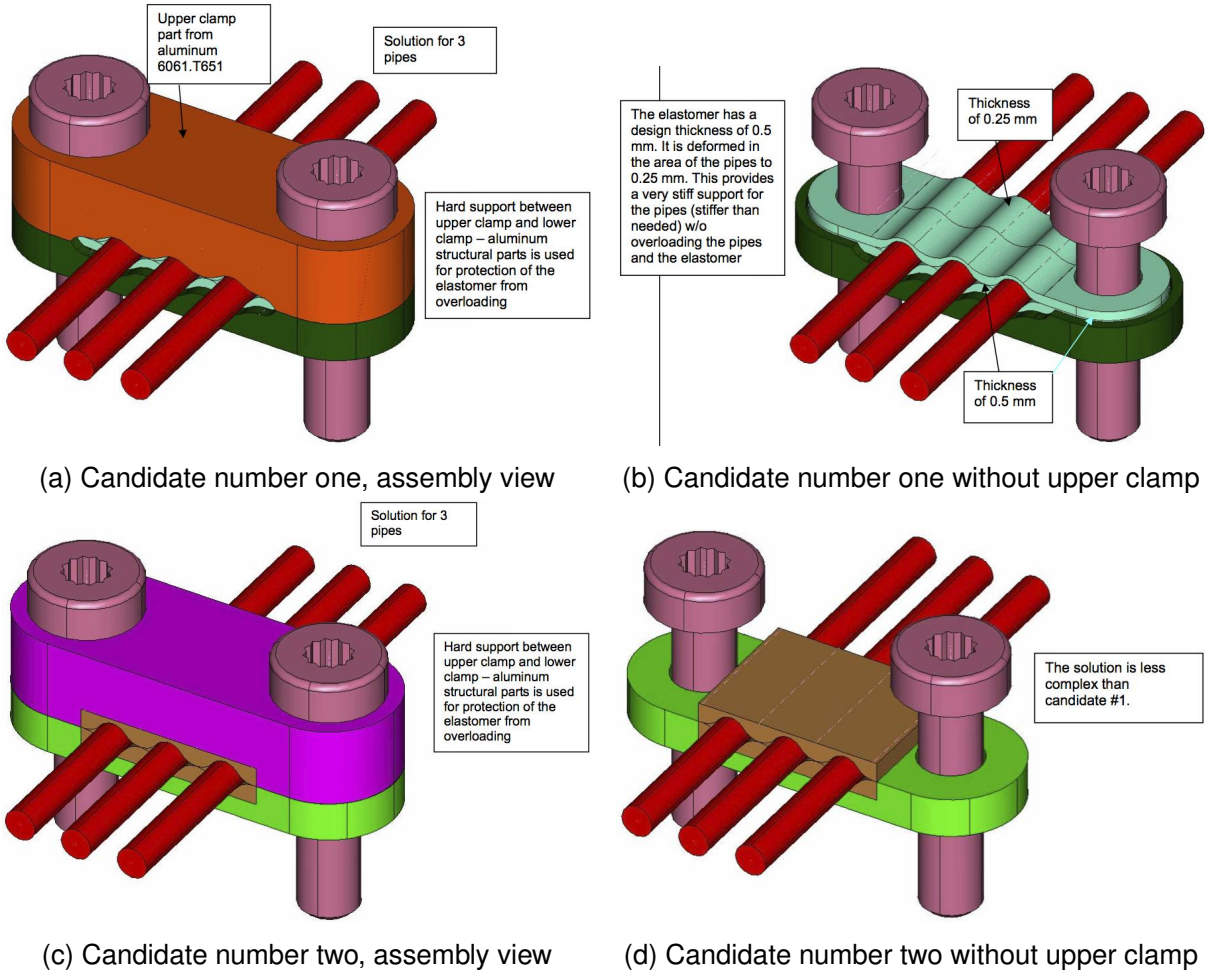

(a) Candidate number one, assembly view

(b) Candidate number one without upper clamp

(c) Candidate number two, assembly view

(d) Candidate number two without upper clamp

Figure 2.15: Clamp part support for the fuel supply pipework[61]

done according to chapter 2.7.2), but for the installation of the fixed part of the cable harness (i.e. cable routing away from the mechanism axis and, for example, along the thruster booms). Based on the support solution for the xenon fuel supply pipework (which is not covered in this diploma thesis), a similar clamping design is feasible for the electric harness itself.

Two different candidates for the clamp part design of the pipework are depicted in figure 2.15. Both candidates consist of a waved elastomer film made of Viton 747.[62] The curly form of the elastomer is adapted to the shape of the pipework and prevents pipe damage while providing sufficient clamping pressure at the same time. Lessons learned from previous missions show that the Viton parts start to distort in the edge areas (where the pipes are entering or exiting the clamps), thus preventing the development of sharp edges. As a consequence, degradation of the cables can be averted when this method is used for the fixed harness routing. Also, the material's Shore A hardness of 75 leads to a Young's

[61] Figures taken from: Janu, 2010, pp. 71–72, 76–77

[62] cf. ibid., p. 76.

modulus of 6 to 10 MPa, which is by far lower than that of the Kapton cable insulation.[63]

Additionally, upper and lower clamp parts made from aluminum 6061.T651 are used as a hard support to prevent overloading of the elastomer.[64] These hard clamp parts are fixed together by two bolts at the ends. The distinction between the two candidates mostly lies in the differently shaped hard clamp parts, which have to feature a corrugated surface adjusted to the elastomer film for the first candidate. The elastomer film in the second candidate is waved only at the inside, while the outside of the film is rectangular. As a consequence, the hard support parts can also feature a straight surface and are therefore easier to manufacture. Candidate number two is to be preferred if the production of candidate number one turns out to be too complicated.[65]

[63] cf. Janu, 2010, p. 70.
[64] cf. ibid., pp. 71–72.
[65] cf. ibid., p. 76.

Chapter 3

Breadboard Testing and Torque Measurements

In this chapter, the different design versions of the electric cable harness shall be described. These versions have been constructed and assemblied in the laboratory in order to investigate their individual geometric and mechanical characteristics. To reach this goal, torque measurements have been performed for the individual test setups in the breadboard testing.

First, two different torque measurement methods shall be explained and compared to each other in terms of precision and usability. After that, a short explanation of the expected measurement results shall be given. Due to the internal friction of the cable harness, a friction hysteresis is expected to occur in the resulting torque-angle characteristic curve. Before describing the results of the laboratory work, an overview of the initial harness design constructed by RSA shall be given. The geometric dimensions and torque characteristics of this initial state will be described in detail, before it is analyzed for possible concepts for improvement. These concepts are to be implemented step-by-step, leading to several different design stages and versions. Lastly, the characteristics, torque measurements and assembly strategies of these versions will be described in detail.

3.1 Torque Measurement Methods

During breadboard testing, three different measurement instruments were used (see figure 3.1). The first instrument is an ordinary spring scale, while the other two instruments are torque wrenches. These two different measurement principles shall be compared by measuring the rotational torque of a harness test setup. The measurement protocol can be found in appendix A. The estimations of mean value and standard deviation of the

(a) Spring scale (HAHN + KOLB) (b) *Torsiometer 760* (STAHLWILLE) (c) Torque wrench (TORQUELEADER)

Figure 3.1: Different measurement instruments used in the laboratory

measurement results are calculated according to

$$\overline{x} = \frac{1}{N} \sum_{i=1}^{N} x_i \tag{3.1}$$

$$s = \sqrt{\frac{1}{N-1} \sum_{i=1}^{N} (x_i - \overline{x})^2} \tag{3.2}$$

and then compared between the two measurement methods. An indicator for the precision of the respective measurement device shall be

$$p = \frac{2s}{\overline{x}} \qquad [\%], \tag{3.3}$$

since according to the so-called *Empirical Rule*, 95 % of observations of variables which are normally-distributed lie in an interval of $\pm 2s$ around the mean value.[66]

3.1.1 Method Using a Spring Scale

One simple way to determine the torque resulting from the torsion of the cable harness is by using a spring scale. The instrument used in this case is made by the company HAHN + KOLB (figure 3.1a) and is classified by RSA as "*Hilfsmittel*", which means that the

[66] cf. http://statweb.stanford.edu/~naras/jsm/NormalDensity/NormalDensity.html (visited on Oct. 19, 2015).

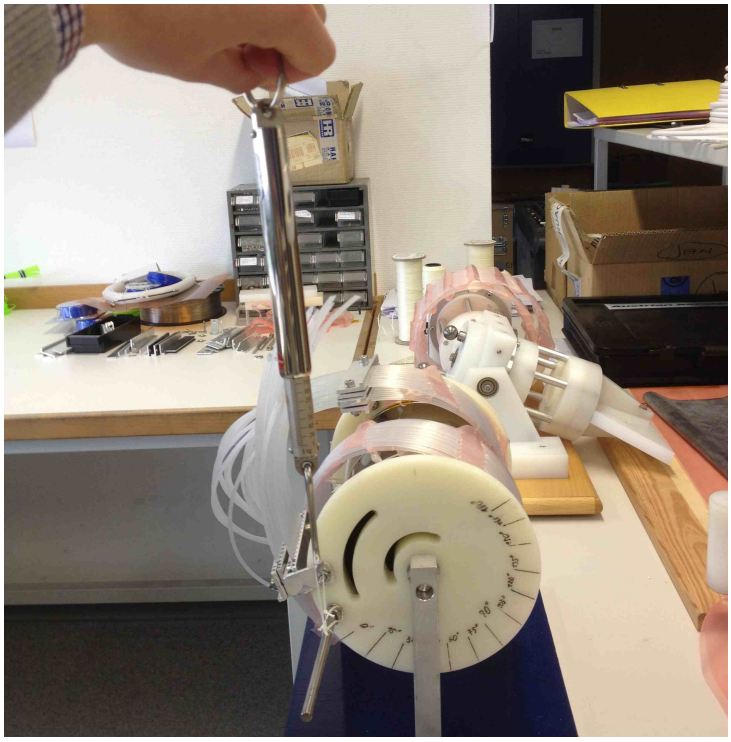

Figure 3.2: Measurement method 1: spring scale

instrument is not calibrated. Still, this method should be accurate enough for this purpose. The measurement method is depicted in figure 3.2.

After the spring scale is attached to the moving end of the harness in a certain distance (lever) to the axis, the moving flange of the test plant can be rotated by a certain angle φ by pulling the spring scale and moving it into the desired position. Hereby it is important to assure that the spring scale always stays in a tangential position to the flange, otherwise the measured force includes also a radial component and cannot be used to calculate the torque of the wire harness.

When the desired angle φ is reached, the current tangential force can be computed from the measure value which is read from the spring scale. Because the spring scale outputs the force in terms of mass, you have to multiply this value with the gravity acceleration ($9.81\,\mathrm{ms}^{-2}$) to get the force. Finally, a multiplication with the lever arm (in this case 62 mm) yields the current torque which is needed to turn the harness by the angle φ.

There are several difficulties and drawbacks to this method which are to be explained:

- When taking the measurements, the spring scale has to be moved through the air free-handedly and without support, but on a specific path which ensures that the scale is always tangential to the moving flange of the test plant. Due to relatively high forces of up to 50 N (the maximum mass which can be measured with the scale is 5 kg), repeated measurements cause an unsteady hand, which leads to imprecise motions and therefore erroneous results. One possibility to tackle this problem could be to use a longer lever arm.

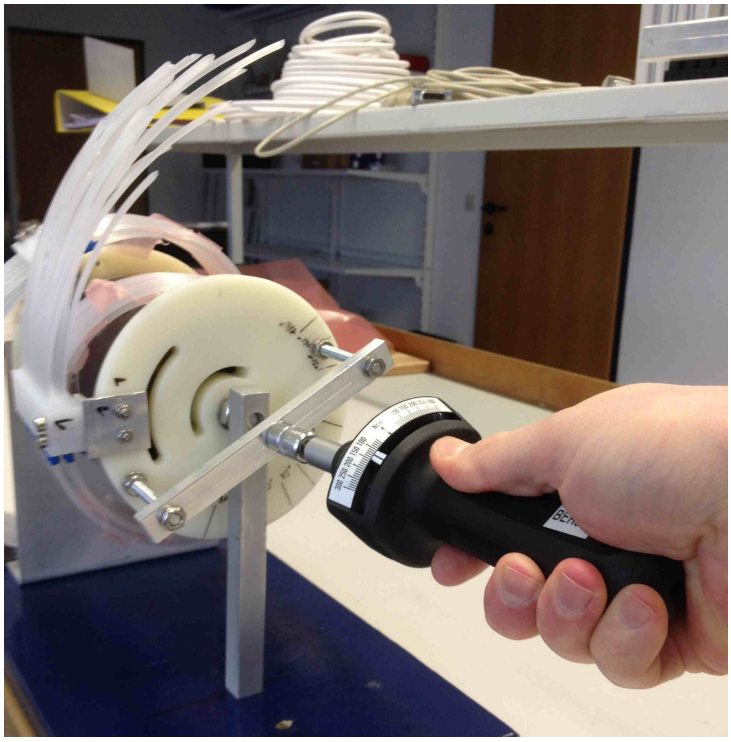

Figure 3.3: Measurement method 2: torque wrench

- As mentioned before, a correct measurement of the tangential force and therefore the resulting torque of the harness is only possible, if the spring scale is in tangential position to the flange and thus orthogonal to the lever arm. In practice it is difficult to ensure this position manually while simultaneously watching the turn angle of the harness and reading the measurements from the spring scale. Slight deviations from the right-angled position lead to varying results, so this problem represents a rather large source of error.

- Another problem is the simultaneous reading of turn angle and force, if the measurements are taken by a single person. The best practice for taking measurements was to watch the turn angle until it reached the desired value, and then look at the spring scale and take the measurement while holding the hand with the scale as still as possible. It turned out that an accurate measurement was almost impossible when done manually without any support.

3.1.2 Method Using a Torque Wrench

To tackle the disadvantages of the method presented before, the measurements can also be taken directly with a torque measuring instrument. This method is depicted in figure 3.3. In the laboratory, the *Torsiometer 760* from the company STAHLWILLE was used, a torque wrench with measuring scale and mounting shank for hexagonal sockets (see figure 3.1b).

The precision of this instrument is given to $\pm 6\,\%$ by the manufacturer.[67]

Attached to the scale of the torque wrench is a drag indicator, a small metal needle which is dragged along the scale while the torque is applied. The drag indicator stays in place after the instrument is loosened, which is a convenient way to freeze the current torque value so that the measurement can be read after the tool is already detached from the test setup.

Another instrument used during breadboard testing is a torque wrench model *ADS 4* by TORQUELEADER (see figure 3.1c), which is based on the same principle as the *Torsiometer*. Both of these torque measuring instruments have been calibrated by RSA.

Before the torque measuring instrument could be used, the test plant had to be adapted in order to provide a point of application for this instrument. At the moving flange of the test bench, a bar holding an M6 bolt in the middle was attached diagonally from end to end of the flange. The bolt located in the middle of the bar provides a point of application for the socket wrench of the *Torsiometer* (see again figure 3.3).

There are many advantages of this method compared to using the spring scale, although not every drawback of the first measurement method could be eliminated.

- Instead of moving the end of the spring scale free-handedly through the air which leads to errors due to an unsteady hand, the measurement procedure with the *Torsiometer* is as ergonomic as the tightening of a screw. This movement can be done easily and without large effort, which leads to a steady hand and therefore more precise results.

- The biggest drawback of the spring scale method was that the orthogonal position of the spring to the lever arm had to be ensured. Obviously, this problem could be eliminated by directly measuring the torque instead of tangential force.

- The problem of having to read turn angle and applied torque simultaneously might be eliminated by the drag indicator. This indicator is attached to the measurement scale and gets dragged along the scale as the applied torque increases. When the instrument is removed from the test object, the drag indicator shows the maximum torque applied during the measurement procedure. However, this is only possible for a single measurement. But, in order to get the torque-angle characteristic curve of the rotation, several measurements in certain steps along the path have to be taken. As the rotation angle is increased, the torque at different values of the angle is measured. This measurement procedure should optimally occur in one go without loosening the torque or returning to the initial position. For this reason, the use of the drag indicator is limited.

[67] cf. http://www.stahlwille-online.de/index.php?amac=03030002000e&sid=-1&lid=1&mid=2&shid=&scmd=pdetail&pcid=4893&cid=4994&pid=4993 (visited on Oct. 16, 2015).

	Turning angle φ	Mean value $\overline{x}$	Std. dev. s	Precision p
Method 1	60°	1600	43.5	5.4 %
	75°	1870	74.8	8.0 %
	90°	2159	62.5	5.8 %
Method 2	60°	1490	51.6	6.9 %
	75°	1745	43.8	5.0 %
	90°	2090	51.6	4.9 %

Table 3.1: Results of the comparison of torque measurement methods (torque values in Nmm)

3.1.3 Comparison of Measurement Methods

In table 3.1, the results of the measurements taken with these two methods are summarized. The complete measurement protocol can be found in appendix A. The precision of the measurement methods is given as a percentage relative to the measured value according to equation (3.3). From these values it can be stated that the two measurement methods show similar precisions, being between 5.4 % and 8.0 % for the spring scale and, slightly lower, between 4.9 % and 6.9 % for the torque meter. The precision of the *Torsiometer* coincides with the value of ± 6 % specified by the manufacturer. For 60° turning angle, the precision of the spring scale is higher than the precision of the torque meter, while it is the other way around at the remaining two measurement points. The mean values at each individual turning angle are smaller for the torque-wrench-method than for the spring-scale-method. This can be explained by the problem of holding the spring scale perfectly tangential to the rotation flange. If there are deviations from this position, the spring scale measures not only the tangential force which can be mapped into the rotational torque, but also a force component radial to the rotation flange. Therefore, the value measured by the spring scale is likely to be higher than the existing rotational torque.

It should be noted that the variance of measurement results is not only due to the uncertainty of the measurement method. A certain portion also comes from slight mechanical differences between each instance of coiling up, which lead to variations in the required rotational torque. This prevents that the value to be measured is exactly the same for each measurement run. With the underlying physical quantity being uncertain, the computed precisions of table 3.1 consist of the uncertainty of the measurement method as well as the uncertainty of the measured value itself.

A comparison of the scales of these two methods reveals that the measurement resolution of the torque meter is only about one third as precise as that of the spring scale. One scale mark of the *Torsiometer* and of the instrument from TORQUELEADER represents **100 Nmm**, while one increment of the spring scale represents 50 g which equals a force of about 490 mN and (with a lever arm of 6.2 cm) a torque of **30.4 Nmm**. Nevertheless, the

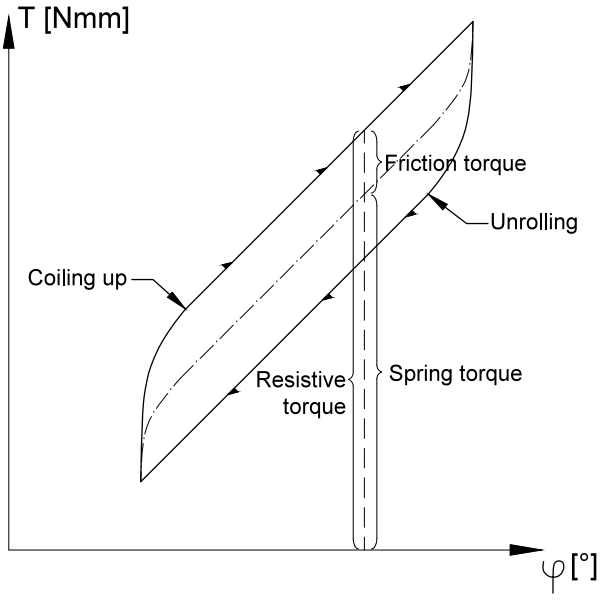

Figure 3.4: Schematic diagram of expected measurement results

resolution of the torque wrenches should be sufficient for this task.

The scale of the spring scale ranges from 0 to 5000 g, which gives a scale range from 0 to about 3000 Nmm. The *Torsiometer* has a scale range from 600 to 3000 Nmm, therefore the lower part of the measurement scale is cut off compared to the spring scale. The instrument from TORQUELEADER has a scale range from 500 to 4000 Nmm. As we will see later, the ability to measure torques of more than 3 Nm is necessary for some harness versions. Also, measurement values below 0.5 Nm do not occur on the test bench. Therefore, the scale range of the torque wrench by TORQUELEADER is sufficient for the laboratory tests.

With the precisions of all three instruments being similar to each other, one of the greatest advantages of the torque wrench is the easy and efficient usability, paired with the reduction of measurement errors. Therefore, during breadboard testing the torque will be measured with one of the torque wrenches (*Torsiometer* for design version 2, instrument from TORQUELEADER for all design versions 3 or later).

3.2 Expected Results

In order to measure the internal friction occurring in the harness design, it is necessary to measure the required rotational torque during coiling up (i.e. increasing the deployment angle) as well as unrolling the harness (i.e. decreasing the deployment angle). The difference between these two measurement values gives information about the amount of internal friction. Taking measurements at certain steps during the process, we get the *torque-angle characteristic curve*, which has the shape of a hysteresis function and is depicted schematically in figure 3.4. From this curve, we can read three different parameters:

- The absolute value which has been measured at a particular angle represents the **resistive torque** of the harness as a whole. In the real application, the motor has to overcome this resistive torque, which is why the torque should stay below a certain threshold. On the other hand, it is desired to have a low level of torque already acting on the flange at the starting position ($\varphi = 0°$) to preload the motor and minimize clearance.

- The mean value between these two measurement series is called **spring torque** $T_{spring} = (T_u + T_d)/2$. When the harness is rotated and the cables are bent, a cutting moment occurs in each one of the cables due to increased flexure. These cutting moments add up and act on the moving flange of the test bench as spring torque. It therefore represents the average torque acting on the motor during operation of the pointing mechanism. The spring torque is important for the strength calculation of the harness cables, because it is responsible for the bending stresses in the cables.

- The **friction torque** $T_{friction} = (T_u - T_d)/2$ is calculated as half of the difference between the two measurement series and becomes visible in the hysteresis loop of the characteristic curve. It represents the static friction acting between the individual cables as well as between the cable harness and the underlying aluminum can. The friction torque is important because it raises the overall resistive torque. The spring torque is more or less given because it depends on parameters of the harness design, such as number and stiffness of cables, number of windings and so on. Large levels of friction torque are able to raise this given spring torque and therefore increase the overall resistive torque acting on the motor.

3.3 Cable Harness Design Versions

3.3.1 Initial State

This chapter serves to describe the initial harness design which was created by RUAG SPACE AUSTRIA. This initial state is the current development status of the electric harness design and serves as point of departure for this diploma thesis.

3.3.1.1 Design of the Test Setup

The initial design is described in chapter 12.5 of the technical report *Thor Harness Routing Experimental*. It consists of an outer harness and two inner harnesses with twenty cables each, which gives a total of sixty cables. For the outer harness, dummy cables made from Nylon with a diameter of 3.1 mm were used, while the wires of the two inner harnesses had a diameter of 2.0 mm and 1.6 mm, respectively. The ribbon cable of the outer harness was

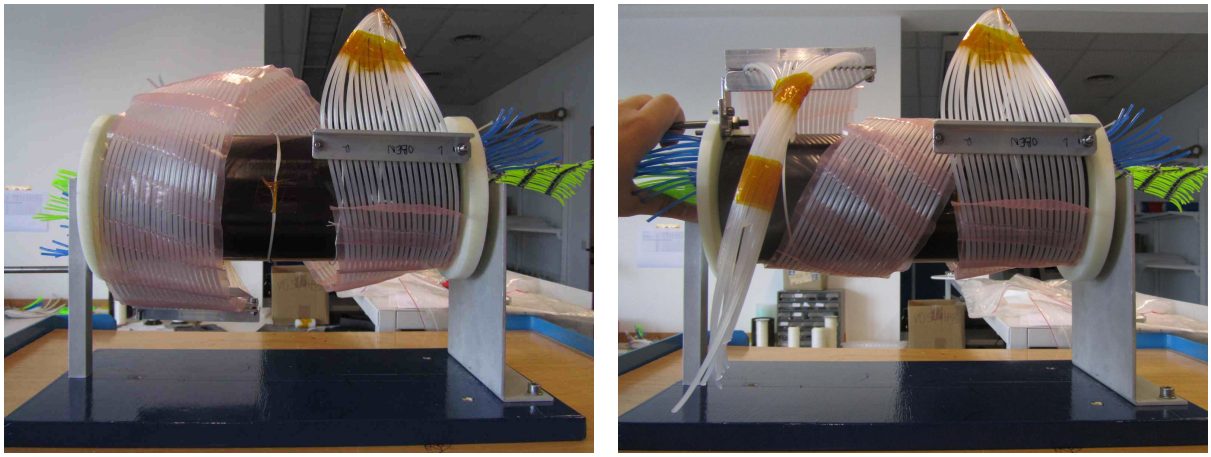

(a) Starting position ($\varphi = 0°$) (b) End position ($\varphi = 120°$)

Figure 3.5: Initial state of the cable harness design[68]

established with a perforated film made of low-density polyethylene (LD-PE). In contrast, both inner harnesses were created using shrink tubes and metal pins.

The test setup of the initial state is depicted in figure 3.5. Two plastic pipes are used to separate the three individual harnesses from each other. A flange is mounted to each end of the pipes, whereby one of them (in this case the right one) is fixed while the other one (left) stays movable. The outer cable harness is winded around the pipe of the test bench one and a half times and is fixed to the flanges with a pair of aluminum brackets. The individual harness cables are laid into the twenty milled grooves of these brackets, and are then fastened by the applied clamping pressure. The inner harnesses are routed around the rotation axis in two resp. three and a half windings. The ends of the inner harnesses are guided through elongated holes in the flanges, which is sufficient for the fixation.

3.3.1.2 Geometric Dimensions and Torque Measurements

The total axial **length** of the harness in this version is **271 mm** and the maximum **diameter** is **181 mm**, which is both far above the specified requirements of about 150 mm for length and 140 mm for diameter. The goal is to minimize these dimensions as far as possible while still keeping the value of the resistive torque, which occurs when the harness is turned, in a reasonable area.

The torque occuring at a rotation by 180 degrees has been measured at a test setup similar to this one and amounts to 3.26 Nm.[69]

[68] Figures taken from: Andre, 2014, pp. 28–29

[69] cf. ibid., p. 27.

3.3.1.3 Concepts for Improvement

The concept of using a perforated film to create a ribbon cable has many advantages (see chapter 2.6.3) and is to be conserved in future design versions.

In order to address the problem of large space requirements in axial direction, the harness could be built with multiple layers of cables arranged above each other. It is easily possible to do this using the perforated film (see again chapter 2.6.3).

Provided that the number of windings around the pipe stays the same, using two layers would reduce the space needed in axial direction by a half, and using three layers would reduce the space to a third of the original value. A drawback of this method is the increasing radial space requirement and, due to a higher thickness of the harness, a higher resistive torque.

3.3.2 Version 1

For the harness routing versions described in the following, only design alternatives for the outer cable harness have been investigated. As due to smaller cable dimensions the inner harness contributes only very little to the overall flexural stiffness (see chapter 4.1.1), it is omitted in the following test setups. The conclusions drawn from testing of the outer cable harness will be transferred to the inner harness in the final design version.

3.3.2.1 Design of the Test Setup

To address the large space requirements of the harness in axial direction which occured in the initial design, the twenty cables were split up in two layers of ten cables each. Arranging these two layers above each other, the axial space requirement could almost be halved while the number of windings around the rotation axis was held constant. At the maximum deployment angle, the harness is winded around the rotation axis two full times, which yields a number of windings of 1.67 in the starting position.

The connection between the individual harness cables was realized using a film similar to the one in the initial design. The principle of this method adapted to a double layer harness is depicted in figure 2.9 on page 22. Hereby, the perforated film is brought into a waveform, before the wires of the top layer are put through the top perforations and the wires of the bottom layer are put through the bottom perforations. The result is a harness with two cable layers above each other, which has the advantage of being half as broad as the original harness (see figure 3.6).

Due to the extension of the harness in radial direction, it is assumed that a higher torque is needed to turn the cable harness as a whole. This is due to the higher flexural stiffness of the harness, which results in a higher cutting torque when the harness is bent to a certain curvature radius. On the other hand, there is no stiff connection between the individual

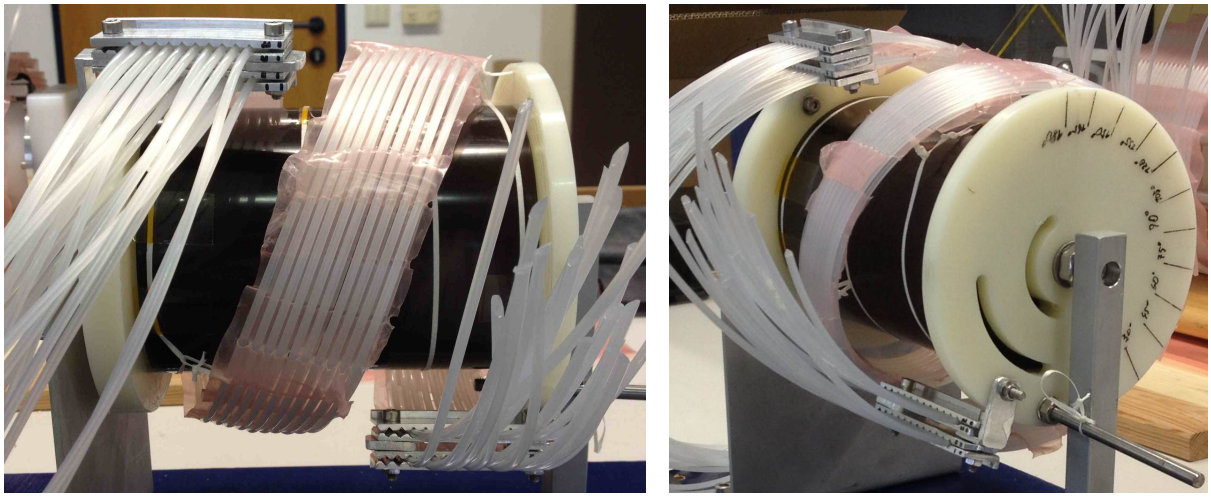

(a) (b)

Figure 3.6: Design version 1 of the cable harness routing

cable layers in longitudinal direction of the wires. The cables of different layers are able to move relatively to each other both in longitudinal direction as well as orthogonally to the layer plane. Because of this relative movement, it is reasonable to reject the assumption that the whole cable harness can be regarded as a single flexural beam. Therefore, the area moment of inertia and thus the occurring resistive torque is expected to be kept within certain limits.

The harness fixation by aluminum brackets was kept for this version, but had to be slightly adapted due to the division of the harness cables into two layers. A new set of brackets consisting of eight jaws had to be manufactured. Each cable layer is fixed between two matching jaws, before the two layers are conjoined by tightening both pairs of jaws together using bolts. This has to be done at both locations where the cable harness is fixed to the flanges, which results in a total number of eight jaws.

In this design version, a possible way of the application of lacing cords was investigated. It may be necessary to fix the harness to the underlying can by applying several lacing cords along its length in order to keep the curvature radius of the wires approximately constant along the cable length. This also has the benefit of keeping the opposite side of the harness away from the underlying can, thus reducing contact and therefore friction between the parts. Lastly, a sideward movement of the individual harness windings can be prevented by connecting the harness to one of the flanges. In this version, the harness has been tied to the can (visible f.i. in figure 3.6a on the bottom left and in figure 3.6b) as well as to the movable flange (visible in figure 3.6a on the top right). It has to be ensured that the connection between the harness and other parts stays movable in longitudinal direction of the cables, because otherwise the lacing cords would impede the relative movement between these components.

Turning angle φ	Measured torque		Spring torque	Friction torque
	Coiling up	Unrolling		
0°	608	426	517	91
15°	912	578	745	167
30°	1125	821	973	152
45°	1277	973	1125	152
60°	1429	1156	1292	137
75°	1673	1247	1460	213
90°	1885	1368	1627	258
105°	2190	1460	1825	365
120°	2585	1946	2266	319

Table 3.2: Measurement results for the cable harness design version 1 (torque values in Nmm)

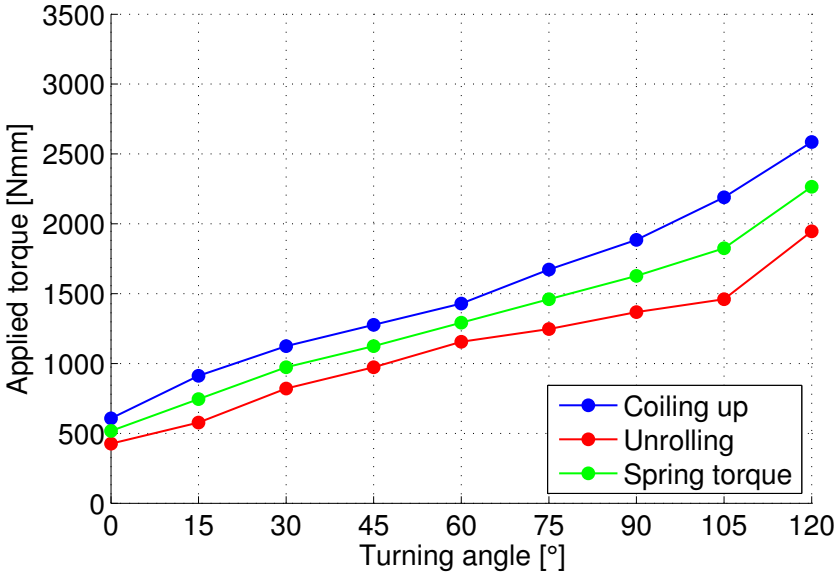

Figure 3.7: Graphic representation of the results in table 3.2 – Measurement results for the cable harness design version 1

3.3.2.2 Geometric Dimensions and Torque Measurements

The length of the harness could almost be halved with respect to the initial design and amounts to 142 mm. The maximum outer diameter of the cable harness is 181 mm, which is equal to the initial state. The goal for the maximum allowed outer diameter (140 mm) which is specified in objective RSA-130 is not met in this design version.

The torque measurements of the first design version have been taken with a spring scale by HAHN + KOLB, see chapter 3.1.1. The lever arm (distance between rotation axis and point of application) is 62 mm. During measurements, the test setup was rotated to a certain deployment angle by pulling the spring scale tangentially to the movable flange. The value displayed by the spring scale (the measured weight) had to be multiplied with

the gravity and the lever arm in order to compute the rotational torque acting against the movement of the harness (resistive torque).

At first, the measurements were taken while increasing the deployment angle stepwise from 0° to 120° (measurements titled “Coiling up”). Afterwards, the deployment angle was decreased down to 0° (“Unrolling”). The difference between these two measurement runs represents the hysteresis loop and is a measure for the internal friction of the cable harness. The *spring torque* is the arithmetic mean between the values of coiling up and unrolling, while the *friction torque* is half the difference between these values (see chapter 3.2 for details).

The measurement results are depicted in table 3.2 and graphically in figure 3.7. The complete measurement protocol can be found in appendix A. As it can be observed from the data, the spring torque increases monotonically with the deployment angle. The highest measured value for the total resistive torque occurs at the maximum deployment angle and amounts to about 2.6 Nm, which is below the limit specified in objective RSA-140. Between the two measurement series (“Coiling up” and “Unrolling”), a pronounced hysteresis loop can be observed. Though the friction torque, which is a measure for this hysteresis, is not increasing monotonically with the deployment angle, there is a positive correlation between these two parameters. The highest value of friction torque occurs at a deployment angle of 105° and amounts to about 0.37 Nm, which is 14 % of the maximum resistive torque.

3.3.2.3 Concepts for Improvement

The method of fixing the harness to the flanges with metal brackets has several downsides, which are described in detail in chapter 2.7.1. In the next harness design version, a different fixation concept (using a plastic block) shall be investigated.

Another disadvantage of this design version is the measurement method by spring scale, which gives probably erroneous results. For this reason, the following version shall be designed in a way that it allows taking measurements directly with a torque measuring instrument.

3.3.3 Version 2

3.3.3.1 Design of the Test Setup

In this version, which is depicted in figure 3.8, an improved concept for the harness fixation to the flanges of the test bench has been implemented. Instead of fixing the cable layers with metal brackets, a plastic block with several drill holes was used (see chapter 2.7.2). The advantages of this method are a significantly easier assembly compared to the metal brackets, equal distribution of the contact pressure to each individual cable, and less critical cable pressure which reduces the risk of damage to the cables.

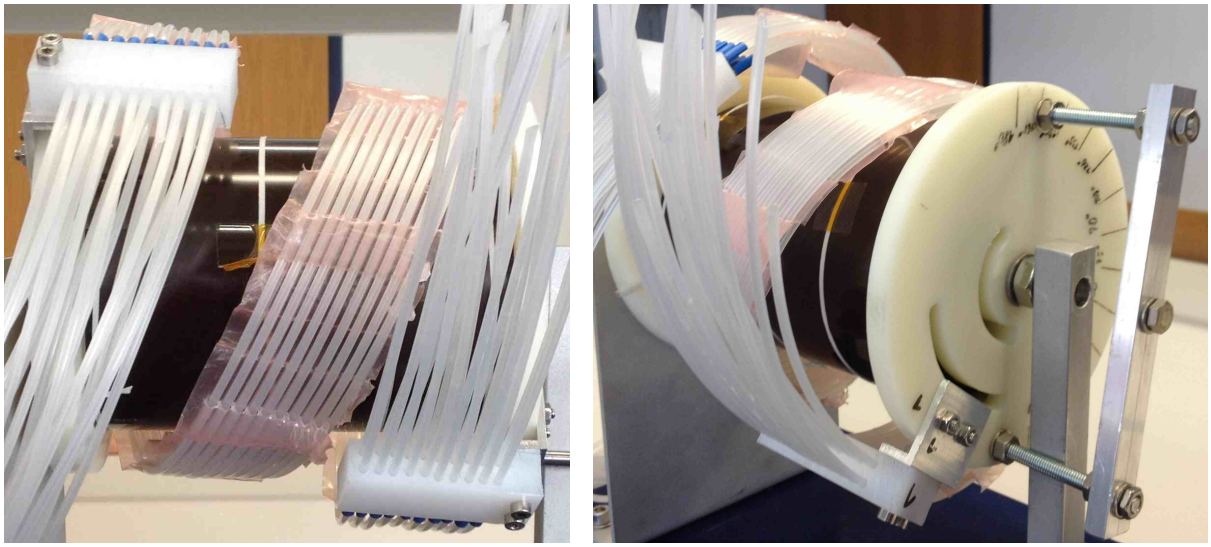

(a) (b)

Figure 3.8: Design version 2 of the cable harness routing

Furthermore, a bar featuring a hexagonal bolt was mounted to the moving flange of the test setup (see figure 3.8b). This bolt can be used as point of application for the torque measuring instrument described in chapter 3.1.2.

Since this version is designed with focus on the investigation of geometric characteristics and the usability of the fixation method by a plastic block, the application of lacing cords was omitted. The routing of the lacing cords will be developed further in the final design version.

3.3.3.2 Geometric Dimensions and Torque Measurements

Other than the features described above, the design of this harness version is the same as version 1. The number of harness windings at the maximum deployment angle (two full windings) as well as the length of the cable harness (142 mm) is equal to version 1. Only the outer diameter of the harness increased slightly to 183 mm because of the different fixation method. Again, objective RSA-130 is not met because the outer diameter is above 140 mm.

The resistive torque of the cable harness was directly measured with the *Torsiometer 760* by the company STAHLWILLE, which is described in chapter 3.1.2. The scale of the *Torsiometer* ranges from 600 Nmm to 3000 Nmm, which is why some of the measurement values (those at the extreme deployment angles) could not be taken correctly. Again, the deployment angle was at first increased stepwise from 0° to 120° (“Coiling up”) before it was decreased to 0° in the same steps (“Unrolling”). Three measurement runs according to this scheme were performed and average values of these runs were computed. The averaged results are depicted in table 3.3 and figure 3.9. The complete measurement protocol can

Turning angle φ	Measured torque		Spring torque	Friction torque
	Coiling up	Unrolling		
0°	850	600[a]	725[b]	125[b]
15°	1083	667	875	208
30°	1200	733	967	233
45°	1350	850	1100	250
60°	1583	1000	1292	292
75°	1783	1167	1475	308
90°	2133	1350	1742	392
105°	2617	1517	2067	550
120°	3500[a]	2433	2967[b]	533[b]

Table 3.3: Averaged measurement results for the cable harness design version 2 (torque values in Nmm)

[a] Estimated value
[b] Quantity derived from an estimated value

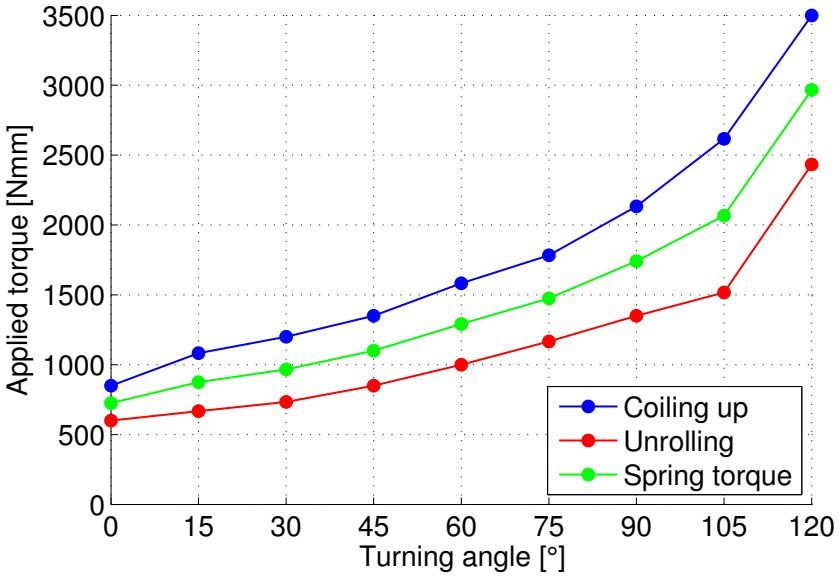

Figure 3.9: Graphic representation of the results in table 3.3 – Averaged measurement results for the cable harness design version 2

be found in appendix A.

Due to a limitation of the measurement scale, the highest measured value (about 3500 Nmm during coiling up) as well as the lowest one (about 600 Nmm during unrolling) could not be measured correctly. The values which are depicted in the table have therefore been estimated intuitively. For the same reason, the values for spring and friction torque at 0° and 120° are an estimation because those quantities were derived from estimated values.

Similar to the first harness design version, the spring torque increases monotonically with the deployment angle. The highest measured value for the total resistive torque occurs again at the maximum deployment angle and lies above 3 Nm, though it could not be measured accurately due to the limitation of the scale range of the instrument. Therefore, objective RSA-140 (resistive torque shall be less than 3 Nm) is not met in this design version.

Again, a hysteresis loop can be observed between the two measurement series. The friction torque increases almost monotonically with the deployment angle, whereby the value at 120° is derived from estimated values and is therefore probably not correct. The highest accurately measured value of friction torque occurs at a deployment angle of 105° and amounts to about 0.55 Nm, which is 16 % of the maximum resistive torque.

3.3.3.3 Concepts for Improvement

The plastic support block is mounted with a relatively large radial distance to the rotation axis, which is visible in figure 3.8. Because of this distance, the middle part of the harness is moving below the support block and there is no contact between these parts during the rotation of the cable harness. This leads to the following improvement opportunities:

The axial length of the whole harness helix can be reduced by telescoping the windings into each other as described in chapter 2.4.2. This overlapped routing form of the harness is possible, because the individual overlapping windings are positioned at different radial distances and therefore produce no friction by touching each other. The onset of reduced axial length will be investigated in version 3 of the harness design, which is described in chapter 3.3.4.

On the other hand, the support block could be mounted closer to the rotation axis in radial direction. As it turned out in the investigation of design version 2, the maximum outer diameter of the harness helix was mainly given by the position of the support block. Because of this, the overall space requirement of the harness in radial direction can be reduced by the described measure. This onset will be investigated in design version 4, which is described in chapter 3.3.5.

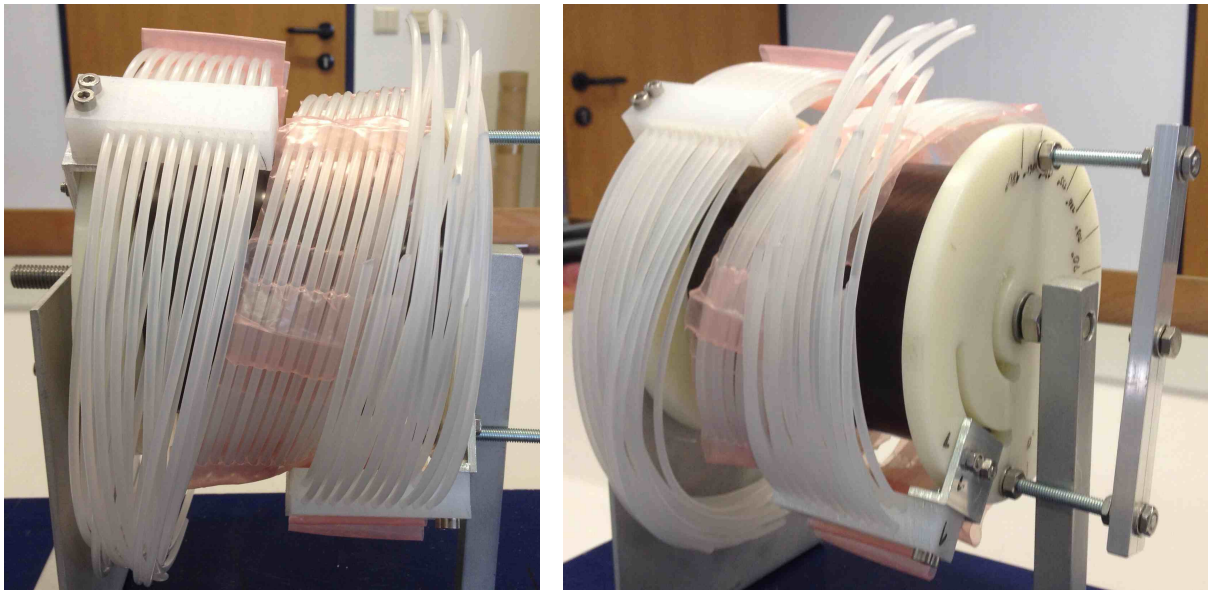

(a) (b)

Figure 3.10: Design version 3 of the cable harness routing

3.3.4 Version 3

3.3.4.1 Design of the Test Setup

Starting from design version 2, the length of the whole test setup in axial direction was reduced while all the other design parameters (i.e. number of cable layers and windings, method of connection between cables, method of fixation to the flanges) were kept the same as in version 2. Moreover, a whole new set of dummy cables was used for this test setup, and also the synthetic film used to connect the cables was renewed. The result is depicted in figure 3.10.

Because the support block is mounted on a different height in radial direction than the middle harness part, there is no contact between these parts and therefore no additional friction. The result is an overlapped routing form of the cable harness (see chapter 2.4.2).

3.3.4.2 Geometric Dimensions and Torque Measurements

Equal to design version 2, the number of harness windings at the maximum deployment angle is two and the maximum outer diameter of the cable harness is 183 mm. Again, objective RSA-130 is not met because the outer diameter is above 140 mm. The overall axial length of the cable harness could be decreased from former 142 mm to 110 mm.

The measuring instrument used during breadboard testing of version 2 was no longer available when this design version was built. Therefore, the resistive torque was measured with a torque wrench model *ADS 4* by the company TORQUELEADER. Its scale ranges from 500 to 4000 Nmm and like the former instrument, the current one features a drag indica-

Turning angle φ	Measured torque		Spring torque	Friction torque
	Coiling up	Unrolling		
0°	850	800	825	25
15°	1017	950	983	33
30°	1200	1067	1133	67
45°	1367	1233	1300	67
60°	1617	1450	1533	83
75°	1850	1600	1725	125
90°	2100	1767	1933	167
105°	2417	1933	2175	242
120°	3167	2500	2833	333

Table 3.4: Averaged measurement results for the cable harness design version 3 (torque values in Nmm)

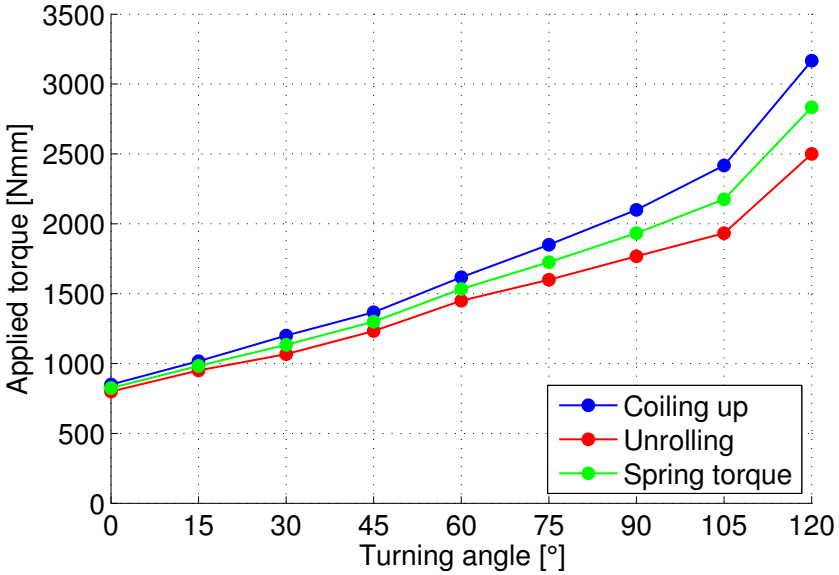

Figure 3.11: Graphic representation of the results in table 3.4 – Averaged measurement results for the cable harness design version 3

tor for eased reading of measurement values. According to the producer, the measuring instrument has a precision of $\pm 3\,\%$ relative to the reading[70] and is therefore even more precise than the former instrument.

The measurement procedure is the same as for design version 2: three measurement runs consisting of coiling up and unrolling of the cable harness and then computing the average measurement values of these runs. The averaged results are depicted in table 3.4 and figure 3.11. The complete measurement protocol can be found in appendix A.

In this design version, the spring torque increases almost linearily with the deployment angle, whereby at the maximum deployment angle of 120°, the slope of the curve is slightly

[70] cf. http://www.torqueleader.com/torque-measuring-tools/ads-dial-measuring-torque-wrenches/ (visited on Dec. 28, 2015).

higher than at all the other measurement points. The maximum resistive torque amounts to about 3.2 Nm and occurs at the maximum deployment angle. Objective RSA-140 is not met in this design version because the resistive torque is above 3 Nm.

The hysteresis loop which can be observed from the measurement values is much lower compared to all of the previous design versions. The reason for these circumstances could be the fact that the harness was built using a completely new synthetic film and dummy cables, thus reducing the internal friction between the moving parts of the harness. Another explanation could be the usage of a different measurement instrument with a higher precision, or the influence of the harness winding form on the resulting friction torque. In chapter 2.4.2 it was stated that the overlapped routing form could increase the friction because of the contact between the individual windings. However, in the current test setup the windings are not at all touching each other. The friction could probably even be reduced compared to the inclined routing form. In the latter, the contact force between the harness windings and the underlying pipe (and therefore the friction torque) is supposed to be higher due to the inclined position of the cable harness, which presses the harness windings against the pipe.

As it can be observed from the measurement values, the friction torque increases monotonically with the deployment angle and reaches its maximum value of 0.33 Nmm at 120°. This amounts to about 11 % of the maximum resistive torque.

3.3.4.3 Concepts for Improvement

The current test setup was designed with the goal of reaching a minimal axial length of the harness helix, given the arrangement of the cables in two layers of ten cables each. This adversely affects the space requirements in radial direction, which are far above the given objectives. For this reason, the next design version will return to the inclined routing form, whereby the support blocks will be attached closer to the rotation axis in order to reduce the overall diameter of the harness helix as much as possible.

3.3.5 Version 4

3.3.5.1 Design of the Test Setup

In the last version of the test setup, a design with minimal space requirement in axial direction was investigated. However, objective RSA-130 has already been met by design version 2 regarding the axial installation length. The focus of this design lies therefore on the reduction of the outer diameter of the harness helix in order to fit into the given objective of 140 mm.

The maximum outer diameter of the harness is determined mostly by the number of windings. The more often the harness is winded around the pipe, the smaller the radial

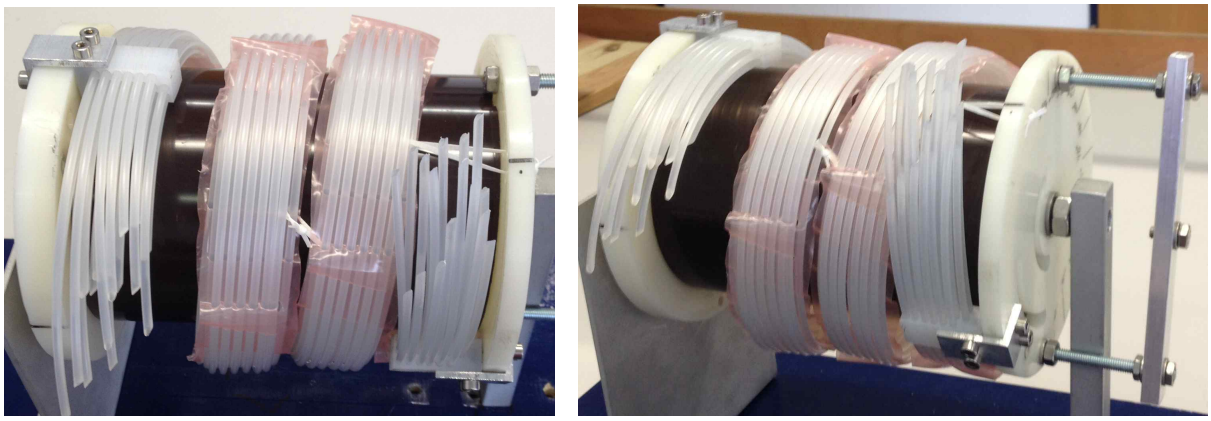

(a) (b)

Figure 3.12: Design version 4 of the cable harness routing

difference between the two extremal positions (i.e. the starting position and the position where the harness is fully turned). Since the minimum diameter is given by the dimensions of the underlying can, a smaller radial difference leads to a smaller maximum outer diameter. However, the outer dimensions of the harness are also affected by the location of the support block, because the block is fixed to the flange and cannot be moved in a radial direction. Therefore, the maximum radius of the harness is always at least the distance of the support block to the turning axis.

Starting from design version 2, the support block was mounted closer to the rotation axis which reduces the radial distance and therefore the outer diameter of the cable harness. Moreover, the number of cable layers was increased. The twenty cables were arranged in three layers (six cables in the outmost layer, seven cables in the other layers). Because the axial length of the harness helix was held constant, the number of windings could thus be increased to three. At the maximum deployment angle, the harness is winded around the rotation axis three full times, which yields a number of windings of 2.67 in the starting position. The resulting design is depicted in figure 3.12.

The method of connection between the individual cables as well as the method of fixation of the harness to the flanges was kept the same as in previous versions, but the used parts (synthetic film and support block) had to be remanufactured.

The support block features two internal threads and is fixed to the flange of the test bench by an aluminum corner plate. Contrary to earlier versions, the support block is fixed as near to the pipe within the harness as possible, which results in a design with a minimal harness diameter, which has been defined as main goal for this version.

The harness is fixed to the test bench solely at its ends, while it is hovering everywhere in between the two support blocks. This may lead to the harness wandering off or deviating at some locations, when the moving flange of the test bench is turned. The result may be unwanted contact between the harness and the support block which leads to friction and, in the worst case, to damage of the harness wires or the harness itself.

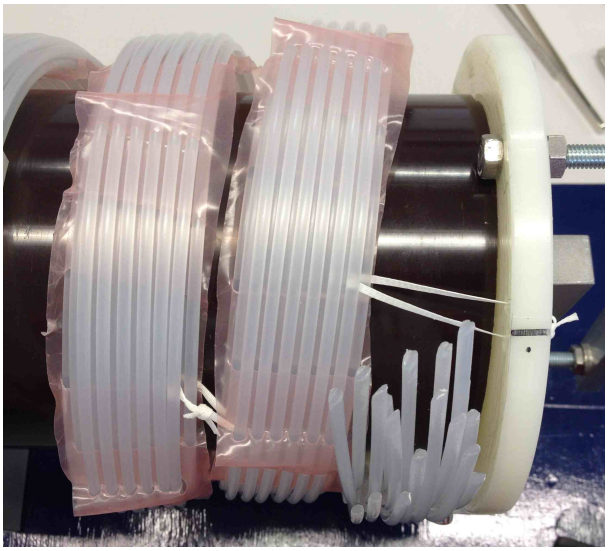

Figure 3.13: Detailed view of the lacing cords which are connecting and stabilizing the harness windings

To prevent this effect and limit the axial motion of the harness windings, a stabilization with lacing cords was created. As depicted in figure 3.13, the third winding from the left was connected to the moving flange by a lacing cord. This ensures a constant distance of the cables to the flange and keeps them from deviating to the left. The relative motion between the flange and the harness is not a problem, because the lacing cords were fixed to the harness in such a way that they are still slideable along the wires. The two middle windings of the harness were also connected together to prevent the cables on the left from running too close to the support block and getting scratched or damaged by it. By this measure, the free movement of the harness windings was limited to keep the cables from wandering off, which has a stabilizing effect on the whole cable harness.

3.3.5.2 Geometric Dimensions and Torque Measurements

At the maximum turning angle, the harness is winded three full times around the underlying pipe. A measurement of the distance between the first and the last cable in axial direction showed a value of 141 mm. The pipe around which the harness is winded is cut to a length of 150 mm and therefore fulfills the requirement defined in objective RSA-130. A measurement of the maximum outer diameter of the cable harness was taken when the harness was fully unrolled ($\varphi = 0°$) and showed a value of 140 mm. As a consequence, the outer dimensions of this harness design version meet objective RSA-130.

As before, the measurements were taken with a torque wrench model *ADS 4* by the company TORQUELEADER. The measurement procedure is the same as for previous design versions (i.e. three measurement runs consisting of coiling up and unrolling of the cable harness and then computing the average measurement values of these runs). At first, the measurements were taken on the finished design of the harness, but before the lacing

Turning angle φ	Measured torque		Spring torque	Friction torque
	Coiling up	Unrolling		
0°	1083	1033	1058	25
15°	1233	1100	1167	67
30°	1383	1200	1292	92
45°	1533	1300	1417	117
60°	1633	1383	1508	125
75°	1717	1467	1592	125
90°	1800	1600	1700	100
105°	1950	1700	1825	125
120°	2333	1950	2142	192

Table 3.5: Averaged measurement results for the cable harness design version 4 (without lacing cords, torque values in Nmm)

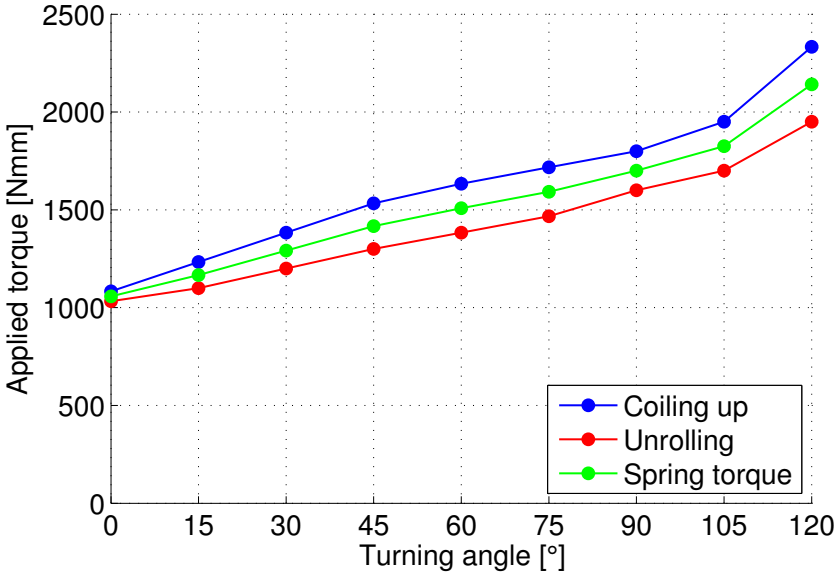

Figure 3.14: Graphic representation of the results in table 3.5 – Averaged measurement results for the cable harness design version 4 (without lacing cords)

cords were applied. These averaged measurement results are depicted in table 3.5 and figure 3.14. The second series of measurements was taken after the application of lacing cords in order to investigate the effects of the harness stabilization with lacing cords. Table 3.6 and figure 3.15 show the averaged measurement results of the harness design with lacing cords. The complete measurement protocols can be found in appendix A.

The measurement data of the harness without lacing cords (table 3.5 and figure 3.14) show a behavior of the resistive torque which is increasing monotonically with the turning angle, although the slope of the blue line (coiling up) is a little lower in the angular range from 60° to 105° than elsewhere. The red line represents measurements taken while the harness was being unrolled, and the increase rate of these values is much more uniform. For both measurement series (coiling up as well as unrolling), the slope is highest at the

Turning angle φ	Measured torque		Spring torque	Friction torque
	Coiling up	Unrolling		
0°	950	633	792	158
15°	1050	717	883	167
30°	1183	817	1000	183
45°	1300	917	1108	192
60°	1400	1017	1208	192
75°	1467	1133	1300	167
90°	1517	1217	1367	150
105°	1683	1300	1492	192
120°	1967	1483	1725	242

Table 3.6: Averaged measurement results for the cable harness design version 4 (with lacing cords, torque values in Nmm)

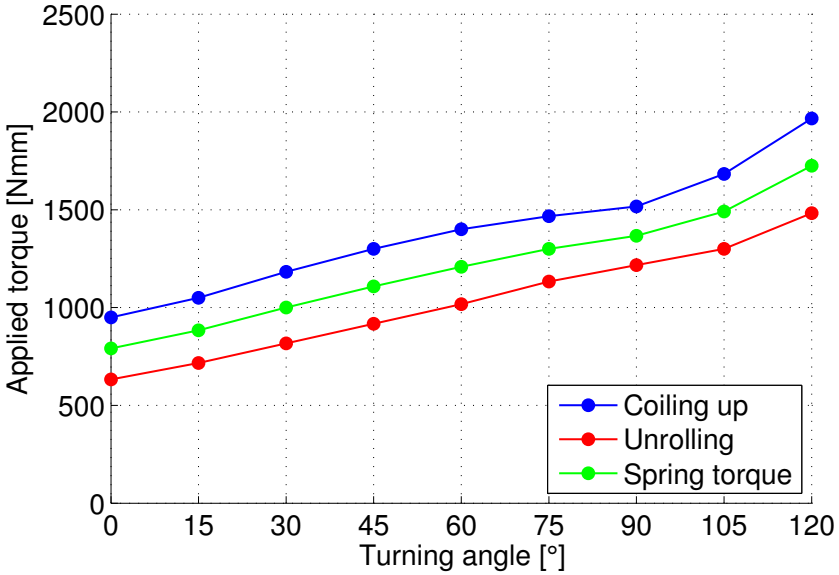

Figure 3.15: Graphic representation of the results in table 3.6 – Averaged measurement results for the cable harness design version 4 (with lacing cords)

maximum turning angle of 120°.

The highest resistive torque occurs at the maximum turning angle and amounts to about 2.3 Nm. This is the smallest value of the maximum resistive torque compared to all previous design versions and it also fulfills the requirements defined in objective RSA-140.

The distance between measurement values on the blue and on the red line represents the static friction at this particular turning angle. It is measured by the friction torque, which is defined as half of this distance. The friction at the starting position is rather small with 25 Nmm and increases with the deployment angle for the first few measurement steps. In the region from 45° to 105° it stays constantly between 100 and 125 Nmm, before it finally increases to its maximum value of 192 Nmm. This can be explained by the fact that the harness is then completely coiled up and pressed against the pipe. The increasing contact pressure between the harness and the pipe leads to higher friction, which is why the hysteresis is most pronounced at this location.

The maximum value of the friction torque hereby amounts to about 8.2 % of the maximum resistive torque, which is the lowest ratio of all design versions so far.

After the harness was fastened with lacing cords, another series of measurements was taken (see table 3.6 and figure 3.15). Again, the otherwise monotonical increase of the measurement values on the blue line (coiling up) is disrupted by a slight drop in the curve's slope at an angle range from 75° to 105°. On a contrary, the measurements on the red line (unrolling) follow an almost linear path over the deployment angle. The highest measured total resistive torque amounts to about 2.0 Nm, which is even smaller than the measured resistive torque of the harness before lacing cords were applied.

In contrast to the system without lacing cords, the friction torque is almost constant over the largest part of the measurement range. It stays between 150 and 200 Nmm everywhere in the range from 0° to 105°, before it increases to its largest value of 242 Nmm at 120°.

Compared to the previous measurements (without lacing cords), the overall level of friction torque is almost twice as high, but its maximum value is only about a quarter higher than the maximum value of the harness without lacing cords. Moreover, the friction torque of the harness with lacing cords is much more uniform over the deployment angle.

The maximum value of the friction torque is 242 Nmm and amounts to about 12 % of the maximum resistive torque.

3.3.5.3 Summary and Conclusion

The properties and results of this harness design can be summarized as follows:

Maximum turning angle:	120°
Number of windings:	3 full windings at maximum angle
Number of cables and layers:	20 cables in 3 layers $(7 + 7 + 6)$

Method of connection between cables:	Perforated plastic film (LD-PE)
Method of fixation to the flanges:	Plastic block with 20 drill holes
Axial length:	141 mm
Maximum outer diameter:	140 mm
Maximum resistive torque (without lacing cords):	2.3 Nm
Maximum spring torque (without lacing cords):	2.1 Nm
Maximum friction torque (without lacing cords):	192 Nmm
Maximum resistive torque (with lacing cords):	2.0 Nm
Maximum spring torque (with lacing cords):	1.7 Nm
Maximum friction torque (with lacing cords):	242 Nmm

This version represents a feasible design solution for the high voltage part of the final electric harness (outer harness), which consists of twenty cables. These cables were arranged in three layers (with seven resp. six cables each). The number of windings around the rotation axis was chosen to be three at the maximum deployment angle of 120°.

The connection between the individual wires was established by a perforated film made of low-density polyethylene (LD-PE). At the ends of the harness, the fixation to the flanges of the test bench was realized by a plastic block with drill holes.

A comparison between the measurement values of the cable harness with and without lacing cords reveals that the total resistive torque of the harness with lacing cords is slightly lower. This is caused by the stabilizing effect of the lacing cords, which limit the deviating motion of the individual harness windings and ensure a constant curvature radius along the length of the cables. The limitation of the sidewards motion of the windings also prevents them from getting into contact with the support block, which would induce scratches and damage to the harness.

For the harness which was braced by lacing cords, the overall level of static friction turned out to be slightly higher but also much more uniform over the deployment angle. This is because the individual windings were tied together and therefore produced friction due to the relative motion between the windings. Still, the maximum value of friction torque of the harness with lacing cords is only about a quarter higher than the friction torque of the harness without lacing cords. The friction torque hereby represents 12 % of the total resistive torque, which fulfills the requirement defined in objective RSA-140, namely that only a small amount of the total torque is caused by internal friction.

As the measurement results of the test setup showed, this design fulfills the geometric and mechanical specifications defined in objectives RSA-130 and RSA-140.

In RSA-130, the outer installation space is restricted to 150 mm in axial direction and 140 mm in diameter. With an axial length of 141 mm and a maximum outer diameter of

exactly 140 mm, the design fulfills these requirements. However, the cavity within the complete electric harness (consisting of the high voltage and low voltage harness) shall provide enough space for the rotary actuator *SA-15*, which has a maximum outer diameter of 82 mm. In chapter 3.3.6, it shall be checked mathematically if the complete harness system consisting of these two parts is able to fulfill this requirement.

The mechanical objective RSA-140 defines the maximum resistive torque to be 3 Nm. With a maximum resistive torque of 2.3 Nm, this requirement is fulfilled by design version 4, though only the high voltage harness is covered in this version. In chapter 4.1.1 it will be showed that the contribution of the low voltage harness to the overall resistive torque is one order of magnitude smaller than the contribution of the high voltage harness, which is why the inner harness was omitted in this design version. In chapter 3.3.7, this assumption will be experimentally validated by testing a system consisting of a high voltage as well as a low voltage harness. The resulting design from version 4 will hereby be adapted to the low voltage harness.

3.3.6 Final Version

Design version 4 covered a feasible design solution for the outer cable harness (high voltage harness). This design shall now be transferred and adapted to the inner cable harness (low voltage harness), which consists of twenty-seven electric cables size AWG 26 according to objective RSA-160. Hereby, all the low voltage cables are united in a single low voltage harness.

3.3.6.1 Outer and Inner Diameter of the Harness Helix

First, the installation space of the complete electric harness consisting of a high voltage harness and a low voltage harness shall be computed in order to check if objective RSA-130 is fulfilled. In particular, the starting point of the calculation shall be the diameter of the inner aluminum can D_i, which is driven by the outer diameter of the rotary actuator. The motor has a maximum diameter of 82 mm and the aluminum can has a thickness of 0.3 mm, which gives a can diameter of $D_i = 82.6$ mm.

As stated in appendix B, the diameter of the cables used in the outer harness is 2.2 mm. The diameter of the inner harness cables was measured in the laboratory to be 2.0 mm. Between the two harnesses there shall be an aluminum can with thickness 0.3 mm and a length of about 150 mm.

The definition of geometric parameters which will be used in the calculation is depicted

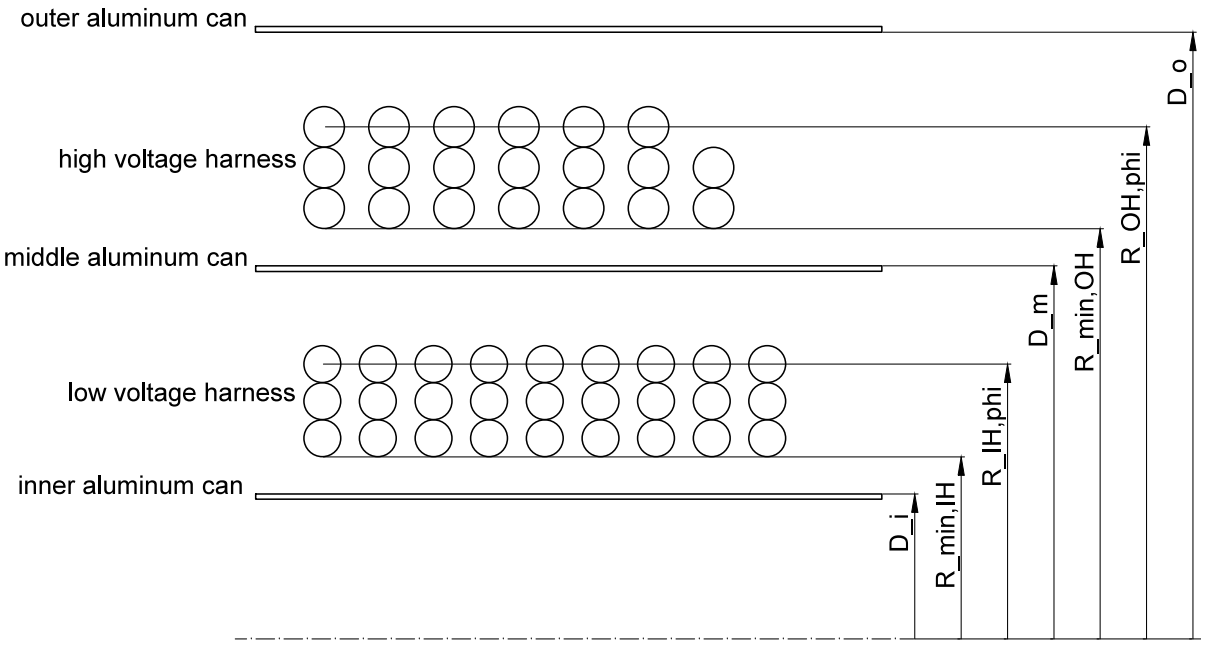

Figure 3.16: Definition of geometric parameters for the calculation of harness radii

in figure 3.16. Their values are the following:

$$\varphi = 120° \quad \text{(maximum deployment angle)} \tag{3.4}$$

$$L = 150\,\mathrm{mm} \quad \text{(axial installation space for harness helix)} \tag{3.5}$$

$$D_i = 82.6\,\mathrm{mm} \quad \text{(outer diameter of inner aluminum can)} \tag{3.6}$$

$$t_{can} = 0.3\,\mathrm{mm} \quad \text{(radial thickness of aluminum cans)} \tag{3.7}$$

$$d_{IH} = 2.0\,\mathrm{mm} \quad \text{(diameter of inner harness cables)} \tag{3.8}$$

$$n_{c,IH} = 27 \quad \text{(number of inner harness cables)} \tag{3.9}$$

$$d_{OH} = 2.2\,\mathrm{mm} \quad \text{(diameter of outer harness cables)} \tag{3.10}$$

$$n_{c,OH} = 20 \quad \text{(number of outer harness cables).} \tag{3.11}$$

The goal is to find the radial space requirements of the inner cable harness in order to define the required diameter of the aluminum can separating the two harnesses. Afterwards, the radial space requirements of the outer cable harness can be calculated in order to check if the maximum outer diameter of the whole harness system lies within the defined installation space. The number of windings is hereby an important parameter for the calculation of the radial space requirements of the individual harnesses.

The cables of the inner harness are arranged in three layers to nine cables each, which gives for the width of a single harness winding

$$w_{IH} = 9d_{IH} + 10 \cdot 1\,\mathrm{mm} = 28\,\mathrm{mm} \tag{3.12}$$

with a distance of 1 mm between the individual cables. From geometrical considerations follows that the maximum possible number of windings is

$$n_{IH,120°} = \frac{L}{w_{IH}} - 1 \approx 4.4 \tag{3.13}$$

$$n_{IH,0°} = n_{IH,120°} - \frac{\varphi}{360°} \approx 4.0. \tag{3.14}$$

From equation (2.7) we get the relation between the maximum and minimum curvature radius at the respective deployment angles

$$R_{max} = R_{min} \left(\frac{n}{n - \frac{1}{3}} \right) \tag{3.15}$$

whereby the parameter n is the number of windings at $\varphi = 120°$. Now the minimum and maximum radius of the harness helix can be calculated. The minimum curvature radius of the inner harness depends on the diameter of the inner aluminum can and amounts to

$$R_{min,IH} = \frac{D_i}{2} + 2\,\mathrm{mm} = 43.3\,\mathrm{mm} \tag{3.16}$$

with a gap of 2 mm between the can and the wire. The curvature radius of the neutral fiber of the outmost cable layer of the inner harness is

$$R_{IH,120°} = R_{min,IH} + 2.5 d_{IH} = 48.3\,\mathrm{mm}, \tag{3.17}$$

which in turn yields for the maximum curvature radius, which occurs at the starting position ($\varphi = 0°$)

$$R_{IH,0°} = R_{IH,120°} \frac{n_{IH,120°}}{n_{IH,0°}} = 52.3\,\mathrm{mm}. \tag{3.18}$$

Finally, the maximum outer diameter of the inner cable harness adds up to

$$D_{max,IH} = 2R_{IH,0°} + d_{IH} = 106.6\,\mathrm{mm}. \tag{3.19}$$

The diameter of the aluminum can which lies in between the high voltage and the low voltage harness was therefore chosen to

$$D_m = 110\,\mathrm{mm}, \tag{3.20}$$

which is about the same as the diameter of the pipe which was used during breadboard testing ($D_{pipe} = 105\,\mathrm{mm}$).

With an analogue calculation scheme, the space requirement of the outer cable harness can be computed. As the cables of the outer harness are split up into three layers of up to

seven wires, the width of a single harness winding is

$$w_{OH} = 7d_{OH} + 8 \cdot 1.2\,\mathrm{mm} = 25\,\mathrm{mm}, \tag{3.21}$$

with a distance of 1.2 mm between the individual cables. The maximum possible number of windings is therefore

$$n_{OH,120°} = \frac{L}{w_{OH}} - 1 = 5 \tag{3.22}$$

$$n_{OH,0°} = n_{OH,120°} - \frac{\varphi}{360°} \approx 4.7. \tag{3.23}$$

The dimension of the aluminum can which separates the outer and the inner harness leads to a minimum curvature radius of the outer harness of

$$R_{min,OH} = \frac{D_m}{2} + 2\,\mathrm{mm} = 57\,\mathrm{mm}, \tag{3.24}$$

whereby again a gap of 2 mm between the can and the wires was considered. The neutral fiber of the outmost cable layer of the outer harness has a curvature radius of

$$R_{OH,120°} = R_{min,OH} + 2.5d_{OH} = 62.5\,\mathrm{mm}, \tag{3.25}$$

which gives with equation (3.15) a maximum curvature radius at the starting position ($\varphi =$ 0°) of

$$R_{OH,0°} = R_{OH,120°}\frac{n_{OH,120°}}{n_{OH,0°}} = 67\,\mathrm{mm}. \tag{3.26}$$

Finally, the maximum outer diameter of the outer cable harness and therefore the maximum outer diameter of the whole electric harness system adds up to

$$D_{max,OH} = 2R_{OH,0°} + d_{OH} = 136.1\,\mathrm{mm}, \tag{3.27}$$

which is less than the specified maximum diameter of the cable harness of 140 mm, as it was defined in objective RSA-130. As a consequence, with a minimum inner diameter of the harness helix of 86.6 mm ($>$ 82 mm), a maximum outer diameter of the helix of 136.1 mm ($<$ 140 mm) and an axial length of the helix of less than 150 mm, objective RSA-130 is fully met.

3.3.6.2 Connection Method Between Individual Harness Cables

During breadboard testing, a film made of low-density polyethylene (LD-PE) with a thickness of 150 µm was used for the connection of the harness cables.

For the final application, polyetheretherketone (PEEK) has been chosen as film material due to its better radiation resistance (see chapter 2.6.3.2). The Austrian company LITE

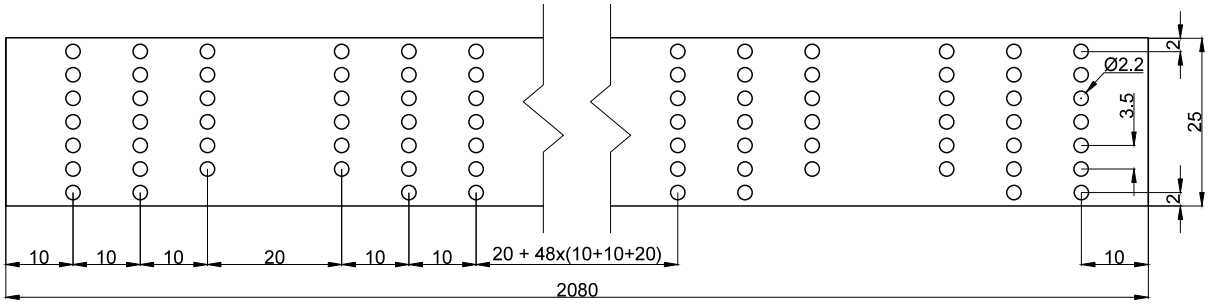

(a) Outer cable harness (high voltage harness)

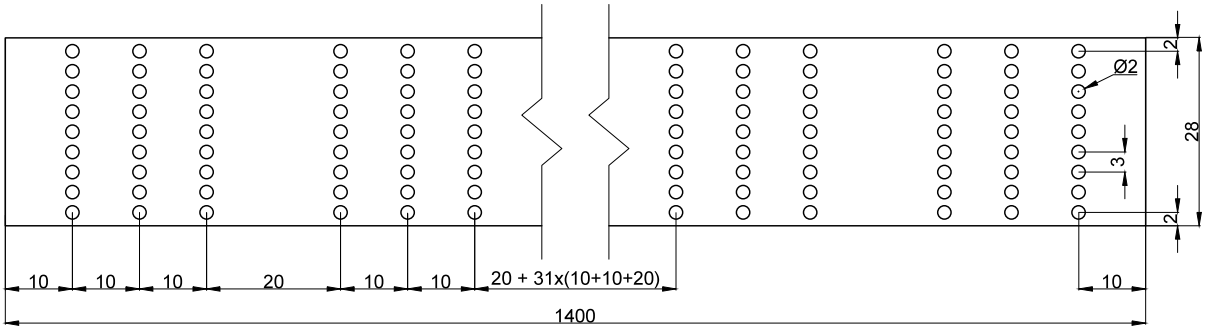

(b) Inner cable harness (low voltage harness)

Figure 3.17: Sketch of the perforated plastic film for the final harness design version (dimensions in mm)

GMBH sells the material under the name *LITE K (PEEK amorph)* as film with a thickness of 100 µm and a roll width of 236 mm. Ten running meters of this film were ordered and can be used for this purpose in future RSA projects.

The design of the perforated film for the outer and the inner cable harness in the final application is depicted in figure 3.17.

3.3.6.3 Fixation Method of the Harness to the Flanges

During breadboard testing, the fixation method by a plastic support block turned out to be the easiest and most reliable method. Therefore, this is the primary choice for the fixation between the cable harness and the flanges of the mechanism in the final harness design. A plastic block measuring $34 \times 16 \times 13$ mm with twenty drill holes will be used for the outer cable harness (see figure 3.18). Using a corner plate, the support block is fixed to the mechanism flange as near as possible in order to keep the axial space requirement of the harness system low. This method of fixation can also be adapted to be used with the inner cable harness.

Figure 3.18: Detailed view of the plastic support block

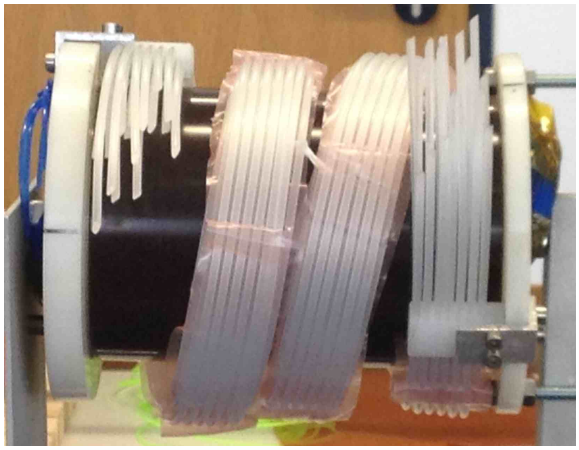

(a)

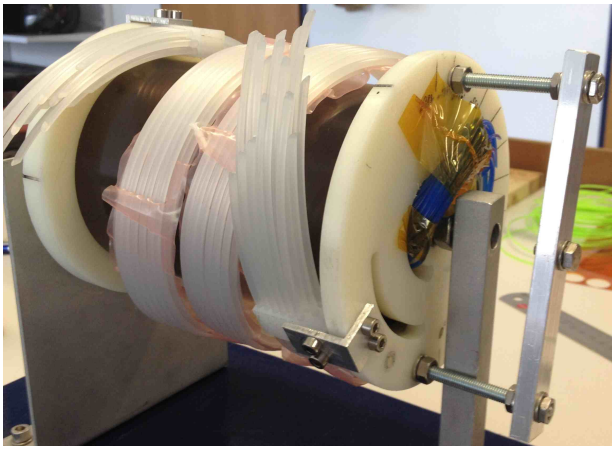

(b)

Figure 3.19: Final design version of the cable harness routing

3.3.7 Breadboard Testing of Final Version

3.3.7.1 Design of the Test Setup

The final harness design, which was created in chapter 3.3.6, shall now be built and tested in the laboratory to investigate its geometric and mechanical characteristics. The test setup which was used is depicted in figure 3.19.

The outer cable harness was carried over from the last test setup and consists of twenty cables arranged in three layers. The individual cables were connected together by a synthetic film and the harness was fixed to the flanges by a plastic support block. The twenty-seven cables of the inner harness were also arranged in three layers and connected together by synthetic film, which can be seen in figure 3.20. Because in the breadboard testing, only the effect of the inner cable harness on the rotational resistive torque should be investigated, the inner harness was just fixed to the flanges by adhesive tape.

Again, lacing cords were used to stabilize the individual harness windings and limit their axial movement. This can be seen for instance in figure 3.19a.

Same as in version 4, the number of windings for the outer harness was three at the maximum deployment angle, although in the calculation in chapter 3.3.6.1, a value of five windings was used. This is due to the dummy cables having a larger diameter than the

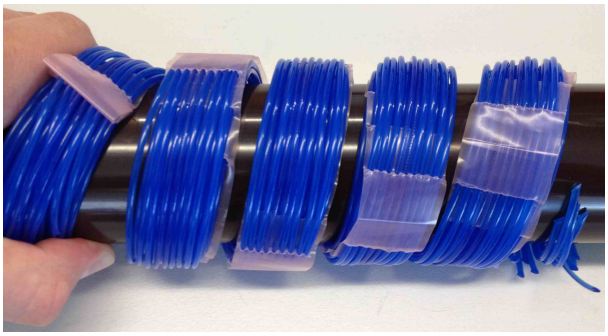

Figure 3.20: Inner cable harness (low voltage harness)

actual electric cables which will be used in the real application. The inner harness could be winded around the rotation axis five and a half times at $\varphi = 120°$, because the width of the harness used in the test setup was a little lower than calculated before.

3.3.7.2 Geometric Dimensions and Torque Measurements

The dimensions of this harness design are the same as in version 4, since the outer cable harness has not been altered. Objective RSA-130 is therefore fully met. The torque measurements which are depicted in table 3.7 and figure 3.21 were taken with the same torque wrench (model *ADS 4* by TORQUELEADER) and using the same measurement procedure as in version 4. Three measurement runs, each one consisting of coiling up and unrolling the cable harness, were performed followed by calculating the averaged measurements of these runs. The complete measurement protocols can again be found in appendix A.

The behavior depicted in the diagram bears a resemblance to the measurement results of design version 4 after the application of lacing cords. All measurement curves increase almost linearily with the turning angle, whereby again at 90 degree turning angle a small drop in the curve's slope is visible. The highest slopes for both measurement series (coiling up as well as unrolling) occur at the ends of the rotational angle range (at 105 and 120 degrees).

The highest resistive torque amounts to about 2.3 Nm and was measured at the maximum turning angle. Compared to design version 4, this value is about 15 % higher than the maximum value of the last version (with lacing cords). This is attributable to the installation of the inner cable harness, which according to chapter 4.1.1 contributes a stiffness to the whole system about one order of magnitude smaller than the stiffness of the outer harness alone.

Similar to the last design version with lacing cords, the friction torque is smooth over the largest part of the measurement range. From 0° to 105°, it stays between 200 and 225 Nmm and is therefore even more uniform than the friction measured on design version 4. However, compared to the last design version the overall level of friction rose from 200 to 225 Nmm and the maximum value rose from 242 to 275 Nmm. Again, this can be

Turning angle φ	Measured torque		Spring torque	Friction torque
	Coiling up	Unrolling		
0°	1133	717	925	208
15°	1200	767	983	217
30°	1333	900	1117	217
45°	1433	1000	1217	217
60°	1550	1133	1342	208
75°	1667	1233	1450	217
90°	1750	1317	1533	217
105°	1967	1517	1742	225
120°	2267	1717	1992	275

Table 3.7: Averaged measurement results for the final cable harness design version (torque values in Nmm)

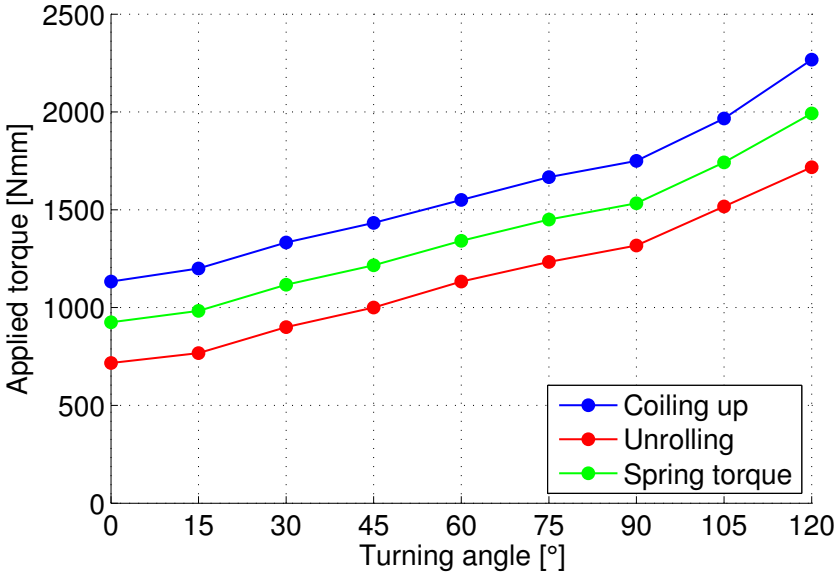

Figure 3.21: Graphic representation of the results in table 3.7 – Averaged measurement results for the final cable harness design version

explained by the influence of the inner cable harness, which poses an additional source of internal friction.

The largest value of the friction torque amounts to 275 Nmm at 120°, which is about 12 % of the maximum resistive torque. With these measurement values, objective RSA-140 is completely fulfilled by the final design version.

3.3.7.3 Summary and Conclusion

In the following, the properties and parameters of the final harness design (as stated in chapter 3.3.6) as well as the measurement results of the breadboard testing are summarized:

Maximum turning angle:	120°
Number of windings (outer harness):	5 full windings at maximum angle
Number of windings (inner harness):	4.4 windings at maximum angle
Number of cables and layers (outer harness):	20 cables in 3 layers ($7 + 7 + 6$)
Number of cables and layers (inner harness):	27 cables in 3 layers (9 cables each)
Method of connection between cables:	Perforated plastic film (PEEK)
Method of fixation to the flanges:	Plastic block with drill holes
Axial length:	141 mm
Maximum outer diameter (outer harness helix):	140 mm
Minimum inner diameter (inner harness helix):	86.6 mm
Maximum resistive torque:	2.3 Nm
Maximum spring torque:	2.0 Nm
Maximum friction torque:	275 Nmm

In the laboratory, a test setup according to this design has been assembled and investigated. Due to differences in the diameters of the dummy cables used in the laboratory and the electric cables which will be used on the real application, the total number of harness windings is not the same for the test setup and the theoretical harness design. The torque measurements should not be influenced by this circumstances as the resistive torque (bending moment in the cables) is not affected by the number of windings.

The final version designed in the laboratory fulfills the following requirements which were stated in chapter 1.2:

The electric cables are designed especially for the use in space applications. They are isolated with Kapton, which provides sufficient resistance against the radiation in space (10^{10} rad according to the data sheet in appendix B). The other components which are

used in the cable harness, as f.i. the PEEK-film, were also chosen to be resistant against the radiation levels during space operations. **RSA-100** is therefore fulfilled.

For breadboard testing, a deployment angle of 120° has been defined. The harness has been designed in order to allow a rotation by this angle, and all the measurements have been taken up to a rotation by 120°. Thus, **RSA-110** is also fulfilled.

The fatigue limits as defined in objective **RSA-120** cannot be tested in the laboratory, but will be verified mathematically in chapter 4.2.

The installation space as defined in **RSA-130** is maintained by the final harness design version, as it has been measured during breadboard testing.

RSA-140 defines the maximum allowed resistive torque to be 3 Nm. Measurement resultes showed that the occurring resistive torque stays below this limit. As we will see in chapter 4.1.1, the dummy cables are stiffer than the electric cables used in the real application, and therefore the measurements are conservative estimations. Furthermore, the friction torque is small compared to the overall resistive torque.

The shielding between the high voltage harness and low voltage harness is required through **RSA-150**. It is established by using shielded electric cables as well as separating these two harnesses by an aluminum can.

The number and cross section of the individual electric cables as defined by **RSA-160** have been taken into account for the harness design and all calculations in chapter 4. The harness was designed to comply with the given electric cable types and sizes.

So apart from objective RSA-120, every requirement is fulfilled by the final harness design. The last remaining objective will be verified by a calculation in chapter 4.2.

Chapter 4

Calculations

4.1 Calculation of Rotational Torque

In this chapter, the rotational torque acting from the harness onto the geared actuator shall be evalued. Based on the measurement results of the rotational torque in the breadboard testing, the values shall be adapted to the conditions of the real application. In order to do that, a comparison of the flexural stiffness of the dummy cables used in the test setup and the electric cables which are installed in the mechanism shall be performed.

Lastly, the results shall be used to validate the choice of the rotational actuator. The standard ECSS-E-ST-33-01C by the EUROPEAN COOPERATION FOR SPACE STANDARDIZATION gives an equation for the dimensioning of actuators used in mechanisms for space flight. With this equation, it shall be checked if the actuator *SA-15* is sufficiently dimensioned for the occurring rotational torque in the application.

4.1.1 Estimation of the Actual Torque Acting upon the Mechanism

In order to estimate the torque acting on the rotational motor in the real application, the flexural stiffness of the cables used during breadboard testing as well as that of the real electric cables needs to be determined. With these results, the measurement values taken at the test setup during breadboard testing can be transferred to estimated values which are expected to occur on the real mechanism.

4.1.1.1 Outer Cable Harness

For the outer cable harness (high voltage harness), Nylon wires with a full circular cross section with a diameter of approximately 3.1 mm were used in the test setup. The flexural stiffness of these cables was determined in the following manner: a piece of the Nylon cable with a length of 100 mm was mounted as cantilever beam. When it was loaded by a mass of 10 g at the end, a vertical displacement of 3 mm was observed. The displacement

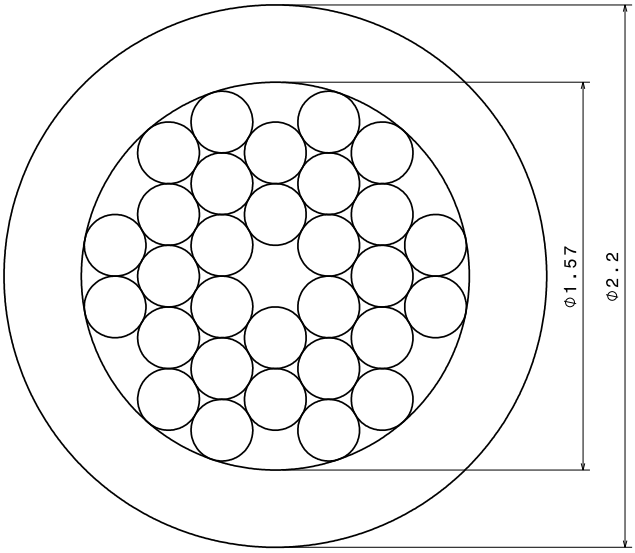

Figure 4.1: Sketch of the cross section of the outer harness cables type *CN4K* (dimensions in mm)

of a cantilever beam is

$$w = \frac{Fl^3}{3EJ_y}, \tag{4.1}$$

which yields for the flexural Stiffness EJ_y of the Nylon cable

$$EJ_{y,dummy} = \frac{Fl^3}{3w} = \frac{0.010 \cdot 9.81 \cdot 100^3}{3 \cdot 3}\,\mathrm{Nmm^2} = 10\,900\,\mathrm{Nmm^2}. \tag{4.2}$$

The area moment of inertia of the circular cross section as well as the Young's modulus of the used synthetic material can now be calculated:

$$J_{y,nylon} = \frac{d^4\pi}{64} = \frac{3.1^4\pi}{64}\,\mathrm{mm^4} = 4.53\,\mathrm{mm^4} \tag{4.3}$$

$$E_{nylon} = \frac{EJ_{y,dummy}}{J_{y,nylon}} = \frac{10900\,\mathrm{Nmm^2}}{4.53\,\mathrm{mm^4}} \approx 2400\ \mathrm{N/mm^2}. \tag{4.4}$$

Because the real electric cables for the outer cable harness were not available during laboratory testing, their flexural stiffness shall be estimated mathematically. The cables which will be used in the outer harness are of type *CN4K* by SILICABLE (see data sheet in appendix B). The core consists of thirty nickel-plated copper strands with a diameter of 0.25 mm each. A jacket of four lapped, heat-sealed Kapton polyimide tapes surrounds the stranding. The cables provide a resistance against radiation of 10^{10} rad and are therefore suitable for the application.

The nominal outer diameter of the whole cable is given as 2.2 mm in the data sheet. Though the thickness of the Kapton layer is not given in the data sheet, it can be estimated by figure 4.1, which shows a possible arrangement of thirty strands with a diameter of 0.25 mm each. In this case, the outer diameter of the stranding would be about 1.57 mm.

With these cross-sectional values, we can estimate the flexural stiffness of the electric cable. The Young's modulus of copper is given by $E_{copper} = 117\,000\,\text{MPa}$[71] and the modulus of Kapton is $E_{kapton} = 2500\,\text{MPa}$.[72] With the area moment of inertia of a single copper strand

$$J_{y,strand} = \frac{d^4\pi}{64} = \frac{0.25^4\pi}{64}\,\text{mm}^4 = 1.92 \times 10^{-4}\,\text{mm}^4 \tag{4.5}$$

and the Kapton jacket

$$J_{y,kapton} = \frac{(D^4 - d^4)\,\pi}{64} = \frac{(2.2^4 - 1.57^4)\,\pi}{64}\,\text{mm}^4 = 0.852\,\text{mm}^4, \tag{4.6}$$

we can calculate the flexural stiffness to

$$EJ_{y,copper} = 30 \cdot E_{copper} \cdot J_{y,strand} = 673\,\text{Nmm}^2 \tag{4.7}$$

$$EJ_{y,kapton} = E_{kapton} \cdot J_{y,kapton} = 2129\,\text{Nmm}^2 \tag{4.8}$$

$$EJ_{y,real} = EJ_{y,copper} + EJ_{y,kapton} = 2802\,\text{Nmm}^2. \tag{4.9}$$

This gives a ratio between the flexural stiffness of the dummy material and the real electric cables in the outer harness (index OH) of

$$r_{flex,OH} = \frac{EJ_{y,dummy}}{EJ_{y,real}} \approx \frac{10900}{2800} = 3.89. \tag{4.10}$$

In this calculation, it was taken into account that the individual strands are not rigidly connected to each other and are therefore able to move relatively to each other in longitudinal direction. However, friction effects between the strands contribute to an increase of the flexural stiffness of the cables. On the other hand, most of this friction will occur in the so-called pre-bending of the cables into their helical form. Afterwards, during normal mechanism operation, the additional flexure of the cables is relatively small compared to the overall bending, and said friction effects will probably have small impact on the harness resistive torque. Nevertheless, this instance would provide an important topic for future research.

Comparing the values of the flexural stiffness of the dummy cables and the real electric cables yields that the dummy cables are almost four times as stiff as the real cables. As a result, the rotational torque acting from the outer harness upon the motor in the real application is estimated to be much lower than the measured torque values of the outer harness in the test setup.

[71] cf. http://www.engineeringtoolbox.com/young-modulus-d_417.html (visited on Nov. 2, 2015).

[72] cf. E. I. du Pont de Nemours and Company. *DuPont™ Kapton® HN polyimide film – Technical Data Sheet*, p. 2. URL: see Bibliography.

4.1.1.2 Inner Cable Harness

In the breadboard testing, Nylon cables with a diameter of 2 mm were used as dummy cables for the measurements of the inner cable harness (low voltage harness). The electric wires which come into operation in the real application are *shielded jacketed twisted pairs* of cables with the reference number ESCC 3901 019 58 (size AWG 26). These cables meet the ESA standard `ESCC 3901/019`. The technical specifications of the cables can be retrieved from the data sheet, which is included in appendix B.

Both the dummy cables and the ESCC cables have been tested for their flexural stiffness. Again, the cables were mounted as cantilever beams, but with a length of 50 mm. The load of 10 g led to a lowering of 6 mm for the Nylon cable and 9 mm for the electric cable. Therefore, the respective flexural stiffness amounts to

$$EJ_{y,dummy} = \frac{Fl^3}{3w} = \frac{0.010 \cdot 9.81 \cdot 50^3}{3 \cdot 6}\,\mathrm{Nmm}^2 \approx 680\,\mathrm{Nmm}^2 \tag{4.11}$$

$$EJ_{y,real} = \frac{Fl^3}{3w} = \frac{0.010 \cdot 9.81 \cdot 50^3}{3 \cdot 9}\,\mathrm{Nmm}^2 \approx 450\,\mathrm{Nmm}^2, \tag{4.12}$$

which leads to a ratio between the flexural stiffness of the dummy material and the real electric cables in the inner harness (index IH) of

$$r_{flex,IH} = \frac{EJ_{y,dummy}}{EJ_{y,real}} = \frac{680}{450} = 1.51. \tag{4.13}$$

From these results we can see that the Nylon cables have a higher flexural stiffness than the real electric cables, both for the outer and for the inner cable harness. Therefore, the test setup is a conservative model regarding the measurements of the rotational torque, i.e. the torque ocurring in the real application is expected to be lower than the measured torque values.

Another observation is that the flexural stiffness of the cables used in the outer harness is about six times higher than that of the inner harness cables. Due to the number of outer harness cables and inner harness cables being about the same (twenty and twenty-seven cables, respectively), the effect of the inner harness on the resistive torque should be about one order of magnitude lower.

4.1.2 Validation of the Designated Rotational Actuator

With the results from the last chapter, the chosen rotational actuator (*SA-15*) can now be validated. The standard `ECSS-E-ST-33-01C` by the EUROPEAN COOPERATION FOR SPACE STANDARDIZATION gives the following equation for the dimensioning of actuators used in space flight mechanisms:

"The minimum actuation torque (T_{min}) shall be derived by the equation:

$$T_{min} = 2 \times (1.1I + 1.2S + 1.5H_M + 3F_R + 3H_Y + 3H_A + 3H_D) + 1.25T_D + T_L$$

where:

- I is the inertial torque applied to a mechanism subjected to acceleration in an inertial frame of reference (e.g. spinning spacecraft, payload or other).
- T_D is the inertial resistance torque caused by the worst-case acceleration function specified by the customer at the mechanism level.
- T_L is the deliverable output torque, when specified by the customer."[73]

Component of resistance	Symbol	Theoretical Factor	Measured Factor
Inertia	I	1.1	1.1
Spring	S	1.2	1.2
Motor mag. losses	H_M	1.5	1.2
Friction	F_R	3	1.5
Hysteresis	H_Y	3	1.5
Others (Harness)	H_A	3	1.5
Adhesion	H_D	3	3

Table 4.1: Validation of geared actuator: minimum uncertainty factors[74]

Table 4.1 defines the other components and variables appearing in the above equation. The various uncertainty factors in this equation may be reduced according to table 4.1, if the resistive torque components used in the calculation are determined through measurement in a test procedure, as it is the case in this situation.

The following values are needed for this calculation:

$$T_{motor} = 12\,\mathrm{Nm} \quad \text{(unpowered holding torque of actuator)} \tag{4.14}$$

$$T_{piping} = 1\,\mathrm{Nm} \quad \text{(spring torque of piping, given by RSA)} \tag{4.15}$$

$$T_{other} = 0.7\,\mathrm{Nm} \quad \text{(other friction torque, given by RSA)} \tag{4.16}$$

$$T_{harness,spring} = 2.0\,\mathrm{Nm} \quad \text{(spring torque of harness, measured)} \tag{4.17}$$

$$T_{harness,friction} = 0.28\,\mathrm{Nm} \quad \text{(friction torque of harness, measured).} \tag{4.18}$$

[73] European Cooperation for Space Standardization, 2009, p. 27.
[74] Table taken from: ibid., p. 27

T_{motor} is the unpowered holding torque of the geared actuator *SA-15*, which is to be compared with the minimum required actuator torque calculated by the equation given in the standard. The margin of safety shall be computed according to the equation

$$MS = \frac{T_{motor}}{T_{min}} - 1 \qquad [\%]. \tag{4.19}$$

The values for T_{piping} and T_{other} are given by RSA, while the torque values of $T_{harness}$ have been measured during breadboard testing (see table 3.7). The torque of the fuel piping consists only of a spring torque as the steel pipes are hovering over the aluminum cans and thus there is no additional friction due to the movement of the piping. T_{piping} is therefore taken into account via the variable S. T_{other} includes various components of the friction torque which are not caused by the cable harness itself but all the other parts of the pointing mechanism. It is therefore reflected in the variables H_Y and H_A. The spring component of the harness torque and the friction component of the harness torque are factorized into the variables S and F_R, respectively. In consultation with RSA, the variables I, H_M, H_D, T_D and T_L can be omitted in this calculation. Therefore, the equation for the minimum required actuator torque reduces to

$$T_{min} = 2 \times (1.2S + 1.5F_R + 1.5H_Y + 1.5H_A). \tag{4.20}$$

Putting in the values from above gives

$$\begin{aligned} T_{min} &= 2 \times (1.2T_{piping} + 1.2T_{harness,spring} + 1.5T_{harness,friction} + 1.5T_{other}) \\ &= 2 \times (1.2 \cdot 1\,\mathrm{Nm} + 1.2 \cdot 2\,\mathrm{Nm} + 1.5 \cdot 0.28\,\mathrm{Nm} + 1.5 \cdot 0.7\,\mathrm{Nm}) = 10.14\,\mathrm{Nm}. \end{aligned} \tag{4.21}$$

The margin of safety is therefore

$$MS = \frac{T_{motor}}{T_{min}} - 1 = \frac{12\,\mathrm{Nm}}{10.14\,\mathrm{Nm}} - 1 = 18.3\,\%. \tag{4.22}$$

The margin of safety is hereby very low. On the other hand, the torque measurements were taken on a system which is according to equation (4.10) more than three times stiffer than the real application. Therefore, the chosen rotational actuator should be sufficiently dimensioned for this use.

4.2 Strength Calculation and Lifetime Prediction

In this chapter, a mechanical stress analysis of the electric cables shall be performed based on material data and the geometric conditions of the cables during the space mission. The stress states in the cables will depend mostly on the global deformations of the cables

which are given by the curvature radius of the harness, which in turn is determined by the angular rotation (i.e. deployment angle) of the EPPM. The flexure of the cables leads to an elongation of the extreme fiber of the cable element, which then causes flexural stresses.

The stress analysis shall be performed both for the outer and the inner cable harness, because the curvature radii differ and a different kind of cables is used. Stresses shall be evaluated in the individual strands made of copper as well as in the jacket made of Kapton. As stated in requirement RSA-120 in chapter 1.2, the cables should be able to withstand over 1000 large cycles and over 100 000 small cycles. A large cycle means a rotation of the deployment mechanism by 120° from one extremal position into the other, while a small cycle means tilting by $\pm 15°$. From the cable strain due to the given curvature radii at these deployment angles, the stress values can be computed. This yields a maximum and minimum stress for each type of cycle, which can be used to calculate a mean stress and stress amplitude for the fatigue analysis.

4.2.1 Fatigue Life Calculation for Low Levels of Plastic Deformations

The calculation methods for fatigue life are mainly used for elastic stresses in components. However, due to the rather large deformations and small cross sections of the copper strands in the electric cables, we will experience a certain plastic strain which is although small compared to the occurring elastic deformations. The aim of this chapter is to find a method to estimate the fatigue life of these copper strands under the occurrence of low levels of plastic strain.

First, it is important to note that the deformation of the electric cables is strain-controlled instead of stress-controlled. The deformation of the cables is mainly controlled by the two different extremal positions given by the deployment angle. The curvature radius of the deformed cables is given by the outer diameter of the aluminum can, around which the cables are winded. The stress occurring in the cables is then a reaction of the material to the underlying strain, which in turn is given and limited due to geometric reasons. Under these circumstances, a stress relaxation can be considered due to the strain cycling between non-varying upper and lower limits (see the stress-strain diagram in figure 4.2a). The rate of stress relaxation depends on several parameters such as plastic strain amplitude and may even be undetectable for “low-plastic-strain-amplitude cycling of medium and high strength materials”.[75] Nevertheless, it is safe to assume that the stresses will at least not increase due to the cyclic loading.

This is an extreme case, because the strain is reduced to zero in each cycle (pulsating strain). As we will see later, in our case the strain reduction during unloading is small compared to the overall level of strain. This prevents plasticizing in opposite direction, and as a result the stresses in each cycle move parallelly to Hooke’s line. This principle is depicted

[75] Klesnil and Lukáš, 1980, p. 134.

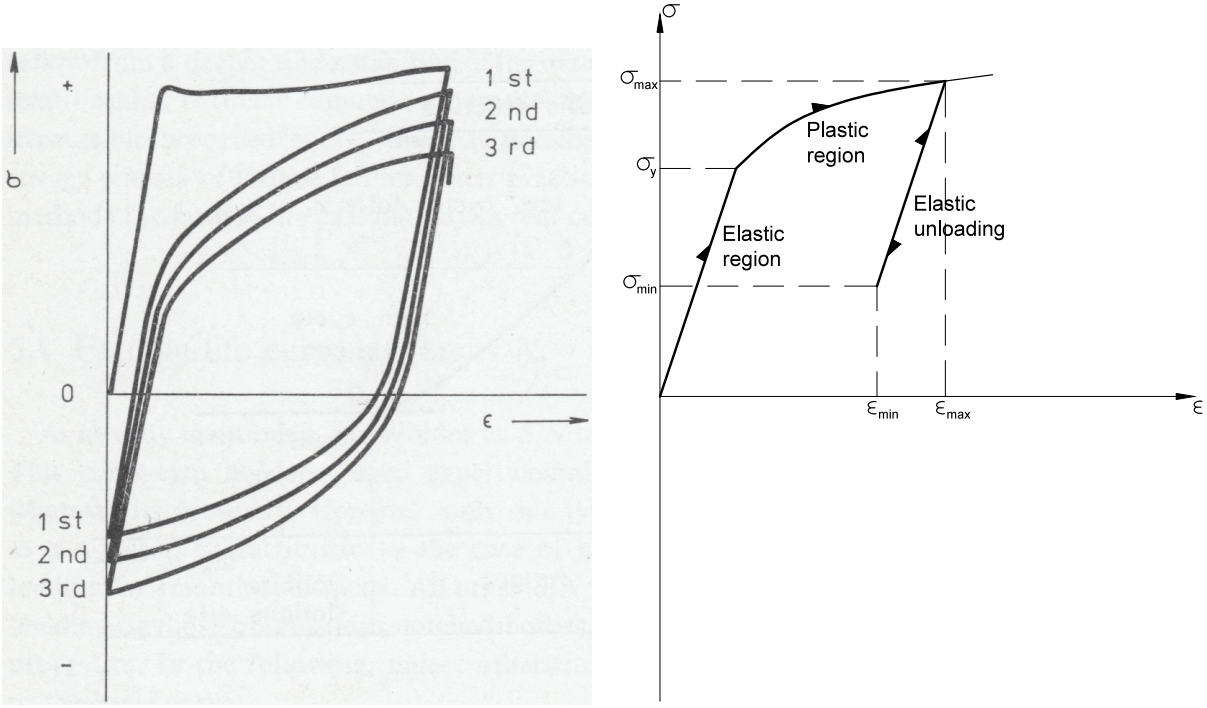

(a) Schematic drawing of stress relaxation for constant pulsating total strain amplitude[76]

(b) Fatigue stresses for cycles with small plastic strains

Figure 4.2: Finding the relevant stresses for the fatigue life calculation in the σ-ε-diagram

in figure 4.2b. During assembly of the system, when the cable harness is brought into its helical form and winded around the rotation axis for the first time, the flexural stresses in the copper strands increase along the corresponding stress-strain curve. At some point, we exceed the yield strength σ_y and leave the elastic region to enter the plastic region. In the first rotation cycle of the mechanism, the flexural stresses are further increased up to the maximum σ_{max}, which occurs at the maximum deployment angle $\varphi = 120°$, where the curvature radius of the electric cables reaches its minimum. When the deployment angle is reduced again, the stresses decrease parallelly to Hooke's line *("Elastic unloading")*, until the minimum σ_{min} is reached. From then on, the stress values move on a straight line between the upper and the lower limit in each and every rotation cycle after the first one. Due to work hardening, the yield strength has been raised to the maximum stress: $\sigma_y = \sigma_{max}$.

Important influence factors for the assessment of fatigue life are the stress ratio

$$\rho = \frac{\sigma_{min}}{\sigma_{max}} \tag{4.23}$$

and the amplitude ratio

$$A = \frac{\sigma_a}{\sigma_m} = \frac{1-\rho}{1+\rho} \tag{4.24}$$

which is defined as the ratio between the stress amplitude $\sigma_a = (\sigma_{max} - \sigma_{min})/2$ and the

[76] Figure taken from: Klesnil and Lukáš, 1980, p. 134

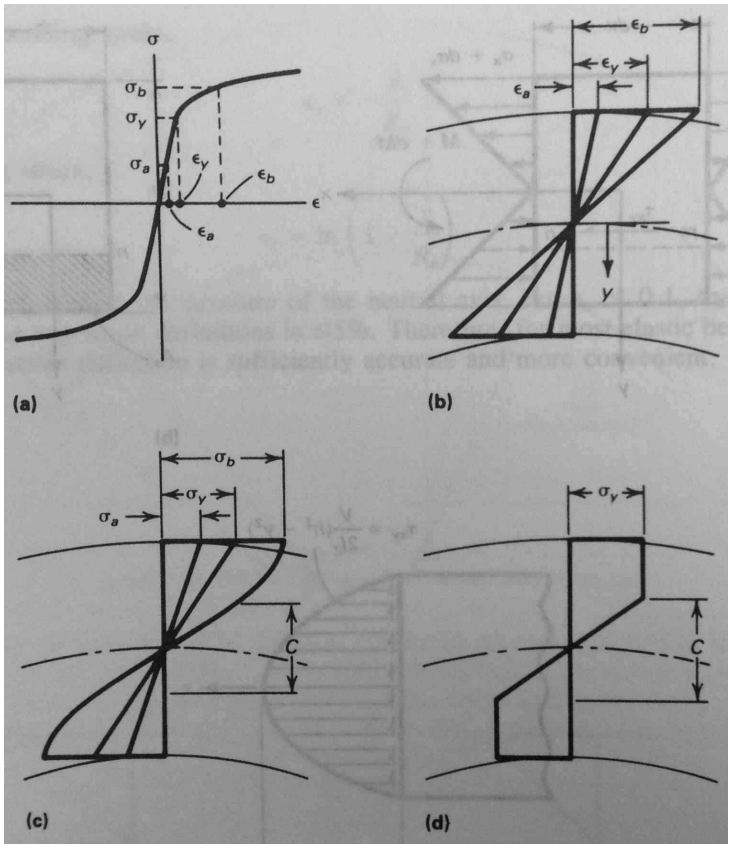

Figure 4.3: Stress-strain distribution in a beam. (a) Stress-strain curve. (b) Strain distribution. (c) Stress distribution. (d) Stress distribution for elastic-perfect plastic material.[77]

mean stress $\sigma_m = (\sigma_{max} + \sigma_{min})/2$.[78]

The maximum and minimum stresses which are required for the calculation of fatigue life can thus be read from the stress-strain curve of the material. They are given by the maximum and minimum strain, which in our case depends only on the geometry of the harness design and the electric cables. Therefore, the relation between the curvature radius of the cables and the resulting strain in the copper strands has to be found. Hereby, the strands are approximated as flexural beams with circular cross section with diameter d. The beam shall be bent to a constant curvature radius R. According to the *Atlas of Stress-Strain Curves*, we can assume a linear distribution of the longitudinal strain over the cross section given by $\varepsilon = -\,y/R$, where y is the distance from the neutral fiber.[79]

Note that this relation holds for elastic as well as plastic stresses, see also figure 4.3b. With the distance $e_u = d/2$ between the neutral fiber and the extreme fiber, the maximum stress in the extreme fiber (index EF) equals

$$\sigma_{EF} = E \cdot \varepsilon_{EF} = E\,\frac{e_u}{R}, \tag{4.25}$$

[77] Figure taken from: Boyer, 1990, p. 74

[78] cf. for example Iowa State University. *Fatigue Life Evaluation*, p. 4. URL: see Bibliography.

[79] cf. Boyer, 1990, p. 74.

as long as we stay in the elastic region. Once the yield strength is exceeded and the plastic region is reached, the stress resulting from the maximum strain in the extreme fiber can be read from the stress-strain curve (see figure 4.3a). The stress in the extreme fiber is therefore given by the function of the stress-strain curve $\sigma = \sigma(\varepsilon)$:

$$\sigma_{EF} = \sigma_{EF}(\varepsilon_{EF}) = \sigma_{EF}\left(\frac{e_u}{R}\right). \tag{4.26}$$

Since the Young's modulus E, the shape of the stress-strain curve and the distance of the extreme fiber e_u are properties of the electric cable, only the curvature radius R has to be determined. The maximum and minimum curvature radius, which the electric cables experience during the lifetime of the EPPM, are important influence factors for the fatigue stresses in the cables. Especially the differences in the curvature radius between two extremal positions in a single load cycle strongly determine those stresses which are the input for the fatigue calculation. Objective RSA-120 defines a large load cycle as deployment by 120° and a small load cycle as pointing by ±15°. This means that in the large cycle, the deployment angle ranges from 0° to 120°, while in the small cycle it ranges f.i. from 90° to 120°. In order to calculate the stresses at these deployment angles, we have to determine the respective curvature radii of the cables in each harness. The index OH represents the outer harness, while IH represents the inner harness.

With the assumption that at the maximum deployment angle ($\varphi = 120°$) the cable harness touches the underlying aluminum can along the whole cable length, the minimum curvature radius of each harness is determined by the diameter of the respective can (these diameters are given in chapter 3.3.6):

$$R_{OH,120°} = \frac{D_{can,OH}}{2} = \frac{110.0\,\mathrm{mm}}{2} = 55.0\,\mathrm{mm} \tag{4.27}$$

$$R_{IH,120°} = \frac{D_{can,IH}}{2} = \frac{82.6\,\mathrm{mm}}{2} = 41.3\,\mathrm{mm}. \tag{4.28}$$

We get the relation between the curvature radii at different deployment angles from the circumstance that the cable length is constant:

$$L = R_\varphi \cdot 2\pi \cdot n_\varphi = R_{120°} \cdot 2\pi \cdot n_{120°} \tag{4.29}$$

$$R_\varphi = R_{120°}\frac{n_{120°}}{n_\varphi}. \tag{4.30}$$

The number of windings for each harness at the maximum turning angle is

$$n_{OH,120°} = 5 \tag{4.31}$$

$$n_{IH,120°} = 4.4, \tag{4.32}$$

while the number of windings n_φ decreases with the difference in deployment angle:

$$n_\varphi = n_{120°} - \frac{\Delta\varphi}{360°} \tag{4.33}$$

with $\Delta\varphi = 120° - \varphi$. Now the curvature radii for the respective deployment angles can be computed:

$$R_{OH,0°} = R_{OH,120°} \frac{n_{OH,120°}}{n_{OH,120°} - \frac{120°}{360°}} = 58.9\,\mathrm{mm} \tag{4.34}$$

$$R_{IH,0°} = R_{IH,120°} \frac{n_{IH,120°}}{n_{IH,120°} - \frac{120°}{360°}} = 44.7\,\mathrm{mm} \tag{4.35}$$

$$R_{OH,90°} = R_{OH,120°} \frac{n_{OH,120°}}{n_{OH,120°} - \frac{30°}{360°}} = 55.9\,\mathrm{mm} \tag{4.36}$$

$$R_{IH,90°} = R_{IH,120°} \frac{n_{IH,120°}}{n_{IH,120°} - \frac{30°}{360°}} = 42.1\,\mathrm{mm}. \tag{4.37}$$

Together with equations (4.27) and (4.28), the curvature radii at the critical deployment angles are defined. From these radii, the elastic (or plastic) strain in the extreme fiber of the copper strands can be computed according to $\varepsilon = d/2R$ with the strand diameter d. Finally, the existing stresses in the strands can be read from the stress-strain diagram. For the stress computation of the Kapton jacket, the same curvature radii as above can be used, but we have to insert the diameter of the whole electric cable instead of the diameter of a single copper strand into the equation.

Once the existing stresses in the copper strands are found, the fatigue life can be assessed via the Smith diagram. Due to work hardening of the material in the very first cycle, the yield point is raised to the maximum stress experienced by the copper strands. Therefore, the upper stress limit used in the fatigue calculation is always equal to the yield strength: $\sigma_{max} = \sigma_y$. The lower stress limit depends on the amount of unloading, which in turn is a function of the difference in curvature radius between two extremal points. An increase in curvature radius (ΔR), which is experienced in a single cycle, leads to elastic unloading and therefore a decrease of the flexural stresses ($\Delta\sigma$). The lower stress limit is therefore $\sigma_{min} = \sigma_{max} - \Delta\sigma$. A higher value of ΔR causes a higher stress decrease $\Delta\sigma$, which results in a higher stress amplitude and therefore a worse load case. According to equation (2.6), a higher number of windings leads to a lower radial difference. Thus it is very effective to plan a high number of harness windings already in the design process in order to increase the fatigue life of the mechanism.

In the Smith diagram (figure 4.4), three possible fatigue load types depending on the level of $\Delta\sigma$ are depicted. As mentioned before, the maximum fatigue stress σ_{max} is always equal to the yield strength. For arbitrary $\Delta\sigma$, the minimum fatigue stress σ_{min} will stay on the line labeled with *"L"* or its dashed extension. This is because due to symmetry reasons

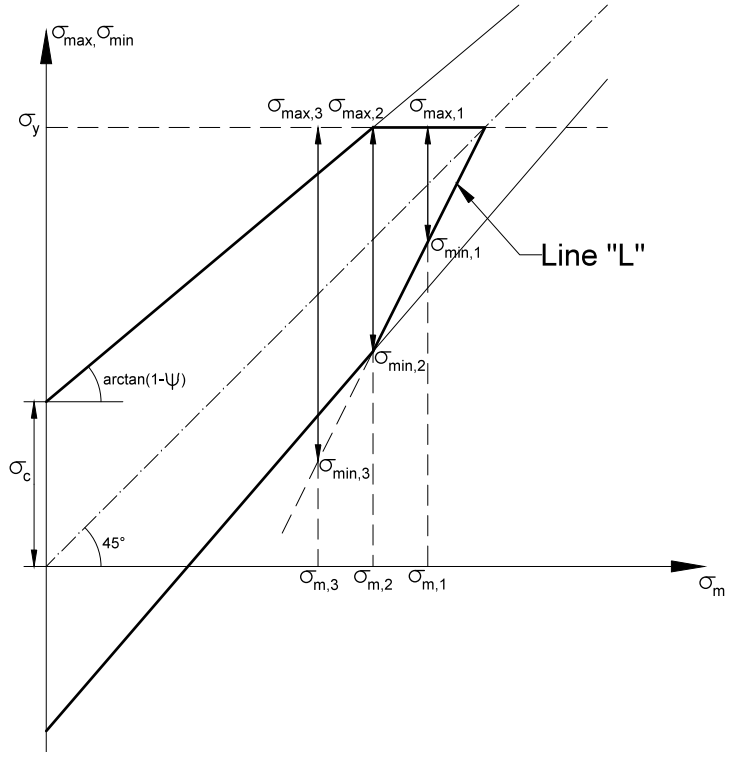

Figure 4.4: Smith diagram for three possible load types depending on $\Delta\sigma$[80]

the vertical distance between the line *L* and the mean stress line (dot-dashed line under 45°) is equal to the distance between the mean stress line and the horizontal line $\sigma = \sigma_y$. Therefore, the mean fatigue stress $\sigma_m = (\sigma_{max} + \sigma_{min})/2 = \sigma_{max} - \Delta\sigma/2$ is located on the mean stress line if and only if the minimum fatigue stress stays on the line *L*.

Load type 1 in figure 4.4 (cycle between $\sigma_{max,1}$ and $\sigma_{min,1}$) is therefore exactly on the borderline of the Smith diagram, which means that the fatigue limit is just reached. We are in the *fail-safe* region, which means that the structure is able to withstand an infinite or very large number of cycles to failure (usually at least 10^7 cycles[81]). The same is true for load type 2, which has a higher $\Delta\sigma$ than the first load type. Also in this case the fatigue limit is just reached and there is no risk of fatigue failure. If we though consider a load type with an even higher $\Delta\sigma$ (load type 3), we leave the fail-safe region and have to evaluate the *safe-life* of the component. This means that the material is only able to withstand a finite number of cycles to failure. This number of cycles cannot be determined with the Smith diagram, as it shows only the fatigue limit under influence of mean stress. Instead, we would have to use the Wöhler curve or S-N-curve in order to determine the number of cycles to failure at the respective stress level.

Load type 2 is therefore just on the boundary between the fail-safe and safe-life region. If the allowed stress amplitude at this location is denoted by σ_c^*, we can define the margin

[80] cf. Figure in: Klesnil and Lukáš, 1980, p. 152

[81] cf. https://www.nde-ed.org/EducationResources/CommunityCollege/Materials/Mechanical/S-NFatigue.htm (visited on Nov. 2, 2015).

of safety for infinite service life for a certain load type given by the level of $\Delta\sigma$ to

$$MS = \frac{\sigma_c^* - \frac{\Delta\sigma}{2}}{\sigma_c^*} = 1 - \frac{\Delta\sigma}{2\sigma_c^*} \qquad [\%]. \tag{4.38}$$

The value of σ_c^* can be calculated from the alternating fatigue strength σ_c and the coefficient ψ, which are both properties of the underlying material. The slope of the upper fatigue limit line is given by the latter according to the equation $\sigma_{Ac} = \sigma_c - \psi\sigma_m$,[82] which yields for the angle of the line $\arctan(1 - \psi)$. Klesnil and Lukáš give the alternating fatigue strength of pure copper to $\sigma_c = 79$ MPa and the ultimate tensile strength to $\sigma_{UTS} = 212$ MPa.[83] The coefficient ψ depends on the ultimate tensile strength and is zero in this case due to the relatively low σ_{UTS}.[84] Therefore, the upper fatigue limit line has an angle of 45° to the abscissa and $\sigma_c^* = \sigma_c = 79$ MPa (for pure copper). Similar values for the alternating fatigue strength σ_c of different copper alloys are given in the literature: about 75 MPa for *Leaded Red Brass*, 120 MPa for *Manganese Bronze*, 150 MPa for different types of *Silicon Brass*, 60 MPa for *Navy "M" Bronze* and 80 MPa for *High-Leaded Tin Bronze*.[85] For a copper-nickel alloy with 10 % nickel, the fatigue strength is given by 93 MPa.[86]

With this result, all necessary equations and parameters for the assessment of fatigue life under small plastic strain values have been found. In the next chapters, the fatigue life of the copper strands and the Kapton jacket will be evaluated.

4.2.2 Evaluation of Fatigue Life for the Copper Strands

Now we can compute the stresses in the individual copper strands. The core of the electric cables used in the outer harness consists of thirty strands made of nickel-plated copper with a diameter of 0.25 mm (see data sheet in appendix B). As mentioned before, the individual strands are not rigidly connected and therefore the stress conditions are similar in every single strand, if the small difference in curvature radius between the inner and outer strands of a single wire is neglected.

The cables used in the inner harness are twisted shielded pairs of wires. The core of each wire consists of nineteen strands with a diameter of 0.1 mm each. They are made of silver-plated copper alloy. The electromagnetic shielding of the wires is realized by a helicoidal shield consisting of silver plated copper strands. The strands of the shielding have a diameter of 0.079 mm and are therefore not as critical as the core strands.

The yield strength and stress-strain diagrams of copper are taken from the COPPER DEVELOPMENT ASSOCIATION INC. The yield strength of the copper alloy No. 706 (cop-

[82] Klesnil and Lukáš, 1980, p. 152.
[83] cf. ibid., p. 161.
[84] cf. ibid., p. 152.
[85] cf. Boyer, 1999, pp. 400–404.
[86] cf. Deutsches Kupferinstitut. *CuNi10Fe1Mn*, p. 7. URL: see Bibliography.

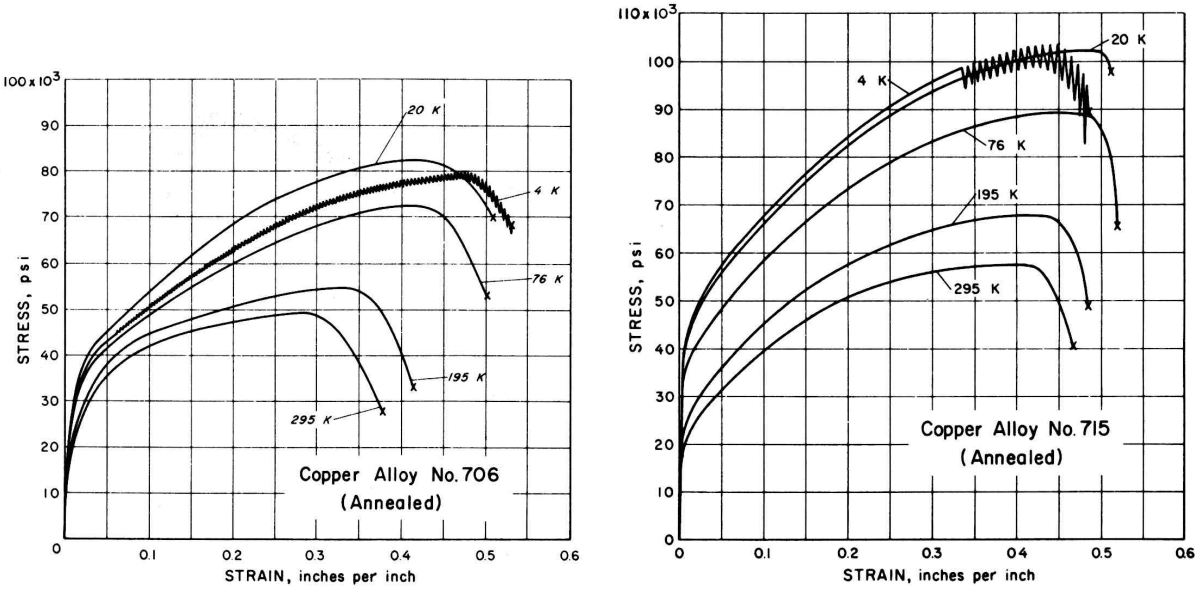

(a) Copper-nickel alloy with 10 % nickel (b) Copper-nickel alloy with 30 % nickel

Figure 4.5: Stress-strain diagrams of different copper-nickel alloys[87]

per with 10 % nickel) equals 21 400 psi or about 148 MPa, while the yield strength of the copper alloy No. 715 (copper with 30 % nickel) equals 18 700 psi or about 129 MPa.[88] The respective stress-strain diagrams are depicted in figure 4.5. It has to be mentioned that the strands of the outer harness cables consist of nickel-plated copper, while the strands of the inner harness cables are made of silver-plated copper alloy. The exact material data for these copper alloys could not be found, which is why the values of the alloys mentioned above have to be used as an estimation.

With the Young's modulus of copper ($E_{copper} = 117\,000$ MPa, see before) and the respective curvature radius taken from equations (4.27) and (4.28), we can calculate the maximum stress in the conductor strands of each harness to

$$\sigma_{OH,120°} = E_{copper}\,\frac{d_{strand,OH}}{2R_{OH,120°}} = 117000 \cdot \frac{0.25}{2 \cdot 55.0}\ \mathrm{N/mm^2} = 265.9\ \mathrm{N/mm^2} \tag{4.39}$$

$$\sigma_{IH,120°} = E_{copper}\,\frac{d_{strand,IH}}{2R_{IH,120°}} = 117000 \cdot \frac{0.1}{2 \cdot 41.3}\ \mathrm{N/mm^2} = 141.6\ \mathrm{N/mm^2}. \tag{4.40}$$

The computed stress of the outer harness cables lies far above the yield strength. Therefore, plastic deformations occur at least in the cables of the outer harness. Since Hooke's law given in equation (4.25) cannot be applied for the calculation of plastic stresses, we have to read the stress directly from the diagram according to equation (4.26). As it was mentioned before, a linear strain distribution over the cross section of the copper strand is

[87] Figures taken from: Copper Development Association Inc. *Application Data Sheet: Mechanical Properties of Copper and Copper Alloys at Low Temperatures*. URL: see Bibliography.

[88] cf. ibid.

assumed. Calculating the elongation in the extreme fiber of the copper strands yields

$$\varepsilon_{OH,120°} = \frac{d_{strand,OH}}{2R_{OH,120°}} = \frac{0.25}{2 \cdot 55.0} = 0.00227 = 0.227\,\% \tag{4.41}$$

$$\varepsilon_{IH,120°} = \frac{d_{strand,IH}}{2R_{IH,120°}} = \frac{0.1}{2 \cdot 41.3} = 0.00121 = 0.121\,\%. \tag{4.42}$$

On the abscissa of the stress-strain diagrams (figure 4.5), the strain is displayed in *inches per inch*. The individual scale lines are plotted at a distance of 0.05 inches per inch, which is equal to an elongation of 5 %. The low strain values in the copper strands, which lie below 0.23 %, make it impossible to read correct stress data from these stress-strain diagrams. All that can be said is that the stress for 0.25 % strain lies under about 22 ksi (`kilopounds per square inch`) for alloy No. 706 or 20 ksi for alloy No. 715. This means that in the worst case, the plastic stress in the extreme fiber equals 151.7 MPa.

Now the relevant stress amplitude for the fatigue calculation is to be found. In our case, regardless of whether or not the yield strength was exceeded in the first load cycle, the stress relief during unloading always occurs parallelly to Hooke's line:

$$\Delta\sigma = E \cdot \Delta\varepsilon. \tag{4.43}$$

This is because of the small levels of unloading compared to the overall level of strain (this was shown in figure 4.2b).

At first, a large cycle (deployment between 0° and 120°) is considered. When the deployment angle of the pointing mechanism is reduced to zero, the harness starts to unroll and the curvature radius goes up to its initial value, which is given in equations (4.34) and (4.35). This leads to the following strain values in the extreme fiber of the copper strands:

$$\varepsilon_{OH,0°} = \frac{d_{strand,OH}}{2R_{OH,0°}} = \frac{0.25}{2 \cdot 58.9} = 0.00212 = 0.212\,\% \tag{4.44}$$

$$\varepsilon_{IH,0°} = \frac{d_{strand,IH}}{2R_{IH,0°}} = \frac{0.1}{2 \cdot 44.7} = 0.00112 = 0.112\,\%. \tag{4.45}$$

For a large cycle (index LC) in fatigue loading we get a stress reduction in the outer and inner harness cables by

$$\begin{aligned}\Delta\sigma_{OH,LC} = E_{copper} \cdot (\varepsilon_{OH,120°} - \varepsilon_{OH,0°}) &= 117000 \cdot (0.00227 - 0.00212)\ \mathrm{N/mm^2} \\ &= 17.6\ \mathrm{N/mm^2}\end{aligned} \tag{4.46}$$

$$\begin{aligned}\Delta\sigma_{IH,LC} = E_{copper} \cdot (\varepsilon_{IH,120°} - \varepsilon_{IH,0°}) &= 117000 \cdot (0.00121 - 0.00112)\ \mathrm{N/mm^2} \\ &= 10.5\ \mathrm{N/mm^2}.\end{aligned} \tag{4.47}$$

For the small cycle (tilting by ±15°), the relevant curvature radii are given in equa-

tions (4.36) and (4.37). With these values, we get a strain in the outer and inner harness cables of

$$\varepsilon_{OH,90°} = \frac{d_{strand,OH}}{2R_{OH,90°}} = \frac{0.25}{2 \cdot 55.9} = 0.00224 = 0.224\,\% \tag{4.48}$$

$$\varepsilon_{IH,90°} = \frac{d_{strand,IH}}{2R_{IH,90°}} = \frac{0.1}{2 \cdot 42.1} = 0.00119 = 0.119\,\% \tag{4.49}$$

and a stress reduction in the small cycle (index SC) by

$$\begin{aligned} \Delta\sigma_{OH,SC} = E_{copper} \cdot (\varepsilon_{OH,120°} - \varepsilon_{OH,90°}) &= 117000 \cdot (0.00227 - 0.00224)\ \mathrm{N/mm^2} \\ &= 3.51\ \mathrm{N/mm^2} \end{aligned} \tag{4.50}$$

$$\begin{aligned} \Delta\sigma_{IH,SC} = E_{copper} \cdot (\varepsilon_{IH,120°} - \varepsilon_{IH,90°}) &= 117000 \cdot (0.00121 - 0.00119)\ \mathrm{N/mm^2} \\ &= 2.34\ \mathrm{N/mm^2}. \end{aligned} \tag{4.51}$$

The highest level of stress reduction therefore occurs in the outer harness cables during a large fatigue cycle. The maximum and minimum stress in this load case amount to

$$\sigma_{max} = \sigma_{OH,120°} = 151.7\ \mathrm{N/mm^2} \tag{4.52}$$

$$\sigma_{min} = \sigma_{max} - \Delta\sigma_{OH,LC} = 134.1\ \mathrm{N/mm^2}. \tag{4.53}$$

The fatigue stress ratio is calculated to

$$\rho = \frac{\sigma_{min}}{\sigma_{max}} = \frac{134.1\ \mathrm{N/mm^2}}{151.7\ \mathrm{N/mm^2}} = 0.884 \tag{4.54}$$

and the amplitude ratio

$$A = \frac{\sigma_a}{\sigma_m} = \frac{8.8\ \mathrm{N/mm^2}}{142.9\ \mathrm{N/mm^2}} = 6.2\,\%, \tag{4.55}$$

which indicates a fluctuating tensile stress history, as opposed to reversed fatigue loading (characterized by $\rho = -1$). The assumption that the stress variations during operation of the mechanism are small compared to the overall level of stress is therefore valid. The material experiences no additional plasticizing in the load cycles after the first one, and the unloading occurs parallelly to Hooke's line in the stress strain diagram.

These results lead to the following conclusion: the majority of mechanical stresses in the copper strands is induced by pre-bending the cable harness to its final form, with the minimum curvature radius at the maximum deployment angle $\varphi = 120°$. This bending leads to slight plastic deformations in the copper strands. When the deployment angle is reduced, the mechanical stresses decrease according to Hooke's law. Since there is no plasticizing in opposite direction upon unloading, every movement of the harness in every

subsequent cycle causes only elastic stresses in the stranding. Work hardening due to the plastic deformation occurs, but is neglectible because the stresses evaluated from the stress-strain diagrams barely lie above the yield strength.

Using the smallest value for the fatigue strength given at the end of chapter 4.2.1, namely $\sigma_c = 60\,\text{MPa}$, we can compute the margin of safety for the worst load case with equations (4.46) and (4.38) to

$$MS = 1 - \frac{\Delta\sigma}{2\sigma_c} = 1 - \frac{17.6\ \text{N/mm}^2}{2 \cdot 60\ \text{N/mm}^2} = 85.3\,\%. \tag{4.56}$$

The margin of safety is very high, which indicates a large safety against fatigue failure during operation. Furthermore, what has been calculated hereby is the margin of safety for the fail-safe region. A structure is considered fail-safe if it is able to withstand an infinite or at least very large number of cycles to failure (typically over 10^7 cycles), while the required number of cycles specified in the objective is around 10^5. Requirement RSA-120 is therefore fulfilled for the copper strands.

4.2.3 Evaluation of Fatigue Life for the Kapton Jacket

For the stress calculation in the Kapton jacket of the harness cables, the same curvature radii as in the last chapter can be used. Instead of the strand diameter, the overall outer diameter of the whole electric cable is used to compute the stresses in the extreme fiber of the Kapton insulation. According to the data sheets in appendix B, the outer diameter of the cables used in the outer harness is 2.2 mm, while the diameter of the inner harness cables is 2.3 mm.

The Young's modulus of Kapton is $E_{kapton} = 2500\,\text{MPa}$ and the yield point is given by the yield strength of 69 MPa at an elongation of 3 %.[89] With the curvature radii taken from equations (4.27) and (4.28), the maximum stress in the insulation can be calculated to

$$\sigma_{OH,120°} = E_{kapton}\,\frac{d_{cable,OH}}{2R_{OH,120°}} = 2500 \cdot \frac{2.2}{2 \cdot 55.0}\ \text{N/mm}^2 = 50.0\ \text{N/mm}^2 \tag{4.57}$$

$$\sigma_{IH,120°} = E_{kapton}\,\frac{d_{cable,IH}}{2R_{IH,120°}} = 2500 \cdot \frac{2.3}{2 \cdot 41.3}\ \text{N/mm}^2 = 69.6\ \text{N/mm}^2\,. \tag{4.58}$$

This time, the critical cables are the ones of the inner harness due to the larger diameter and smaller curvature radius. The maximum stress is just slightly above the yield strength, but taking a look at the occurring strain in the extrem fiber of the critical cables

$$\varepsilon_{IH,120°} = \frac{d_{cable,IH}}{2R_{IH,120°}} = \frac{2.3}{2 \cdot 41.3} = 0.0278 = 2.78\,\%, \tag{4.59}$$

[89] cf. E. I. du Pont de Nemours and Company. *DEC Kapton – Summary of Properties*, p. 4. URL: see Bibliography.

we can conclude that the strain still lies below the yield point which is given by an elongation of 3 %.

The other relevant stress values for the large and small fatigue cycles can be calculated using the curvature radii from equations (4.34) to (4.37):

$$\sigma_{OH,0°} = E_{kapton}\,\frac{d_{cable,OH}}{2R_{OH,0°}} = 2500 \cdot \frac{2.2}{2 \cdot 58.9}\ \mathrm{N/mm^2} = 46.7\ \mathrm{N/mm^2} \tag{4.60}$$

$$\sigma_{IH,0°} = E_{kapton}\,\frac{d_{cable,IH}}{2R_{IH,0°}} = 2500 \cdot \frac{2.3}{2 \cdot 44.7}\ \mathrm{N/mm^2} = 64.3\ \mathrm{N/mm^2} \tag{4.61}$$

$$\sigma_{OH,90°} = E_{kapton}\,\frac{d_{cable,OH}}{2R_{OH,90°}} = 2500 \cdot \frac{2.2}{2 \cdot 55.9}\ \mathrm{N/mm^2} = 49.2\ \mathrm{N/mm^2} \tag{4.62}$$

$$\sigma_{IH,90°} = E_{kapton}\,\frac{d_{cable,IH}}{2R_{IH,90°}} = 2500 \cdot \frac{2.3}{2 \cdot 42.1}\ \mathrm{N/mm^2} = 68.3\ \mathrm{N/mm^2}. \tag{4.63}$$

From this we can calculate the stress variation in the individual harnesses during the different load cycles:

$$\Delta\sigma_{OH,LC} = \sigma_{OH,120°} - \sigma_{OH,0°} = 50.0\ \mathrm{N/mm^2} - 46.7\ \mathrm{N/mm^2} = 3.3\ \mathrm{N/mm^2} \tag{4.64}$$

$$\Delta\sigma_{IH,LC} = \sigma_{IH,120°} - \sigma_{IH,0°} = 69.6\ \mathrm{N/mm^2} - 64.3\ \mathrm{N/mm^2} = 5.3\ \mathrm{N/mm^2} \tag{4.65}$$

$$\Delta\sigma_{OH,SC} = \sigma_{OH,120°} - \sigma_{OH,90°} = 50.0\ \mathrm{N/mm^2} - 49.2\ \mathrm{N/mm^2} = 0.8\ \mathrm{N/mm^2} \tag{4.66}$$

$$\Delta\sigma_{IH,SC} = \sigma_{IH,120°} - \sigma_{IH,90°} = 69.6\ \mathrm{N/mm^2} - 68.3\ \mathrm{N/mm^2} = 1.3\ \mathrm{N/mm^2}. \tag{4.67}$$

Besides the highest amount of stress, the inner harness cables experience also the highest level of stress reduction during a large fatigue cycle. From the maximum and minimum stress in this load case, we get the fatigue stress ratio

$$\rho = \frac{\sigma_{min}}{\sigma_{max}} = \frac{64.3\ \mathrm{N/mm^2}}{69.6\ \mathrm{N/mm^2}} = 0.924 \tag{4.68}$$

and the amplitude ratio

$$A = \frac{\sigma_a}{\sigma_m} = \frac{2.65\ \mathrm{N/mm^2}}{66.95\ \mathrm{N/mm^2}} = 3.96\,\%, \tag{4.69}$$

As the fatigue strength of Kapton could not be retrieved, the values of Vespel will be used as an estimation, which is also a polyimide manufactured by DUPONT.[90] The flexural fatigue (endurance limit) at 10^3 cycles is given by 65.5 MPa and the endurance limit at 10^7 cycles is 44.8 MPa.[91] However, these are the values for a fully reversed stress history with $\sigma_{min} = -\sigma_{max}$ and $\rho = -1$, which is the worst load case. For the same level of

[90] cf. http://www.dupont.com/products-and-services/plastics-polymers-resins/parts-shapes/brands/vespel-polyimide/products/vespel-s.html (visited on Nov. 23, 2015).

[91] cf. E. I. du Pont de Nemours and Company. *DuPont™ Vespel® SP-1 – Polyimide Isostatic Shapes*, p. 1. URL: see Bibliography.

maximum stress, a fluctuating tensile stress (load case with $0 < \rho < 1$) as it is found in our case leads to a longer fatigue life and is therefore much more favorable.[92]

The same scheme of calculation as for the copper strands can be used, but it must be pointed out that the fatigue calculation methods and the principle of the Smith diagram were developed for metallic materials and can only be adapted to synthetic materials with great caution. Therefore, the worst value of ψ given by Klesnil and Lukáš ($\psi = 0.25$)[93] is to be used for the calculation of σ_c^*. As pointed out above, the upper fatigue limit line is given by the equation

$$\sigma_u = \sigma_c + \sigma_m(1 - \psi) = \sigma_c + 0.75\sigma_m. \tag{4.70}$$

The value of σ_m where the upper fatigue limit line crosses the yield strength is calculated to

$$\sigma_c + 0.75\sigma_m^* = \sigma_y \tag{4.71}$$

$$\sigma_m^* = \frac{\sigma_y - \sigma_c}{0.75} \tag{4.72}$$

and the maximum allowable stress amplitude at this location is

$$\sigma_c^* = \sigma_y - \sigma_m^* = \frac{\sigma_c - 0.25\sigma_y}{0.75}. \tag{4.73}$$

With $\sigma_c = 44.8\,\text{MPa}$ for 10^7 cycles and $\sigma_y = 69\,\text{MPa}$, we get

$$\sigma_c^* = \frac{44.8 - 0.25 \cdot 69}{0.75}\ \text{N/mm}^2 = 36.7\ \text{N/mm}^2. \tag{4.74}$$

The margin of safety for the worst load case in the Kapton jacket is finally calculated via the equations (4.65) and (4.38) and amounts to

$$MS = 1 - \frac{\Delta\sigma}{2\sigma_c^*} = 1 - \frac{5.3\ \text{N/mm}^2}{2 \cdot 36.7\ \text{N/mm}^2} = 92.8\,\%. \tag{4.75}$$

Again, the margin of safety for fail-safe is very high. Thus also the Kapton insulation is able to withstand more than the required number of load cycles and objective RSA-120 is fully reached.

[92] cf. engr.bd.psu.edu/rxm61/MET210/Lecture/Chapter5_partA.ppt, p. 24 (visited on Nov. 20, 2015).
[93] cf. Klesnil and Lukáš, 1980, p. 152.

Chapter 5

Summary

5.1 Tasks and Methodological Approach

The goal of this diploma thesis was to find a feasible solution for the electric cable harness routing via several rotation axes of the so-called *Electric Propulsion Pointing Mechanism* (EPPM) developed by RUAG SPACE AUSTRIA (RSA). The pointing mechanism is a device used for mounting and control of electric propulsion thrusters (ion thrusters or Hall-effect thrusters). A schematic sketch of the mechanism is given in figure 1.1. The ion thruster can be moved around several rotation axes by geared actuators. The electric cable harness serving as supply and control of the thruster as well as the actuator must be able to compensate this rotational movement as it connects the thruster to the spacecraft via these rotation axes. The challenge for the designer of the cable harness is on the one hand the high flexural stiffness of these cables leading to a resistive torque to be overcome by the geared actuator, and on the other hand the repeated flexing of these cables leading to fatigue of the material and probable damage of the cables. The requirements for the harness design have been defined in chapter 1.2 and are as follows:

- X-ray radiation resistance of all materials against at least 100 Mrad
- Deployment angle of up to 120°
- Fatigue life of 1000 large cycles and 100 000 small cycles
- Axial installation length smaller than 150 mm, inner diameter of helix larger than 82 mm and outer diameter smaller than 140 mm
- Maximum resistive torque of 3 Nm
- Separation between high voltage harness and low voltage harness by electromagnetic shielding

- Twenty cables with nominal cross section of 1.5 mm^2 for the high voltage harness and twenty-seven cables size AWG 26 for the low voltage harness

Based on these objectives, a trade-off between several design alternatives of certain cable harness features was performed. This was done partly by analytical computations and partly by investigations of the laboratory model which was set up in the Mechanical AIV of RSA. Hereby, the cable harness was recreated with Nylon wires with a full circular cross section. For the cable harness routing, the *torsion spring layout* according to figure 2.1 was chosen as it has already been found by RSA to be the best suited layout for this application.

An important parameter for the harness design is the number of windings around the rotation axis. In chapter 2.3, we found that the amplitudes of repetitive flexural stresses and resistive torque are inversely proportional to the number of windings according to equation (2.6). Therefore an increase in the number of windings leads to a higher fatigue life and a more uniform load characteristic for the geared actuator.

Two different winding forms were investigated in the laboratory: the inclined routing (see figure 2.2), where all the windings are positioned next to each other without overlapping, and the overlapped routing (figure 2.3) with the extreme form of perpendicular routing, where all the windings are positioned completely above each other. A detailed description is given in chapter 2.4. All of these winding forms have their individual advantages and disadvantages on the axial and radial installation space, respectively. The inclined routing saves radial space but spreads out in axial direction, while the perpendicular routing takes up minimal space in axial direction but has large space requirements in radial direction. Due to the other downsides of the perpendicular routing form (difficult assembly procedure, geometric instability and increased friction torque), this method was discarded and the inclined routing form was chosen.

In chapter 2.5, we investigated the possibility of creating a multiple-layer harness by arranging the harness cables of the individual windings above each other. By this means, the axial space requirement can be significantly reduced, leading to a decrease of installation space, a possible increase in the number of windings, or both. The number of cable layers in radial direction is therefore a powerful parameter in order to reach the different design goals.

The different methods for the conjunction of individual harness cables are described in chapter 2.6. Possible conjunction methods are: connection by lacing cord and metal pins, connection by ovally-bent copper pins and connection by a perforated plastic film. A comparison and trade-off between these methods was done using the *weighted point rating system* according to chapter 2.1. The assessment criteria were: Expenditure of time for production and assembly, strength of conjunction, possibility of creating a multi-layer harness, effect on resistive torque, and geometric stability of the resulting harness. The conjunction method using a synthetic film was clearly dominating and was therefore

chosen for the final design of the harness.

With this method, the harness cables are pulled through the perforations in the plastic film in order to be connected together. As depicted in figure 2.9, this method is also feasible for a multi-layer harness. A simple but also convenient production method for the film was found with manual punching. Furthermore, a usable material for the film had to be found. The requirements were a sufficient resistance against radiation, a not too high Young's modulus in order for the cables not to get damaged, and about the same flexural stiffness as the film used in the laboratory. With polyetheretherketone (PEEK), a material was found which fulfills all these requirements. Eventually, a film made from this material was ordered from the Austrian company LITE GMBH.

Finally, several possible methods for the fixation of the cable harness to the EPPM flanges were investigated in chapter 2.7. Hereby, different methods were chosen for the moving part of the harness (i.e. the part winded around the rotation axis) and the fixed part of the harness (the part fixed to the boom or the spacecraft itself, which is therefore not movable). For the latter, the well-tried method using a clamp part support (figure 2.15) was chosen because of its simplicity and the sufficient usability at the low load levels occurring at these locations. For the moving harness on the other hand, the fixation method using a drilled plastic block was chosen (figure 2.13). The harness cables are pulled through these drill holes and stay there by the friction between the cable surface and the inner surface of the hole. The block itself is then mounted to the flange by a corner plate. This method is characterized by its stability, a significantly easier assembly than the other methods, and almost no risk of cable damage due to contact forces.

5.2 Results

5.2.1 Measurement Results

One main task for this diploma thesis was the laboratory work, where different design versions of the cable harness were modelled (using dummy cables made from Nylon) and torque measurements were performed. The test setup was improved to the effect that the measurements could be taken by a torque wrench instead of a spring scale (see chapter 3.1). This gives way to a much more convenient measurement procedure where errors generated by human imperfection were greatly reduced while the precision was even increased.

The expected measurement results are schematically given in figure 3.4. Due to internal friction in the harness system, a hysteresis loop was expected to occur in the torque-angle characteristic curve. The mean value of this hysteresis is defined as spring torque, which is caused by the elastic flexure of the harness cables during rotation of the mechanism. The friction torque is defined as half the width of the hysteresis loop and is a measure

for the level of friction in the harness system. The maximum value of torque (spring torque plus friction torque) is called resistive torque and has to be overcome by the geared actuator.

Starting point for the laboratory work was the initial harness design developed by RSA, which is described in chapter 3.3.1. It consisted of an outer harness (high voltage harness) and two inner harnesses (low voltage harnesses) with a total of sixty cables. The wires were arranged in a planar cable consisting of a single layer only. The cable connection was realized by a perforated film made of low-density polyethylene for the outer harness and by lacing cord and metal pins for the inner harnesses. The cables were fixed to the flanges by aluminum brackets. According to the RSA technical report, the measured torque for a rotation by 180° amounted to 3.26 Nm. A measurement in the lab revealed that the axial length of the harness was about 270 mm and the diameter was about 180 mm.

The history of laboratory design versions is described in chapters 3.3.2 to 3.3.5. All of these versions have in common that the conjunction method between the individual cables was kept the same (perforated plastic film). The number of cable layers was increased to eventually three layers, which brought many geometric advantages. The axial length of the harness were reduced while the number of windings were increased from one and a half windings in the initial state to three full windings in the last version. This also had a positive effect on the torque characteristic of the harness. The fixation of the cables to the flanges was realized by a plastic block. The outer radius of the harness was even more reduced by mounting the block as near to the rotation axis as possible.

In chapter 3.3.6, the results from the previous versions were used in order to determine the parameters of the final harness design. In contrast to the initial version, there was only one inner cable harness (low voltage harness) consisting of twenty-seven cables in order to comply with the thesis objectives. The inner harness was designed after the same principle than the outer harness. At first, the required diameters and possible number of windings of both harnesses were computed. Starting from a minimum inner diameter of the inner harness of 82.6 mm, a maximum outer diameter of 106.6 mm was calculated. The diameter of the aluminum can separating the high voltage and low voltage harness was chosen to be 110 mm. Finally, the maximum outer diameter of the outer cable harness was calculated to 136.1 mm, which fulfills the requirement of being below 140 mm. The maximum possible number of windings is 5 for the outer harness and 4.4 for the inner harness. The number of layers of each harness was fixed to be three.

Finally, in chapter 3.3.7 the breadboard testing of this final version is described. With an axial length of 141 mm, a maximum outer diameter of 140 mm and a minimum inner diameter of 86.6 mm, the geometric requirements are fulfilled. Torque measurements (see table 3.7 and figure 3.21) revealed a maximum resistive torque of 2.3 Nm, which is below the allowed value of 3 Nm. The friction torque amounts with its maximum value of 275 Nmm to only 12 % of the resistive torque and behaves uniformly over the measurement range.

With these results, also the requirements for the torque characteristic are fulfilled.

5.2.2 Computational Results

In order to check if the chosen geared actuator *SA-15* is sufficiently dimensioned for this application, an estimation of the actual rotational torque had to be made first. Afterwards, the measurement values obtained in chapter 3 were used in an equation for the dimensioning of actuators in space flight according to the standard ECSS-E-ST-33-01C by the EUROPEAN COOPERATION FOR SPACE STANDARDIZATION (ECSS).

The estimation of the actual torque was performed in chapter 4.1.1. The flexural stiffness of the dummy cables used for the outer cable harness during breadboard testing was determined by mounting a cable piece as cantilever beam. It amounts to 10 900 Nmm^2. The stiffness of the real electric cables was estimated mathematically and is about 2800 Nmm^2. The flexural stiffness of the dummy cables used in the inner harness as well as those electric cables was again determined by means of a cantilever beam and amounts to 680 Nmm^2 and 450 Nmm^2, respectively. This yields a stiffness ratio of 3.89 for the outer harness and 1.51 for the inner harness. Both types of dummy cables (inner harness as well as outer harness) have therefore a higher flexural stiffness than the real electric cables which will be used in the mechanism. The laboratory test setup is thus a conservative model regarding the measurements of the rotational torque. Furthermore, the effect of the inner cable harness on the resistive torque was estimated to be about one order of magnitude lower than the effect of the outer cable harness.

Inserting the torque measurement values with their respective uncertainty factors (see table 4.1) into said equation gave us a minimum actuation torque of 10.14 Nm. This calculation was done in chapter 4.1.2. The geared actuator is able to deliver an unpowered holding torque of 12 Nm, which gives a margin of safety of 18.3 %. Although this margin is very low, the chosen geared actuator should be sufficiently dimensioned because the measurements were taken on a system which is more than three times as stiff as the real application.

Another important task was the strength calculation and fatigue lifetime prediction of the harness system, which was done in chapter 4.2. The requirement was that the harness system is able to withstand 1000 large cycles and 100 000 small cycles, characterized by the magnitude of angular rotation of the mechanism. The flexural stresses in the cables depend on the global deformations, which are given by the geometry and the current deployment angle of the mechanism. The stress calculation was performed for the copper conductors of the electric cables as well as for the insulation made from the synthetic material Kapton.

In chapter 4.2.1, we developed a procedure for the calculation of fatigue life for low levels of plastic deformations. This was important because the copper strands experience

plastic stress, which is though only slightly above the yield strength of copper. Bearing in mind that the deformation of the electric cables is strain-controlled, we found that the stress history in the copper strands is qualitatively similar to the one depicted in figure 4.2b. Due to the amplitude of the load cycles being much smaller than the overall stress level, we have only elastic unloading during normal operation of the mechanism. The upper stress limit is hereby equal to the yield strength due to work hardening, while the lower stress limit and therefore the stress amplitude of the fatigue calculation depends on the amount of unloading during a single cycle. As mentioned in chapter 2.3, the radial difference between the extremal deployment positions and therefore the stress amplitude is inversely proportional to the number of windings. This means that a higher number of windings leads to a lower stress amplitude and thus higher fatigue life of the harness system. In figure 4.4, we see three possible load types with different stress amplitudes. As mentioned before, the maximum stress is in each case equal to the yield strength because of the small plastic deformation. Load type 1 and 2 lie exactly at the fatigue limit, which means that the component is able to resist at least 10^7 load cycles. Load type 3 lies outside the boundaries of the Smith diagram, which leads to a finite fatigue life of the structure. With these considerations, a margin of safety for a fail-safe dimensioning of the harness was defined according to equation (4.38). This equation compares the existing stress amplitude of the relevant load cycle with the maximum allowed one, which is equal to the stress amplitude of load type 2 in figure 4.4.

The geometric and mechanical properties of the copper strands as well as the geometric parameters of the whole harness are described in chapter 4.2.2. By applying the procedure described above to the copper strands of the outer harness and the inner harness, we computed a maximum stress reduction of 17.6 MPa. This value occurs in the outer harness during a large load cycle. The fatigue stress ratio in this case amounts to 0.884, which indicates that the stress variations during operation of the mechanism are small compared to the overall level of stress. A stress ratio slightly below 1 characterizes fluctuating tensile stress, as opposed to reversed fatigue loading characterized by a stress ratio of -1 which is the worst load case. The margin of safety was finally computed with the maximum allowable stress amplitude of 60 MPa to 85.3 %. Not only does this margin of safety imply a large safety against fatigue failure, but it was also calculated as safety factor for the fail-safe region. This region is defined by an infinite or at least very large number of cycles to failure, which is two orders of magnitude above the demanded number of cycles.

The evaluation of fatigue life for the Kapton jacket was done in the same manner as for the copper strands, but this time there were only elastic deformations in the first place. The geometric parameters of the harness are the same as for the copper strands, and the geometric and mechanical properties of the Kapton insulation are given chapter 4.2.3. The maximum stress reduction occurs during a larce cycle, this time in the inner harness cables, and amounts to 5.3 MPa. The fatigue stress ratio is 0.924 and therefore even higher than for

the copper strands. The maximum allowable stress amplitude was estimated to 36.7 MPa, which yields a margin of safety of 92.8 %. Again, this high margin of safety indicates a large safety against fatigue failure, whereby the demanded number of cycles is exceeded by two orders of magnitude.

5.3 Conclusion

It was stated in chapter 3.3.7.3 that every set objective except RSA-120 (fatigue behavior) is fulfilled by the final harness design. The remaining objective was verified mathematically in chapter 4.2.

- All of the used components provide sufficient radiation resistance against a dosage of at least 10^{10} rad.
- The test setup during breadboard testing was designed for a deployment angle of 120°, and this value was also taken into account for all of the mathematical consideration.
- The individual components of the electric cables all have a positive margin of safety not only for a finite life as required, but for the fail-safe region.
- By calculation and also measurements on the final harness design, it was ensured that the harness fulfills the geometrical requirements (axial length and diameters).
- The measured resistive torque of the harness stayed below the maximum allowed resistive torque, and the equation for the actuator dimensioning given by ECSS is fulfilled.
- An electromagnetic shielding between the two harnesses was established by using shielded cables and also by separating them using an aluminum can.
- The test setup was built with the same number and approximate diameter of cables as demanded by the objective.

With this diploma thesis, the aim of finding a feasible harness design which fulfills all set requirements was reached. Furthermore, the suitability of the test setup used in the laboratory was verified. It was shown that the measurement values are a good approximation of the true resistive torque and the behavior of the real mechanism can be modelled with this test setup. Also the amount of internal friction in the harness system can be evaluated through breadboard testing. The dummy material used instead of the real electric cables provides a conservative model which is a few times stiffer than the real system. However, internal friction effects between the individual copper strands of the electric cables are not

taken into account by this model. Although most of this friction occurs during pre-bending of the harness into its final shape and has therefore little influence during normal operation of the mechanism, the friction effects are able to raise the stiffness of the cable harness and therefore the resistive torque. An assessment of this quantity would be an important topic for future research.

Finally, a mathematical procedure was found with which the fatigue life of such cables can be assessed. Because of the small plastic deformations in the copper strands and the strain-controlled nature of the loading, conventional fatigue calculation methods are not sufficient for the estimation of the safe-life of the components. These methods had therefore to be adapted to the given circumstances in order to provide a computation procedure which can also be used in future design problems similar to this one.

The following design parameters and aspects turned out to be most helpful in achieving the objectives:

- By arranging the cable harness in three layers, the axial length was greatly reduced while the number of windings was increased. This higher number of windings led to a decrease of the curvature radius difference between two extremal deployment positions and therefore a smaller stress amplitude for the fatigue calculation. As mentioned repeatedly, an increase of the number of windings also leads to an increase of fatigue life. The disadvantage of using more cable layers is the increased thickness of the harness, which leads to a larger radial space requirement. This effect is partially cancelled out by the smaller radial difference between the extremal positions.

- With the harness fixation method, where the ends of the movable part of the cable harness are fixed to the flanges by a plastic block with drill holes, production and assembly time as well as the risk of cable damage due to contact pressure was greatly reduced. A further development of this method could consist of using shrink tubes for more favorable fastening of the cables to the block.

- The cable connection method by a perforated plastic film, which was already used in the initial harness design, was assessed together with other methods by means of a weighted point rating system and turned out to be the preferred solution out of the available ones. In the course of this thesis, a feasible synthetic material as well as an efficient production procedure was found.

- The stress ratio ρ in the fatigue life calculation was very close to 1, which lies in the fact that the majority of stresses is induced by the pre-bending of the cables and the deviations during normal operation of the mechanism are small compared to the overall stress level. This has a great positive effect on the fatigue life of the structure, as load types with ρ close to 1 are the most favourable ones. Furthermore, there are only elastic deformations during the individual cycles because due to the small stress

amplitude there is no plasticizing in opposite direction upon unloading. Although the copper strands experience small plastic deformations during pre-bending, the stress history during normal operation behaves according to Hooke's law.

Bibliography

Altorfer, Rahel (2014). “Mit Elektroantrieb durchs Weltall”. In: *InsideSpace* 1 (2014), pp. 5–6.

Andre, Florian (2014). *Thor Harness Routing Experimental*. Tech. rep. Vienna: RUAG Space Austria.

Boyer, Howard E., ed. (1990). *Atlas of Stress-Strain Curves*. 2nd ed. Metals Park, Ohio: ASM International.

— ed. (1999). *Atlas of Fatigue Curves*. 4th ed. Metals Park, Ohio: American Society for Metals.

Copper Development Association Inc. *Application Data Sheet: Mechanical Properties of Copper and Copper Alloys at Low Temperatures*. URL: http://www.copper.org/resources/properties/144_8/ (visited on June 11, 2015).

Deutsches Kupferinstitut. *CuNi10Fe1Mn*. URL: https://www.kupferinstitut.de/fileadmin/user_upload/kupferinstitut.de/de/Documents/Shop/Verlag/Downloads/Werkstoffe/Datenblaetter/Kupfer-Nickel/CuNi10Fe1Mn.pdf (visited on Nov. 12, 2015).

Domininghaus (2008). *Kunststoffe – Eigenschaften und Anwendungen*. Ed. by Peter Elsner, Peter Eyerer, and Thomas Hirth. 7th ed. Berlin; Heidelberg: Springer Verlag.

E. I. du Pont de Nemours and Company. *DEC Kapton – Summary of Properties*. URL: http://www.dupont.com/content/dam/assets/products-and-services/membranes-films/assets/DEC-Kapton-summary-of-properties.pdf (visited on Nov. 23, 2015).

— *DuPont™ Vespel® SP-1 – Polyimide Isostatic Shapes*. URL: http://www.dupont.com/content/dam/dupont/products-and-services/plastics-polymers-and-resins/parts-and-shapes/vespel/documents/VPE-A10861-00-B0614.pdf (visited on Nov. 23, 2015).

— (2011). *DuPont™ Kapton® HN polyimide film – Technical Data Sheet*. URL: http://www.dupont.com/content/dam/assets/products-and-services/membranes-films/assets/DEC-Kapton-HN-datasheet.pdf (visited on June 30, 2015).

Ensinger GmbH. *Radiation resistance*. URL: http://www.ensinger-online.com/en/technical-information/properties-of-plastics/various-other-properties/radiation-resistance/ (visited on May 7, 2015).

— *TECAFLON PVDF natural - Stock Shapes*. URL: http://www.ensinger-online.com/modules/public/sheet/createsheet.php?SID=1343&FL=0&FILENAME=HZ_TECAFLON_PVDF_natural_IN_DE_201505.pdf&ZOOM=1.2 (visited on June 26, 2015).

Ensinger GmbH. *TECATRON natural - Stock Shapes*. URL: http://www.ensinger-online.com/modules/public/sheet/createsheet.php?SID=1380&FL=0&FILENAME=HZ_TECATRON_natural_IN_DE_201505.pdf&ZOOM=1.2 (visited on June 26, 2015).

European Cooperation for Space Standardization (2009). *Space engineering – Mechanisms (ECSS-E-ST-33-01C)*. Noordwijk: ECSS Secretariat, ESA-ESTEC, Requirements & Standards Division.

Goebel, Dan M. and Ira Katz (2008). *Fundamentals of Electric Propulsion: Ion and Hall Thrusters*. Pasadena: Jet Propulsion Laboratory, California Institute of Technology. URL: http://descanso.jpl.nasa.gov/SciTechBook/series1/Goebel__cmprsd_opt.pdf (visited on May 14, 2015).

Iowa State University. *Fatigue Life Evaluation*. URL: http://www.public.iastate.edu/~e_m.424/Fatigue.pdf (visited on Nov. 17, 2015).

Janu, Paul (2010). *Flexlines – TN 2 Preliminary Designs, Analyses and Performance Predictions*. Tech. rep. Vienna: RUAG Space Austria.

Klesnil, Mirko and Petr Lukáš (1980). *Fatigue of Metallic Materials*. Amsterdam; Oxford; New York: Elsevier Scientific Publishing Company.

Lindemann, U. (2007). *Methodische Entwicklung technischer Produkte – Methoden flexibel und situationsgerecht anwenden*. 2nd ed. Berlin: Springer Verlag.

National Institute of Standards and Technology (2008). *The International System of Units (SI)*. Ed. by Barry N. Taylor and Ambler Thompson. Gaithersburg, Maryland. URL: http://physics.nist.gov/Pubs/SP330/sp330.pdf (visited on June 30, 2015).

Pahl, Gerhard and Wolfgang Beitz (2013). *Konstruktionslehre – Methoden und Anwendung erfolgreicher Produktentwicklung*. Ed. by Jörg Feldhusen and Karl-Heinrich Grote. 8th ed. Berlin: Springer Verlag.

RUAG Space Austria. *RUAG SPACE GmbH*. URL: http://www.ruag.com/de/space/ruag-space-austria/ (visited on June 25, 2015).

Sforza, Pasquale (2012). *Theory of Aerospace Propulsion*. Oxford: Butterworth-Heinemann.

Tajmar, Martin (2003). *Advanced Space Propulsion Systems*. Wien: Springer Verlag.

Turner, Martin J. L. (2009). *Rocket and Spacecraft Propulsion – Principles, Practice and New Developments*. 3rd ed. Berlin; Heidelberg; New York: Springer Verlag.

W. L. Gore & Associates. *FAQ - Improving Cable Performance in Harsh Environments*. URL: http://www.gore.com/en_xx/products/cables/improving_cable_performance_in_harsh_environments_faq.html (visited on Apr. 29, 2015).

— *GORE Space Cables and Assemblies*. URL: https://escies.org/download/webDocumentFile?id=61092 (visited on May 18, 2015).

Woebcken, Wilbrand, ed. (1998). *Kunststoff Lexikon*. 9th ed. München; Wien: Carl Hanser Verlag.

List of Abbreviations

AWG	American Wire Gauge; *Code for electric cable sizes*
cf.	confer; *compare (used in footnotes)*
CN2K, CN4K	*Types of electric cables manufactured by SILICABLE*
e.g.	example given
ECSS	European Cooperation for Space Standardization
EPPM	Electric Propulsion Pointing Mechanism
ESA	European Space Agency
ESCC	*Type of electric cables in compliance with ESA standards*
f.i.	for instance
HD-PE	High-density polyethylene
HET	Hall-effect thruster
i.a.	inter alia; *among other things*
i.e.	id est; *that is*
ibid.	ibidem; *in the same place (used in footnotes)*
LD-PE	Low-density polyethylene
mag.	magnetic
No.	number
p.	page
pp.	pages
PA	Polyamide
PE	Polyethylene
PEEK	Polyetheretherketone
PI	Polyimide
POM	Polyoxymethylene
PPS	Polyphenylene sulfide
PTFE	Polytetrafluoroethylene
PVDF	Polyvinylidene fluoride
resp.	respectively
RSA	RUAG Space Austria
std. dev.	standard deviation
wtd. pts.	weighted points *(used in the point rating system)*

List of Figures

List of Tables

Appendix A

Measurement Protocols

Comparison of both torque measurement methods

Date: 06.02.2015 / 11.02.2015

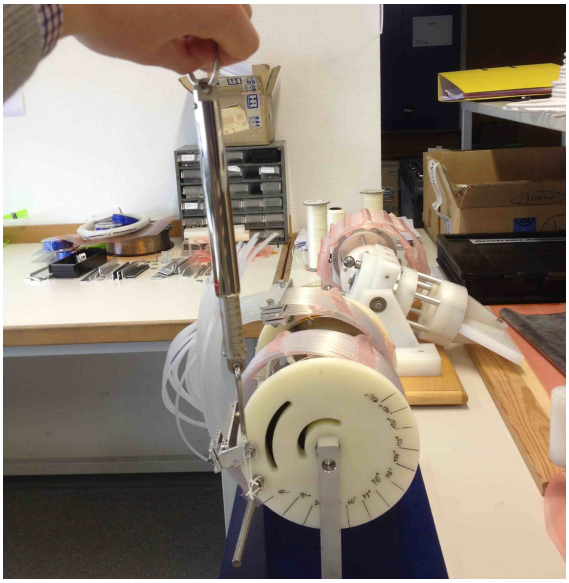

Method 1							Method 2		
Measure-	Measured weight w [g]			Torque ($w \cdot g \cdot h$) [Nmm]			Torque [Nmm]		
ment no.	60°	75°	90°	60°	75°	90°	60°	75°	90°
1	2750	3250	3600	1673	1977	2190	1500	1800	2100
2	2600	3050	3600	1581	1855	2190	1400	1800	2100
3	2750	3300	3750	1673	2007	2281	1450	1750	2000
4	2600	3050	3500	1581	1855	2129	1450	1700	2100
5	2650	3100	3600	1612	1885	2190	1500	1750	2100
6	2650	3050	3550	1612	1855	2159	1600	1700	2050
7	2550	2950	3500	1551	1794	2129	1500	1800	2200
8	2550	3000	3500	1551	1825	2129	1500	1700	2100
9	2600	2900	3350	1581	1764	2038	1500	1700	2050
10	2600	3100	3550	1581	1885	2159	1500	1750	2100
Mean value				**1600**	**1870**	**2159**	**1490**	**1745**	**2090**
Std. dev.				**43,5**	**74,8**	**62,5**	**51,6**	**43,8**	**51,6**

Measurement method 1:
- Date of measurement: 06.02.2015
- Device: *Hahn + Kolb* spring scale
- Calibrated: no
- Scale increment: 50 g (≙ 30,4 Nmm)

Measurement method 2:
- Date of measurement: 11.02.2015
- Device: *Stahlwille Torsiometer 760*
- Calibrated: yes
- Scale increment: 100 Nmm
- Precision (according to manufacturer): ± 6 %

Measurement procedure:
Using the two methods described above, ten consecutive torque measurements have been taken at deployment angles of 60°, 75° and 90°. The weight w measured with the spring scale had to be multiplied by the gravity g and lever arm h (62 mm) in order to get the rotational torque.

Breadboard testing: torque measurement of test setup version 1

Date: 15.12.2014

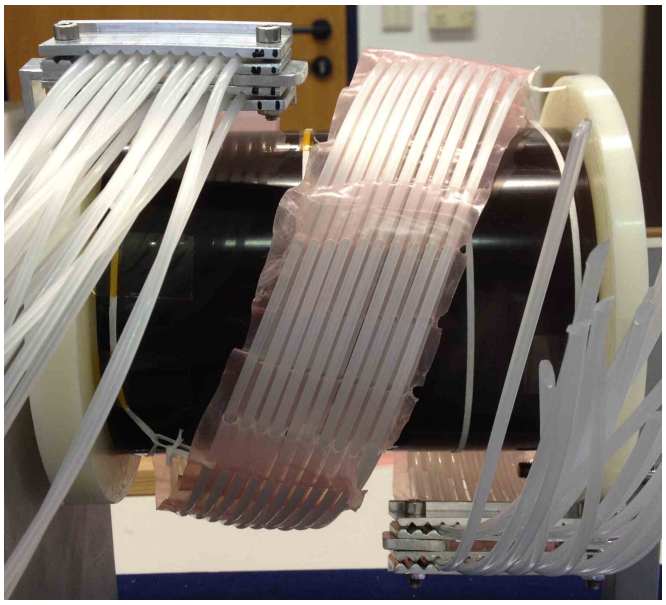

Design details:
- Number of windings (at φ = 120°): 2.0
- Winding form: inclined routing
- Application of lacing cords: yes
- Number of cable layers: 2 layers
- Connection between cables: LD-PE film
- Harness fixation: milled metal brackets
- Measuring device: *Hahn + Kolb* spring scale

Space requirements:
- Length in axial direction: L = 142 mm
- Diameter in radial direction: $Ø$ = 181 mm
- Lever arm of spring scale: h = 62 mm

Turning angle φ [°]	Measured weight w [g]		Torque ($w \cdot g \cdot h$) [Nmm]	
	Coiling up	Unrolling	Coiling up	Unrolling
0	1000	700	608	426
15	1500	950	912	578
30	1850	1350	1125	821
45	2100	1600	1277	973
60	2350	1900	1429	1156
75	2750	2050	1673	1247
90	3100	2250	1885	1368
105	3600	2400	2190	1460
120	4250	3200	2585	1946

Measurement procedure:
The measurements have been taken by turning the cable harness to the respective deployment angle with the attached spring scale. The value displayed by the spring scale (the measured weight w) has to be multiplied by the gravity g and lever arm h in order to get the torque acting against the rotation (*spring torque*). At first, the measurements were taken while increasing the deployment angle from 0° to 120° (measurements titled *"Coiling up"*). Afterwards, the deployment angle was decreased down to 0° (*"Unrolling"*). The difference between these two measurement runs represents the hysteresis loop and is a measure for the internal friction of the cable harness.

Breadboard testing: torque measurement of test setup version 2

Date: 11.02.2015

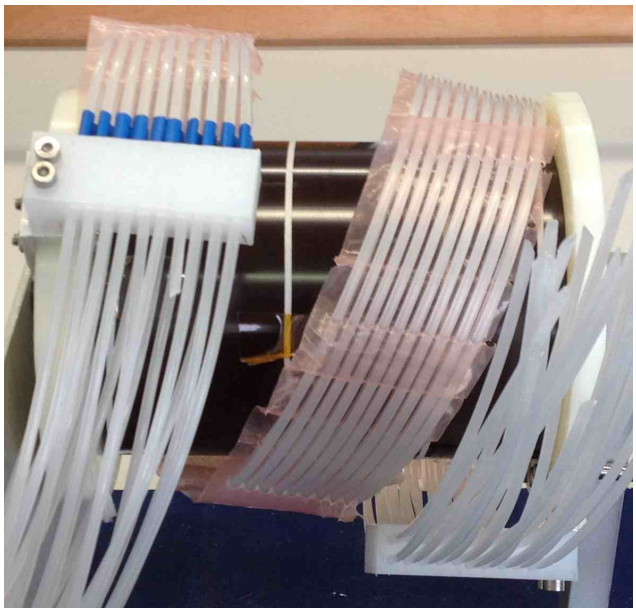

Design details:
- Number of windings (at φ = 120°): 2.0
- Winding form: inclined routing
- Application of lacing cords: no
- Number of cable layers: 2 layers
- Connection between cables: LD-PE film
- Harness fixation: plastic block
- Measuring device: *Stahlwille Torsiometer 760*

Space requirements:
- Length in axial direction: L = 142 mm
- Diameter in radial direction: $Ø$ = 183 mm

Turning angle φ [°]	Torque [Nmm] (series 1)		Torque [Nmm] (series 2)		Torque [Nmm] (series 3)	
	Coiling up	Unrolling	Coiling up	Unrolling	Coiling up	Unrolling
0	900	600	850	600	800	< 600
15	1100	700	1050	700	1100	600
30	1200	700	1200	800	1200	700
45	1400	800	1350	950	1300	800
60	1600	900	1650	1200	1500	900
75	1850	1100	1800	1300	1700	1100
90	2100	1300	2200	1450	2100	1300
105	2550	1500	2600	1650	2700	1400
120	> 3000	2200	> 3000	2600	> 3000	2500

Measurement procedure:
The measurements have been taken by turning the cable harness to the respective deployment angle using a torque wrench, which directly displays the torque acting against the rotation (*spring torque*). At first, the measurements were taken while increasing the deployment angle from 0° to 120° (measurements titled *"Coiling up"*). Afterwards, the deployment angle was decreased down to 0° (*"Unrolling"*). The difference between these two measurement runs represents the hysteresis loop and is a measure for the internal friction of the cable harness. In total, three measurement series were performed according to the described procedure.

Remarks:
The scale span of the *Torsiometer* reaches from 600 Nmm to 3000 Nmm, which is why some of the measurement values could not be taken accurately. In the table above, they are displayed as *"< 600"* or *"> 3000"*.

Breadboard testing: torque measurement of test setup version 3

Date: 25.02.2015

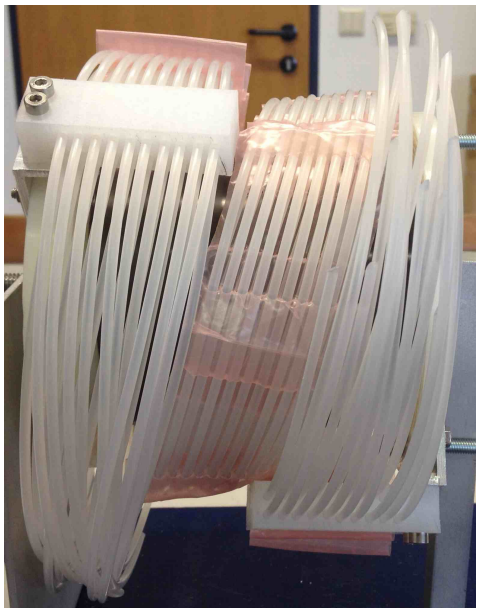

Design details:
- Number of windings (at φ = 120°): 2.0
- Winding form: inclined routing
- Application of lacing cords: no
- Number of cable layers: 2 layers
- Connection between cables: LD-PE film
- Harness fixation: plastic block
- Measuring device: *Torqueleader* torque wrench

Space requirements:
- Length in axial direction: L = 110 mm
- Diameter in radial direction: $Ø$ = 183 mm

Turning angle φ [°]	Torque [Nmm] (series 1)		Torque [Nmm] (series 2)		Torque [Nmm] (series 3)	
	Coiling up	Unrolling	Coiling up	Unrolling	Coiling up	Unrolling
0	900	800	800	800	850	800
15	1050	1000	1000	950	1000	900
30	1250	1050	1200	1050	1150	1100
45	1400	1200	1350	1300	1350	1200
60	1700	1450	1550	1500	1600	1400
75	1850	1550	1900	1700	1800	1550
90	2150	1800	2100	1800	2050	1700
105	2600	2050	2300	1950	2350	1800
120	3400	2500	3000	2500	3100	2500

Measurement procedure:
The measurements have been taken by turning the cable harness to the respective deployment angle using a torque wrench, which directly displays the torque acting against the rotation (*spring torque*). At first, the measurements were taken while increasing the deployment angle from 0° to 120° (measurements titled *"Coiling up"*). Afterwards, the deployment angle was decreased down to 0° (*"Unrolling"*). The difference between these two measurement runs represents the hysteresis loop and is a measure for the internal friction of the cable harness. In total, three measurement series were performed according to the described procedure.

Breadboard testing: torque measurement of test setup version 4

(without lacing cords)

Date: 10.03.2015

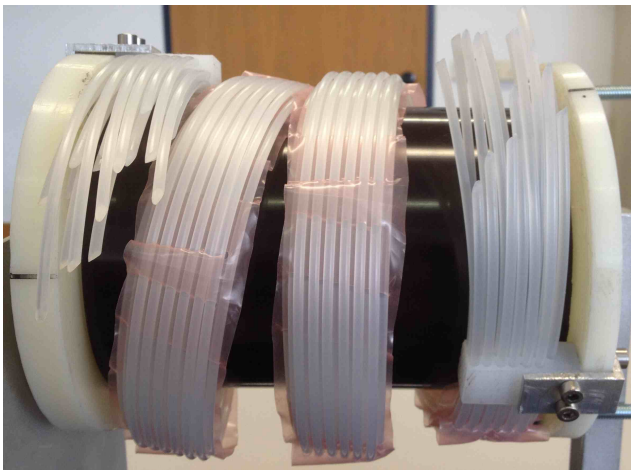

Design details:

- Number of windings (at φ = 120°): 3.0
- Winding form: inclined routing
- Application of lacing cords: no
- Number of cable layers: 3 layers
- Connection between cables: LD-PE film
- Harness fixation: plastic block
- Measuring device: *Torqueleader* torque wrench

Space requirements:

- Length in axial direction: L = 141 mm
- Diameter in radial direction: $Ø$ = 140 mm

Turning angle φ [°]	Torque [Nmm] (series 1)		Torque [Nmm] (series 2)		Torque [Nmm] (series 3)	
	Coiling up	Unrolling	Coiling up	Unrolling	Coiling up	Unrolling
0	1150	1000	1100	1050	1000	1050
15	1250	1100	1250	1100	1200	1100
30	1450	1200	1350	1200	1350	1200
45	1600	1300	1500	1300	1500	1300
60	1700	1350	1600	1400	1600	1400
75	1750	1450	1700	1500	1700	1450
90	1800	1600	1800	1600	1800	1600
105	1900	1700	2000	1700	1950	1700
120	2350	2000	2300	1900	2350	1950

Measurement procedure:

The measurements have been taken by turning the cable harness to the respective deployment angle using a torque wrench, which directly displays the torque acting against the rotation (*spring torque*). At first, the measurements were taken while increasing the deployment angle from 0° to 120° (measurements titled *"Coiling up"*). Afterwards, the deployment angle was decreased down to 0° (*"Unrolling"*). The difference between these two measurement runs represents the hysteresis loop and is a measure for the internal friction of the cable harness. In total, three measurement series were performed according to the described procedure.

Breadboard testing: torque measurement of test setup version 4

(with lacing cords)

Date: 17.03.2015

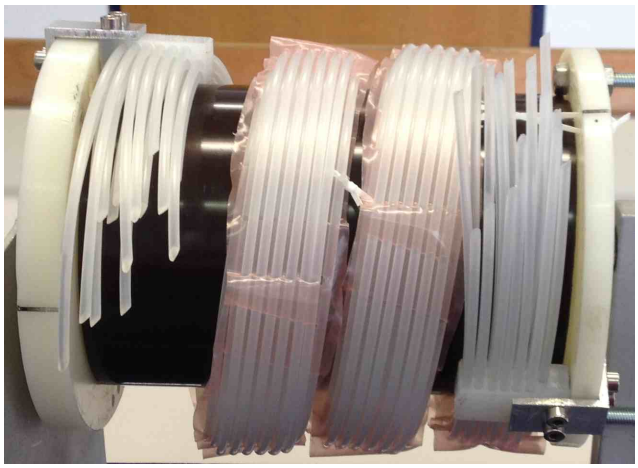

Design details:

- Number of windings (at φ = 120°): 3.0
- Winding form: inclined routing
- Application of lacing cords: yes
- Number of cable layers: 3 layers
- Connection between cables: LD-PE film
- Harness fixation: plastic block
- Measuring device: *Torqueleader* torque wrench

Space requirements:

- Length in axial direction: L = 141 mm
- Diameter in radial direction: $Ø$ = 140 mm

Turning angle φ [°]	Torque [Nmm] (series 1)		Torque [Nmm] (series 2)		Torque [Nmm] (series 3)	
	Coiling up	Unrolling	Coiling up	Unrolling	Coiling up	Unrolling
0	900	700	950	600	1000	600
15	1050	750	1050	700	1050	700
30	1200	850	1200	800	1150	800
45	1300	900	1300	900	1300	950
60	1400	1000	1400	1000	1400	1050
75	1500	1100	1450	1200	1450	1100
90	1550	1200	1500	1250	1500	1200
105	1700	1300	1650	1300	1700	1300
120	2000	1400	1900	1550	2000	1500

Measurement procedure:

The measurements have been taken by turning the cable harness to the respective deployment angle using a torque wrench, which directly displays the torque acting against the rotation (*spring torque*). At first, the measurements were taken while increasing the deployment angle from 0° to 120° (measurements titled *"Coiling up"*). Afterwards, the deployment angle was decreased down to 0° (*"Unrolling"*). The difference between these two measurement runs represents the hysteresis loop and is a measure for the internal friction of the cable harness. In total, three measurement series were performed according to the described procedure.

Breadboard testing: torque measurement of test setup version 5

(final design version with outer and inner cable harness)

Date: 12.05.2015

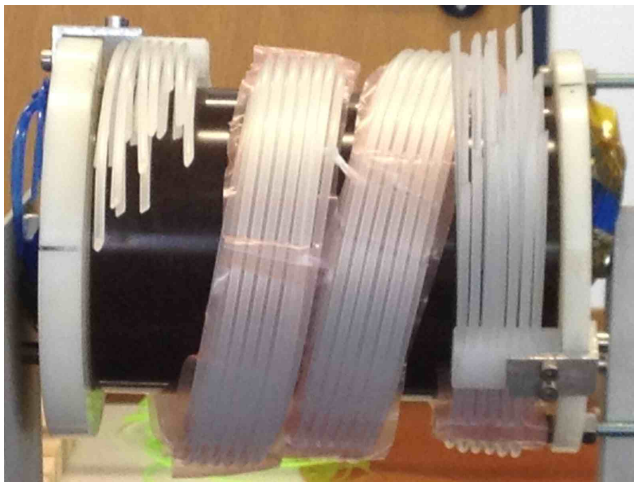

Design details:

- Number of windings (at $\varphi = 120°$):
  - Outer harness: 3.0; inner harness: 5.5
- Winding form: inclined routing
- Application of lacing cords: yes
- Number of cable layers: 3 layers
- Connection between cables: LD-PE film
- Harness fixation: plastic block
- Measuring device: *Torqueleader* torque wrench

Space requirements:

- Length in axial direction: $L = 141$ mm
- Diameter in radial direction: $Ø = 140$ mm

Turning angle φ [°]	Torque [Nmm] (series 1)		Torque [Nmm] (series 2)		Torque [Nmm] (series 3)	
	Coiling up	Unrolling	Coiling up	Unrolling	Coiling up	Unrolling
0	1150	750	1150	700	1100	700
15	1200	800	1200	750	1200	750
30	1350	900	1350	950	1300	850
45	1450	1050	1450	1000	1400	950
60	1550	1150	1550	1150	1550	1100
75	1700	1250	1650	1250	1650	1200
90	1800	1350	1750	1350	1700	1250
105	2000	1550	1950	1550	1950	1450
120	2300	1750	2250	1700	2250	1700

Measurement procedure:

The measurements have been taken by turning the cable harness to the respective deployment angle using a torque wrench, which directly displays the torque acting against the rotation (*spring torque*). At first, the measurements were taken while increasing the deployment angle from 0° to 120° (measurements titled *"Coiling up"*). Afterwards, the deployment angle was decreased down to 0° (*"Unrolling"*). The difference between these two measurement runs represents the hysteresis loop and is a measure for the internal friction of the cable harness. In total, three measurement series were performed according to the described procedure.

Appendix B

Data Sheets

SILICABLE®

CN2K and CN4K

- 190°C to + 260°C

CHARACTERISTICS

Physical-chemical

- Continuous working temperatures: - 190°C to + 260°C - Peaks at + 300°C.
- Good resistance to thermal shock.
- Excellent ageing resistance.
- Good resistance to humidity and UV.
- Good resistance to aggressive chemical atmospheres.
- Excellent resistance to radiation: 1.10^{10} rad.

Electrical

- Working voltage: 300/500 V.
- Test voltage: 2000 V.
- Increased dielectric strength: ref. CN4K.

PRODUCTS

- CN2K: 0.14 to 6 mm².
- CN4K: 0.14 to 50 mm².
- Colour: amber.

OPTIONS

- Pure nickel core: ref. N2K and N4K.
- Silver-plated copper core: ref. A2K and A4K.
- Multiconductor assembly under a Kapton® polyimid sheath: ref. MK-CN2K and MK-CN4K.
- Other cross-sections, core compositions and flexibility classes: consult us.

1 - Flexible nickel-plated core.
2 - Two lapped, heat-sealed Kapton® polyimide tapes.
3 - Four lapped, heat-sealed Kapton® polyimide tapes.

APPROVALS - STANDARDS

- Nickel-plated copper meets standard ASTM B355.
- VERITAS inspection certificate N° 153624.

PACKAGING

- Rolls, spools or drums.

APPLICATIONS

- Wiring of heating elements, cartridges, bands, and hot plates.
- All wiring in aggressive environments (nuclear, chemical, etc.).

CN2K

CN4K

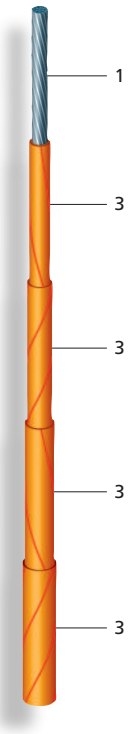

C

CORE

Nominal cross-section mm²	Nominal stranding	Max. linear resistance at 20°C Ω/km
0.14*	7 x 0.15	178
0.22*	7 x 0.20	99.4
0.25	8 x 0.20	86.9
0.34*	7 x 0.25	63.6
0.5*	7 x 0.30	43.8
0.6*	19 x 0.20	36.3
0.75	24 x 0.20	28.7
0.93*	19 x 0.25	23.2
1	32 x 0.20	21.5
1.34*	19 x 0.30	16.1
1.5	30 x 0.25	14.7
1.91*	27 x 0.30	11.3
2.5	50 x 0.25	8.21
2.62*	37 x 0.30	8.21
3.18*	45 x 0.30	6.75
4	56 x 0.30	5.09
6	84 x 0.30	3.39
10	80 x 0.40	1.95
16	126 x 0.40	1.24
25	196 x 0.40	0.795
35	276 x 0.40	0.565
50	396 x 0.40	0.394

* Concentric cores.

INSULATED WIRE OR CABLE

Nominal outer diameter mm CN2K	Nominal outer diameter mm CN4K	Approx. linear weight kg/km
0.8	1.1	1.50
0.9	1.2	2.80
1.0	1.3	3.40
1.1	1.4	3.90
1.2	1.5	4.70
1.3	1.6	6.00
1.5	1.8	7.40
1.6	1.9	10.3
1.6	1.9	12.2
1.8	2.1	14.2
1.9	2.2	17.7
2.2	2.5	21.3
2.3	2.6	29.7
2.4	2.7	29.9
2.8	3.1	35.6
2.9	3.2	41.5
3.5	3.8	71.0
	5.0	125
	6.0	195
	7.4	312
	8.8	393
	10.6	553

Kapton® is a registered trademark of Du Pont de Nemours.

Zone Industrielle - F 63600 AMBERT
Tel: (33) 04 73 82 50 00 - Fax: (33) 04 73 82 50 10
omerin@omerin.com - www.omerin.com

omerin division principale

Shielded jacketed twisted pairs

ESCC 3901 019

CELLOFLON® / Polyimide tape

Operating temperature: -200°C up to +200°C

Voltage rating: 600 VAC max.

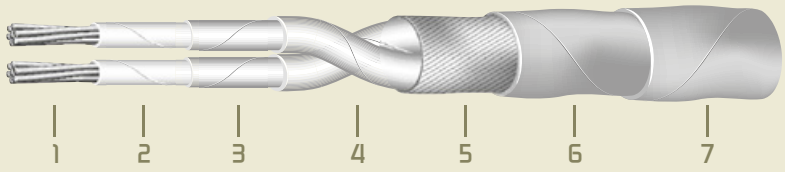

Construction

1 - Stranded silver plated copper or copper alloy conductor,
2 - Expanded PTFE tape (CELLOFLON®),
3 - Polyimide tape,
4 - Polyimide tape,
5 - Silver plated copper helicoidal shield,
6 - Polyimide tape,
7 - Polyimide tape.

Colour: Amber (except other specification)

Main characteristics

Excellent physical, chemical and electrical properties:

- excellent penetration resistance under pressure,
- excellent radiation resistance,
- resist large overloads with no fire risk,
- non-flammable,
- good flexibility,
- resistant to most chemicals,
- suited for thermal, mechanical or laser stripping.

AXON' REFERENCE	CONDUCTOR					SHIELD STRAND Ø mm	SINGLE WIRE MAX. Ø mm	OVERALL MAX. Ø mm	MAX. WEIGHT g/m
	AWG	STRANDING Nb x Ø mm	MAX. Ø mm	NOM. CROSS SECTION mm²	MAX. DC RESISTANCE AT 20°C Ω / km				
ESCC 3901 019 56*	30	7X0.102 SPCA	0.32	0.057	383	0.063	0.78	1.90	5.10
ESCC 3901 019 57	28	7X0.127 SPCA	0.47	0.09	258	0.079	0.87	2.10	6.10
ESCC 3901 019 58	26	19X0.10 SPCA	0.57	0.15	170	0.079	0.96	2.30	7.70
ESCC 3901 019 59	24	19X0.12 SPCA	0.58	0.25	120	0.079	1.13	2.70	9.50
ESCC 3901 019 60	22	19X0.15 SPC	0.76	0.40	63	0.079	1.25	2.90	13.40
ESCC 3901 019 61	20	19X0.20 SPC	0.99	0.60	35	0.079	1.48	3.30	19.60
ESCC 3901 019 62	16	19X0.30 SPC	1.49	1.20	15	0.079	1.98	4.30	35.00
ESCC 3901 019 63	12	37X0.32 SPC	2.18	3.00	7.50	0.079	2.73	5.80	67.00

SPC: silver plated copper - SPCA: silver plated copper alloy -*=according to the ESA standard